Technical Review: Performance of the Composite Barrier Layers and Lateral Drainage Layers of the U.S. Department of Energy 2020 Performance Assessment for the Savannah River Site Saltstone Disposal Facility

Date

April 18, 2023

Reviewer

Hans Arlt, Sr. Risk Analyst, U.S. Nuclear Regulatory Commission
Stuart Stothoff, Principal Scientist, Center for Nuclear Waste Regulatory Analyses, Southwest Research Institute®

1.0 Purpose and Scope

The purpose of this U.S. Nuclear Regulatory Commission (NRC) staff Technical Review Report (TRR) is to document the NRC staff review of technical bases for modeled material properties of three types of barriers within the closure caps or surface covers: (i) composite barriers consisting of high-density polyethylene (HDPE) geomembrane in combination with a geosynthetic clay liner (GCL); (ii) HDPE geomembranes without GCLs, used as liners; and (iii) lateral sand drainage layers, which are used in conjunction with HDPE/GCL composite barriers modeled in the U.S. Department of Energy (DOE) 2020 Performance Assessment (PA) for the Saltstone Disposal Facility (SDF) at the Savannah River Site (SRS) (the DOE document SRR-CWDA-2019-00001). The performance of these risk-significant cover barriers is discussed in detail in this TRR; however, the NRC staff also addresses the overall hydraulic performance of the closure cap in the context of the PA in other TRRs. The NRC staff performed this review to support a future decision about whether the DOE has demonstrated that radioactive waste disposal activities at the SDF are in compliance with the performance objectives of Title 10 of the *Code of Federal Regulations* (10 CFR) Part 61, "Licensing Requirements for Land Disposal of Radioactive Waste," at the SRS SDF pursuant to Section 3116(b) of the Ronald W. Reagan National Defense Authorization Act for Fiscal Year 2005. This technical review also supports the NRC monitoring of the SDF under Monitoring Factor (MF) 2.01, "Hydraulic Performance of Closure Cap," under Monitoring Area (MA) 2, "Infiltration and Erosion Control," as detailed in the current NRC Monitoring Plan for the SDF (available in the NRC's Agencywide Documents Access and Management System under Accession No. ML13100A113).

The 2020 DOE SDF PA completely replaced the previous DOE 2009 SDF PA and includes altered design concepts and newer data. In response to the NRC request for supplemental information (ML20254A003), the DOE provided two documents (SRR-CWDA-2021-00031, Rev. 1 and SRR-CWDA-2021-00033, Rev. 1).

The current DOE design plan includes 15 existing and proposed disposal structures. The initial free-standing concrete vaults of those disposal structures will be backfilled and covered by one of two closure caps, including lateral sand drainage layers and HDPE/GCL composite barrier layers. Composite barriers will also be used within mud mats underlying some of the disposal structures. In addition, some of the disposal structure walls will be wrapped with HDPE geomembranes prior to backfilling. In the 2020 SDF PA, the composite barrier layers provided risk-significant performance with respect to limiting flow of water through the disposal structures. Also, the review scope included the NRC staff's evaluation of parameters and equations used in the DOE models to calculate or simulate flow in the covers.

2.0 Background

Hydraulic performance of closure cap of the DOE SRS SDF is described in the current NRC Monitoring Plan for the SDF in MF 2.01. Besides the 2020 SDF PA, the NRC staff and the Center for Nuclear Waste Regulatory Analyses (CNWRA®) staff reviewed and evaluated information from various DOE and non-DOE documents, including annual SDF groundwater monitoring reports. This TRR relies on findings of the CNWRA's 2021 "Technical Report: Performance of HDPE Geomembrane Layers, Composite Barrier Layers, and Lateral Sand Drainage Layers of the 2020 Saltstone Disposal Facility Performance Assessment" (ML21287A328) for technical topics where information has been consistent and relatively unchanged since that report was issued.

In addition, this review also was informed by the following documents:

- the 2012 NRC Technical Evaluation Report (TER) (ML121170309)
- the current NRC Monitoring Plan for the SDF (ML13100A113)
- the DOE Fiscal Year (FY) 2013 SDF Special Analysis Document (the DOE document SRR-CWDA-2013-00062, Rev. 2, [ML14002A069])
- the DOE Responses to the NRC Request for Additional Information (RAI) Comments and Questions on the DOE FY 2013 SDF Special Analysis Document (the DOE document SRR-CWDA-2014-00099, Rev. 1, [ML15020A672])
- the DOE FY 2014 SDF Special Analysis Document (the DOE document SRR-CWDA-2014-00006, Rev. 2, [ML15097A366])
- the DOE Responses to the NRC RAI Questions and Comments on the DOE FY 2014 SDF Special Analysis Document (the DOE document SRR-CWDA-2016-00004, Rev. 1, [ML16105A043])
- the DOE Responses to the NRC Request for Supplemental Information for the 2020 SDF PA (the DOE documents SRR-CWDA-2021-00031, Rev. 1, [ML21160A061] and SRR-CWDA-2021-00033, Rev. 1, [ML21160A062])
- the DOE Comment Response Matrix for the Third Set of U.S. NRC RAI Questions and Comments on the 2020 SDF PA (the DOE document SRR-CWDA-2022-00003, Rev. 0, [ML22083A049])
- the Report for the July 2018 NRC SDF Onsite Observation Visit (ML18219B859).

3.0 Information from the Previous PA, Special Analyses Documents, and the Current PA

3.1 *Context for the TRR*

This TRR examines performance aspects of three types of barriers: (i) HDPE geomembranes used as liners; (ii) HDPE geomembranes combined with a GCL; and (iii) lateral sand drainage layers, which are used in conjunction with an HDPE/GCL composite barrier. This TRR is intended to better understand performance claims for these barrier components in the DOE 2020 SDF PA, which builds upon and completely replaces the previous DOE 2009 SDF PA (2009, SDF PA).

The SDF consists of disposal structures that receive a low-level waste (LLW) salt waste solution into which dry feeds (e.g., Portland cement) are added to produce a grout slurry called "Saltstone." The 2020 SDF PA assumed that the final SDF configuration will include two existing rectangular disposal structures (Saltstone Disposal Structure (SDS) 1 and SDS 4), six existing "150-Foot" diameter cylindrical disposal structures (SDS 2A, SDS 2B, SDS 3A, SDS 3B, SDS 5A, and SDS 5B), and seven "375-Foot" diameter cylindrical disposal structures (SDS 6 through SDS 12).

The cylindrical disposal structures each have a conical roof, with nominal radial slopes of 2 percent for the small ones and 1.5 percent for the large ones. The 15 disposal structures will be sequestered beneath two covers, also called closure caps (Figure **3-*1***). Cross sections through the covers are shown in Figure **3-*2***. The 2020 SDF PA describes the closure cap design as preliminary and conceptual in nature. The presented design sequesters SDS 1 and SDS 4 within the smaller southern cover and the other 13 disposal structures within the larger northern cover.

The closure cap design indicates a continuous upper lateral sand drainage layer in each of the two SDF closure caps and indicates 15 separate lower lateral sand drainage layers below these two upper drainage layers (i.e., each of the disposal structures has a separate lateral sand drainage layer above its roof). A composite barrier will be installed below each of these drainage layers. Composite barriers will also be found within mud mats underlying some of the disposal structures, and some of the walls of the disposal structures will be wrapped with HDPE geomembranes prior to backfilling.

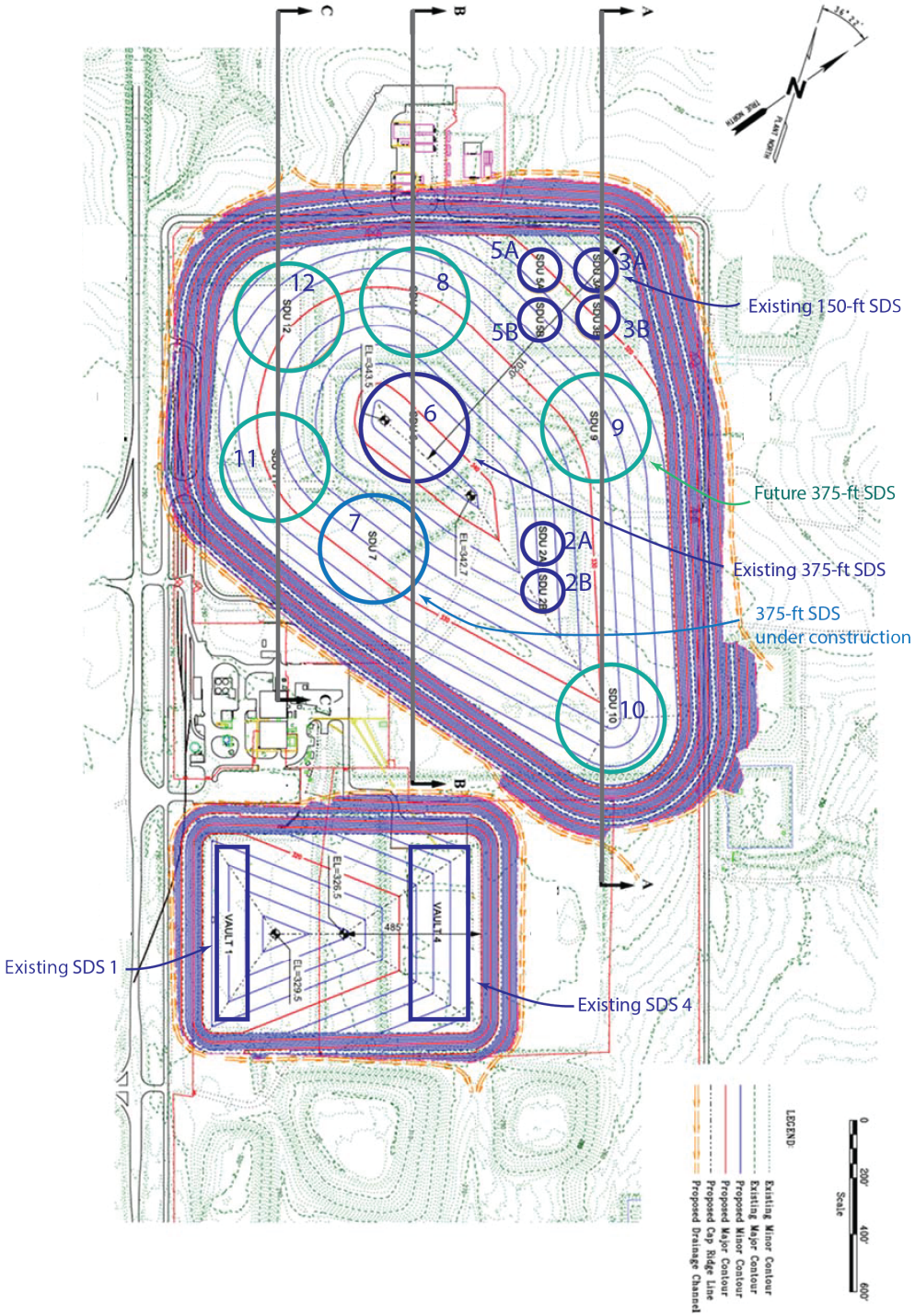

Figure 3-1: SDF Conceptual Closure Cap Design Configuration (labeled arrows indicate position of cross sections in Figure 3-2)
(modified from Figure 3.2-29 in the DOE 2020 SDF PA Figure 3.2-29)

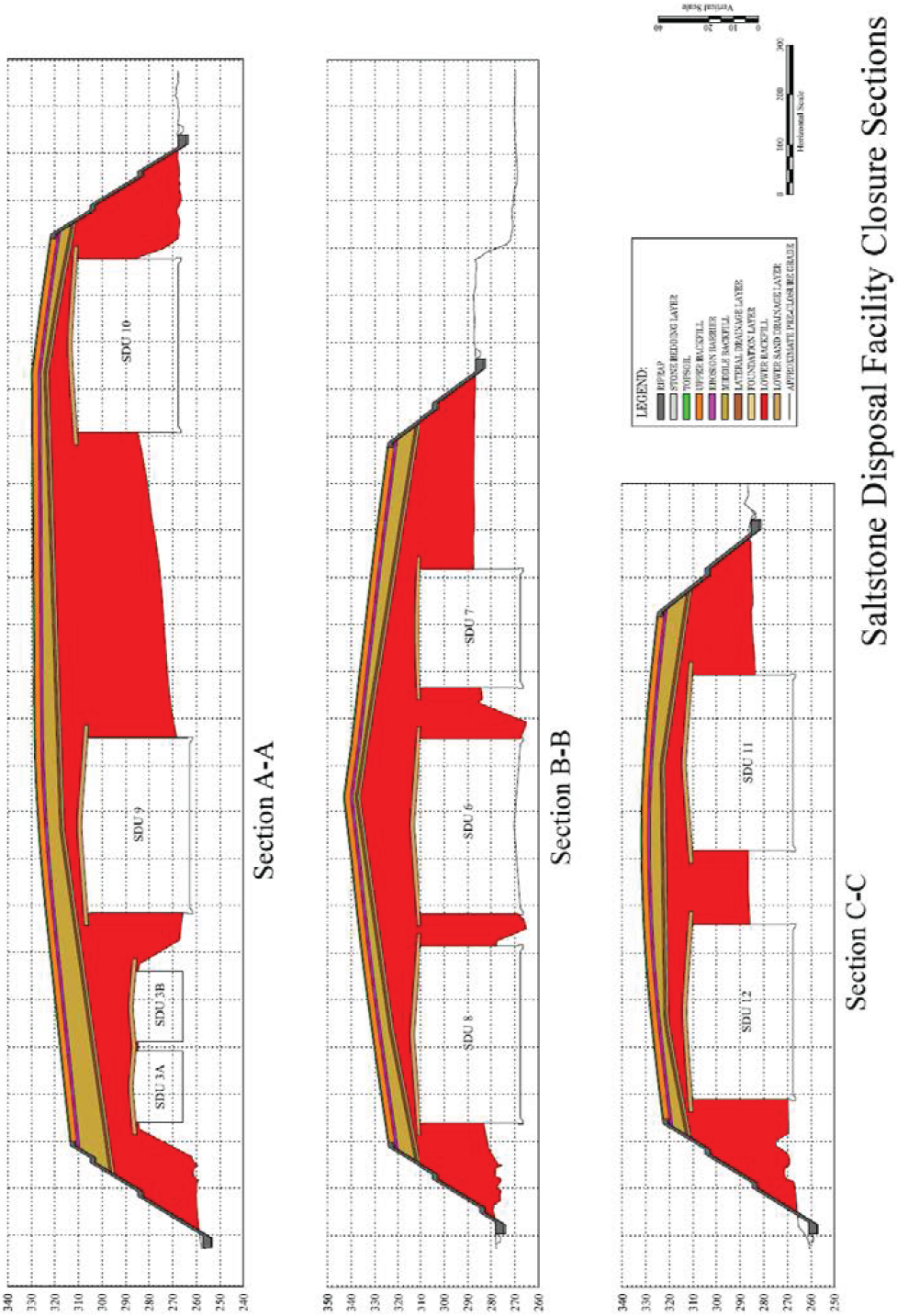

Figure 3-2: Selected Cross Sections in the SDF Conceptual Closure Cap Design Configuration (modified from Figure 3.2-30 in the DOE 2020 SDF PA)

For consistency and clarity, this TRR uses the following terminology:

- lateral sand drainage layers in the two SDF closure caps are referred to as the Upper Lateral Drainage Layers (ULDL). The 15 separate lateral sand drainage layers that overlie each of the 15 SDSs are referred to as the Lower Lateral Drainage Layers (LLDL)

- an HDPE geomembrane used alone as a barrier layer is referred to as an "HDPE geomembrane layer." The DOE plans to use HDPE geomembrane layers for vertical barriers on several of the disposal structures. If the discussion is about the polyethylene substance itself, then it is referred to as HDPE

- a barrier layer comprising an HDPE geomembrane and GCL is referred to as a "composite barrier layer". The HDPE geomembrane component of a composite barrier layer is referred to as an "HDPE geomembrane" and the GCL component of the composite barrier layer is referred to as a "GCL." The composite barrier layer below the ULDL, below the LLDL, and between the mud mats are referred to as the ULDL composite barrier layer, the LLDL composite barrier layer, and the mud-mat composite barrier layer, respectively

- the ULDL barrier in the closure cap refers to the combined layers of the HDPE/GCL composite barrier layer and the ULDL above it. The LLDL barrier above the roof of the disposal structure refers to the combined layers of the HDPE/GCL composite barrier layer and the LLDL above it

- a composite barrier layer or a HDPE geomembrane layer is generically referred to as a "liner" when referring to any HDPE-based barrier layer adjacent to a disposal structure roof or exterior wall, or within a mud mat underlying a disposal structure floor

Figure 4-1 in Section 4.0 below shows the future location of some of those barriers within the SDF.

Both the DOE Radioactive Waste Management Manual 435.1-1 (ML20206L014) and 10 CFR Part 61, "Licensing Requirements for Land Disposal of Radioactive Waste," indicate that a PA should provide reasonable expectation or assurance that LLW disposal will comply with specified performance objectives, requiring assessments of impacts to hypothetical receptors that include future members of the public and inadvertent human intruders. The DOE Radioactive Waste Management Manual 435.1-1 also requires assessments for impacts to water resources. The 2020 SDF PA addressed a 1,000-year Compliance Period after facility closure and informational 10,000-year Performance and Long-Term Exploratory (greater than 10,000-year) Periods to identify potential peak doses occurring beyond the regulatory Compliance Period.

Aqueous transport is the primary mode for radionuclides to contact potential receptors, however the saltstone sequestration strategy limits the amount of flow contacting the saltstone by: (i) placing the disposal structures above the water table, (ii) emplacing backfill around and above the disposal structures, and (iii) using multiple barriers, including composite barriers and lateral drains, to redirect flow away from the disposal structures.

Although annual precipitation at the SRS is significantly larger than annual potential evapotranspiration, the fraction of water removed by evapotranspiration is not insignificant. However, the large fraction of water remaining must either run off the surface or infiltrate into the ground. The conceptual design allows substantial infiltration into the cover in order to minimize erosion due to runoff at the surface. Based on numerical simulations using the WINUNSAT-H model, DOE calculated that annual excess infiltration (i.e., escaping evapotranspiration) might range from ~250 to ~650 millimeters (mm) (9.8 – 26 inches (in.)) from year to year because of variability in precipitation rates and other factors, and would average approximately 400 mm/year (yr) (16 in./yr). The conceptual design removes essentially all the excess infiltration with the ULDL (see **Figure 3-*3***). The LLDL, immediately above each disposal structure, is a backup to reduce any remaining flow that might reach the disposal structure. As shown in Figure **3-*3***, the ULDL will be continuous across the cover, but each disposal structure will have a separate LLDL that extends 7.6 meters (m) (25 feet (ft.)) past the edge of the disposal structure roof to shed water into a gap between disposal structures. Both drainage layers are underlain by a composite barrier layer. The 2020 SDF PA described the composite barrier as essentially impermeable for thousands of years, which: (i) keeps infiltrating flow within the drainage layer and (ii) minimizes oxygen exchange. In the LLDL concept, the DOE will place the GCL directly on the disposal structure roof. The HDPE/GCL combination will not extend beyond the roof, unlike the lateral drainage layer, which extends beyond the roof.

The performance of the composite barrier layer is critical for performance of a lateral drainage layer (and vice versa) where the underlying material is permeable. A HDPE geomembrane is typically manufactured in rectangular 1.0 to 2.5 mm (40 to 100 mil (thousandth of an inch)) (0.04 – 0.1 in.) thick sheets of solid flexible HDPE, typically supplied in rolls that are 1.8 to 10 m (5.9 – 33 ft.) wide and up to 305 m (1000 ft.) long (U.S. Bureau of Reclamation, 2018). The seams between the sheets are welded together during installation or construction. The 2020 SDF PA specifies the HDPE geomembranes as 1.5 mm and 2.5 mm (0.06 - 0.1 in.) under the ULDL and LLDL, respectively. A GCL is another manufactured product, typically consisting of a thin layer of bentonite wrapped in geotextiles and stitched together to resist shear. The 2020 SDF PA specifies that the GCLs for the two drainage layers are both 5 mm thick. GCLs are usually supplied as rolled sheets that are 4 to 5.5 m (13 - 18 ft.) by 30 to 60 m (98 - 200 ft.) (U.S. Environmental Protection Agency, 2001).

Figure **3-*3*** indicates several other aspects of the closure cap that are related to cover performance. One aspect involves the foundation layer below the ULDL and composite barrier layer, or the ULDL barrier. It is intended to provide a relatively low-permeability layer to provide required drainage contours and will consist of the backfill material mixed with bentonite. Other aspects pertain to different cover components having different slopes so that the thickness of backfill will vary between these components. The near-surface part of the cover is designed to minimize surface erosion, with the 3 percent surface slope set to minimize erosion from runoff. The ULDL has a steeper slope (4 percent) to enhance drainage, while the LLDL slope is determined by the disposal structure roof slope (1.5 percent or 2 percent). From geometric constraints, the middle backfill is thinnest and the lower backfill is thickest at the center of the cover as seen in Section B-B in Figure 3-2. The various emplaced geotextile fabric layers are intended to: (i) protect the HDPE during construction, (ii) minimize the transport of fine soil particles that might clog the drainage layers, and (iii) restrain penetration of erosion stones into the middle backfill and prevent development of open flow channels along preferential pathways

(piping) in the middle backfill through the erosion barrier voids. Geotextile performance is not explicitly represented in flow simulations.

Two additional barriers featuring a HDPE geomembrane layer or composite barrier layer are not shown in
Figure **3-3**. The 13 cylindrical disposal structures are designed to have an additional composite barrier layer encased within two layers of the underlying concrete mud mat. In addition, the smaller ones are designed to have a HDPE layer wrapping the exterior of the disposal structure walls. Those barriers are intended to reduce transfer of water, reduce inflow of carbon dioxide and oxygen; and reduce release of radionuclides.

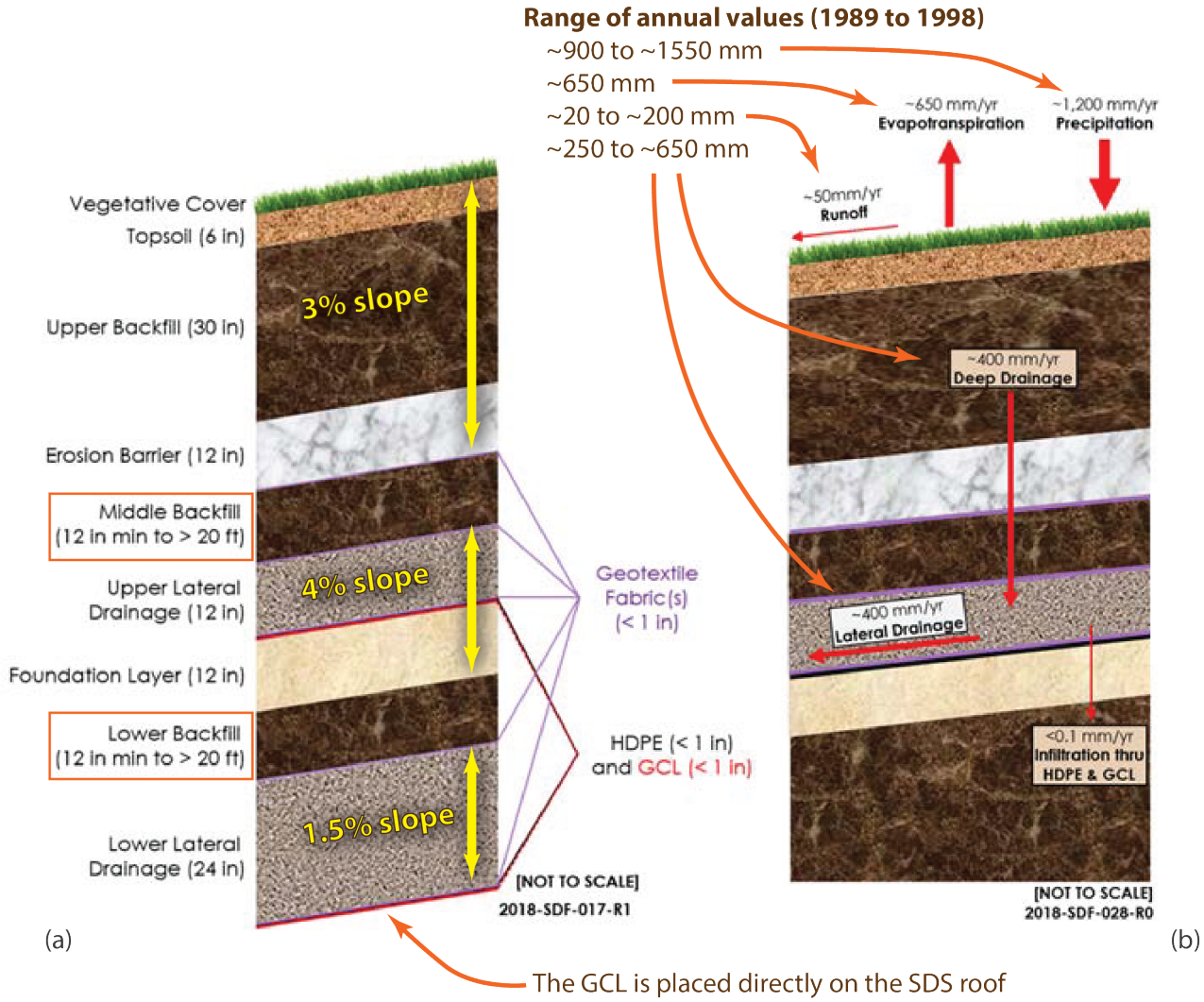

Figure 3-3: SDF Conceptual Closure Cap Design: (a) Components of the cover above each disposal structure and(b) Water balance summary above the ULDL (modified from Figure 3.2-33 and Figure 3.2-35 in the DOE 2020 SDF PA)

3.2 *Information from the Previous PA and Special Analyses Documents*

In an NRC TRR from 2017 (ML17081A187), the NRC staff documented a technical review related to the performance of HDPE geomembrane layers, composite barrier layers, and the LLDL. The NRC 2017 TRR summarized aspects of the earlier NRC 2012 SDF TER (ML121170309), then reviewed updates to SDF modeling approaches found in the DOE SDF FY 2013 and FY 2014 Special Analysis Documents (the DOE documents SRR-CWDA-2013-00062, Rev. 2, and SRR-CWDA-2014-00006, Rev. 2, respectively). In the NRC 2012 TER, which considered the DOE 2009 SDF PA (the DOE document SRR-CWDA-2009-00017), the NRC staff evaluated the hydraulic properties assigned to: (i) the composite barrier layers on the roof and under the floors, and (ii) the HDPE geomembrane layer on the walls of the smaller cylindrical disposal structures. In that 2012 TER, the NRC concluded that the properties appeared to be reasonable. In that 2012 TER, the NRC evaluated the DOE consideration of potential sources of HDPE and GCL degradation and concluded that most major potential degradation modes were considered. In that 2012 TER, the NRC also determined that the application of the methods that the DOE used to estimate antioxidant depletion were reasonable. Using the method in the 2004 Environment Agency of England and Wales Research and Development Technical Report P1-500/1/TR (Needham et al., 2004), the DOE estimated the creation of defects (i.e., pinholes, holes, tears, and cracks) in the closure cap HDPE from the combination of antioxidant depletion, thermal oxidation, and tensile stress. With respect to estimation of the combination of the effects of antioxidant depletion, thermal oxidation and tensile stress cracking, in general, in that 2012 TER, the NRC determined that the DOE application of the method in Technical Report P1 500/1/TR was reasonable. The DOE also considered chemical attack from groundwater and saltstone leachate but found the degradation mechanism to be limited. Many chemicals were not expected to adversely affect HDPE (e.g., calcium sulfate, calcium nitrate, up to 50 percent phosphoric acid, and up to 20 percent nitric acid aqueous solutions below 60°C), although no literature information could be found on the effects of sodium nitrite, sodium nitrate, sodium sulfate, and sodium phosphate aqueous solutions on HDPE (Schweitzer, 2004). Although there was limited information about the effects of those chemicals on HDPE performance in the long term (i.e., thousands of years), in that 2012 TER, the NRC determined that the potential effects of those chemicals on the HDPE were accounted for, at least in part, by the DOE modeled rapid degradation of HDPE hydraulic conductivity and diffusivity.

The NRC ended the evaluation in the 2012 NRC TER by stating that "… the use of a material with which there is limited long-term engineering experience and no natural analogues, such as HDPE, introduces conceptual model uncertainty." The 2012 NRC TER included the example that if the HDPE geomembrane layer performs better than expected and forms few defects for thousands of years after placement, then the saltstone could oxidize substantially from gas-phase transport of oxygen while being exposed to very little water. If the HDPE geomembrane layer were to begin to fail several thousand years after placement, when the closure cover and disposal structure roofs may have degraded, then the oxidized saltstone could quickly be exposed to a sudden flow of water that could cause the release of a significant fraction of the Tc-99 inventory in a relatively short amount of time. Hypothetical sudden failures of the composite barrier layer on the roof and under the floor of the disposal structures were expected to be mitigated to some extent by the GCL, which the NRC indicated could be expected to fail more gradually. However, if both layers fail as the result of a disruptive event (e.g., an earthquake or formation of a sink), then water flow through the disposal structures could increase significantly in a relatively short time. Thus, the NRC deemed information regarding the potential for sudden failure of the composite barrier layers to be important to an evaluation of predicted site performance.

The 2017 NRC TRR discussed a concern related to observations of water in the leak detection system of SDS 3A, attributing the water to: (i) potential sources such as unusual welds and/or penetrations or (ii) failure of the HDPE material or an HDPE seam. In the 2017 TRR, the NRC staff concluded that the leaks undermine the technical bases for the expected barrier performance of the HDPE geomembrane layer and the composite barrier layer. That TRR also discussed changes in the conceptual model in the PORFLOW model from the 2009 SDF PA to the DOE SDF FY 2014 Special Analysis Document. PORFLOW is a numerical software package for creating two- or three-dimensional flow and transport models. In the 2017 TRR, the NRC staff concluded that the conceptual model from the DOE 2009 SDF PA represented HDPE/GCL performance that the DOE expected and the model from the FY 2014 Special Analysis Document represented a more conservative assumption with regard to the composite barrier performance. The NRC staff was concerned that the evaluation case in the FY 2014 Special Analysis Document may not be fully supported or appropriate for all relevant time periods and recommended that both conceptual models should be carried forward as sensitivity cases.

As described in the DOE 2009 SDF PA, the 0.6 m (2 ft.) thick LLDL placed above the geotextile fabric will extend approximately 7.6 m (25 ft.) from the disposal structure walls, draining infiltration water to the backfill material that will be placed adjacent to the disposal structures. The LLDL will be designed to divert infiltrating water away from the underlying disposal structures and transport the water beyond each disposal structure perimeter in conjunction with the underlying composite barrier layer and to prevent perched water on top of the disposal structures. The hydraulic properties of the backfill layer above the drainage layer are not expected to change; however, over time colloidal clay will migrate with the water flux from the lower backfill layer to the underlying LLDL. That water flux-driven clay was modeled as accumulating in the LLDL from the bottom up. The thickness of the clay-filled portion was modeled as increasing with time, while the thickness of the unfilled portion was modeled as decreasing with time. Those changes will result in an overall decrease in the hydraulic conductivity and porosity of the LLDL; so that, after approximately 19,000 years, the hydraulic conductivity and porosity of the LLDL was estimated to be similar to those for the overlying backfill layer.

In the 2012 NRC TER, the NRC questioned support for several assumptions in the DOE base case analysis. The NRC determined that the DOE base case in the 2009 SDF PA, which relied on references from the study of soils, did not have an adequate technical basis to support the projected rate of infill for the LLDL and that the model support for both the geotextile filter fabrics and the lateral drainage layers was not commensurate with their expected long-term performance and risk significance. Both the DOE SDF FY 2013 Special Analysis Document and the DOE SDF FY 2014 Special Analysis Document described the decreasing hydraulic conductivity of the sand unit within the LLDL as being controlled by the assumed annual precipitation rate and the associated sediment load. The DOE modeled the process of filling in with fine-grained sediment (e.g., migration of colloidal clay) with three different precipitation and infiltration rates.

In the 2017 NRC TRR, the NRC staff continued to question: (i) the technical basis for the process model for colloidal clay particle filtration within the LLDL and (ii) the consequences of infill on performance. The NRC staff suggested that alternative conceptual models for infill might be plausible, such as preferential flow through the soils allowing an uneven deposition of colloids to occur in the sand drain layer and recommended that the DOE further develop the technical basis for the current conceptual fill in or clogging model. The NRC staff also

recommended that the filling in process of the LLDL be reevaluated by the DOE if the range of infiltration rates is revised, because the influx of colloids is determined by the cumulative flux into the LLDL.

3.3 *Information from and relevant to the DOE 2020 SDF PA*

The DOE described four major assumptions in the 2020 SDF PA Closure Cap Model: (i) sufficient engineering controls on erosion will be in place such that overall impacts to closure cap performance will be minimal; (ii) roots will penetrate the upper sand drainage layer, reducing the saturated hydraulic conductivity and thereby raising the perched water level in the drainage layer and increasing the estimated infiltration rate to <0.1 mm/yr (0.0004 in./yr) ; (iii) the HDPE geomembrane will be impermeable to flow except through holes, will have a service life of at least 2,000 years, will not develop new holes, and will perform well for the 10,000-year Performance Period; and (iv) climatic conditions at SRS will remain approximately the same over the Performance Period.

Inflow rates through the composite barrier layer that were calculated with the 2020 SDF PA Closure Cap Model are dramatically smaller than infiltration rates calculated with the 2009 SDF PA Closure Cap Model (
Figure Error! No text of specified style in document.-4**Error! Reference source not found.**) with every 2020 SDF PA inflow rate orders of magnitude smaller than the 2009 SDF PA inflow rate. In
Figure Error! No text of specified style in document.-4, the two uppermost curves represent the 2009 inflow calculated: (i) with backfill in place of the ULDL structure and (ii) with the ULDL structure in place (including the composite barrier layer). The remaining curves are from the 2020 SDF PA, generated with two assumptions about climate (percolation rate of 400 and 650 mm/yr [16 – 26 in./yr]), ULDL saturated conductivity (0.01 and 0.05 cm/s [0.004 – 0.02 in/s]), HDPE defect diameter (2 and 10 mm [0.08 – 0.4 in)], and GCL saturated hydraulic conductivity (10^{-9} and 10^{-8} cm/s [$0.4x10^{-9}$ and $0.4x10^{-8}$ in/s]).

The cases that the DOE referred to as the “Reasonable Upper Bound” cases (Compliance Cases) use the smaller value for ULDL saturated hydraulic conductivity. In order to drain a given inflow to the ULDL when the hydraulic conductivity is decreased by a factor of five, the depth of flow within the ULDL must increase by a factor of five. The equation (Giroud, 1997) used to calculate flow through the underlying composite barrier layer is:

$$Q = C_{qo}[1 + 0.1(h/t_s)^{0.95}]a^{0.1}h^{0.9}k_s^{0.74} \quad (3\text{-}1)$$

where Q is the flow through the defect, h is the head above the defect, a is the defect area, t_s and k_s are the thickness and hydraulic conductivity of the underlying low-permeability layer, and C_{qo} is a dimensionless contact quality factor. The equation applies for defect diameters between 0.5 and 25 mm (0.2 – 9.8 in.) and head values less than 3 m (10 ft.) (Giroud, 1997). Giroud (1997) does not describe the pressure or flow condition applied at the bottom of the low-permeability layer. The equation sums terms proportional to $h^{0.9}$ and $h^{1.85}$, respectively. As a result, a larger head disproportionately increases flow through the underlying composite barrier layer. In the 2020 SDF PA, head is calculated using the formula:

$$h = \frac{qL}{K_d \sin\beta} \quad (3\text{-}2)$$

where q is the inflow rate to the ULDL, L is the upslope length, K_d is the ULDL hydraulic conductivity, and β is the slope angle. The formula assumes that the water level is less than the thickness of the ULDL. With this formula, decreasing the ULDL saturated hydraulic conductivity by a factor of five increases infiltration by a factor of 15 to 16.

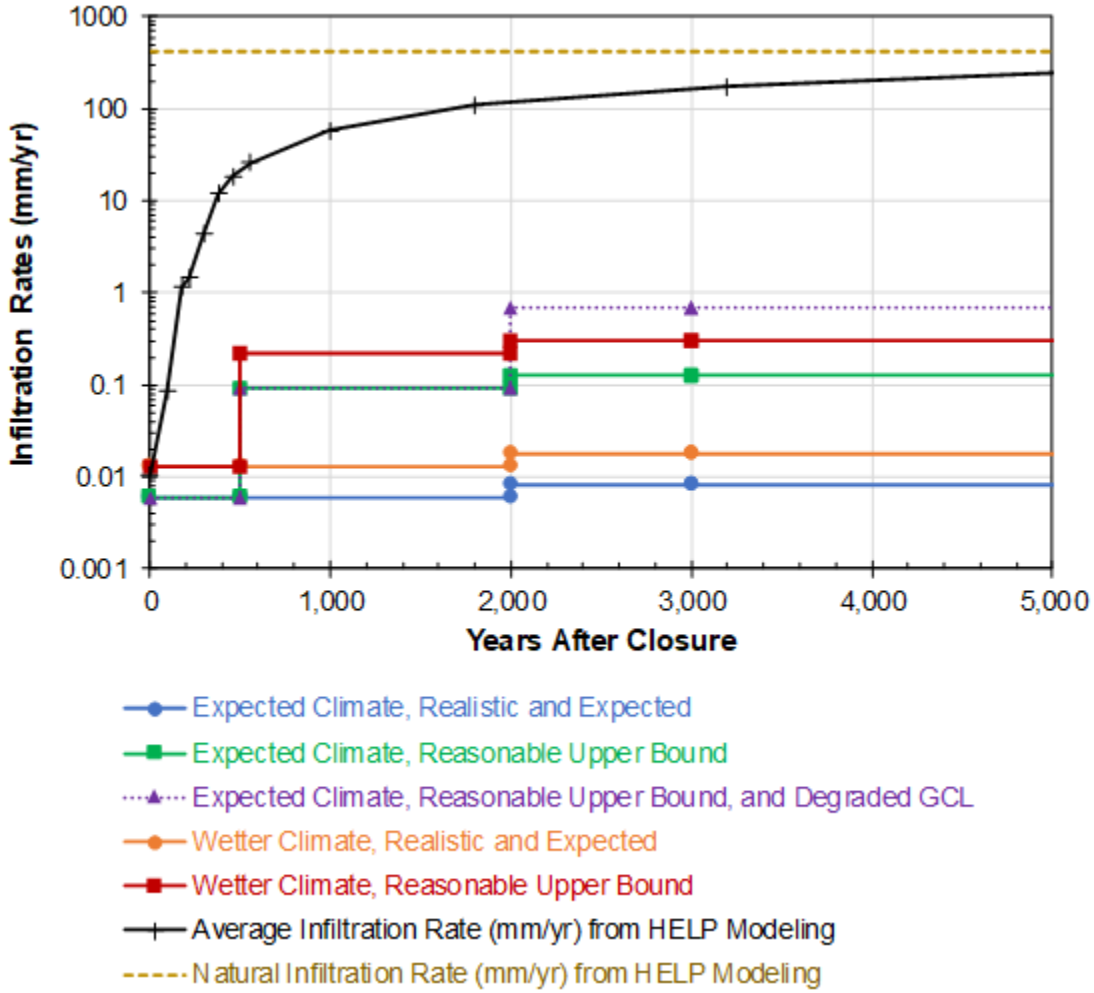

Figure Error! No text of specified style in document.**-4: DOE-Recommended Infiltration Rates from the 2009 and 2020 Closure Cap Models (the two HELP modeling results (black and dashed tan lines) are from the 2009 SDF PA Closure Cap Model the other five results are from the 2020 SDF PA Closure Cap Model) (Reproduced from Figure 4.4-11 in the DOE 2020 SDF PA)**

The primary difference between the 2009 and 2020 Closure Cap Models is in the treatment of post-closure defects. Both models assume that the HDPE geomembrane is impermeable except at holes or other defects. The 2009 model assumes that tree roots will penetrate the ULDL composite barrier layer once forest conditions are established, continually creating new holes that deteriorate the composite until it no longer offers a barrier. The 2020 model assumes that the HDPE geomembrane in the ULDL composite barrier layer loses strength over time, but the weakened geomembrane remains functionally intact because it never experiences stress levels

(including stresses from tree roots) that are large enough to create new defects; however, the initial defects are assumed to enlarge from 2 to 10 mm (0.08 – 0.4 in) over time.

The 2009 and 2020 Closure Cap Models differ in the parameter values for the GCL layer. The 2009 SDF PA assumes that the hydraulic conductivity value is initially 5×10^{-9} cm/s ($2x10^{-9}$ in/s), increasing to 5×10^{-8} cm/s ($2x10^{-8}$ in/s) after 500 years to account for divalent cation replacement. The 2020 SDF PA assumes the hydraulic conductivity value is 1×10^{-9} cm/s ($4x10^{-10}$ in/s) as a best estimate, with an upper bound of 1×10^{-8} cm/s ($4x10^{-9}$ in/s) as a pessimistic estimate. For comparison, Scalia and Benson (2011) provide data suggesting that new GCLs have a hydraulic conductivity of approximately 1×10^{-9} cm/s ($4x10^{-10}$ in/s). In most scenarios, the 2020 SDF PA holds the GCL hydraulic conductivity value constant through time.

3.3.1 Influence of Composite Barrier Layers and HDPE Geomembrane Layers on Performance

The DOE 2020 SDF PA uses several PA models in sequence, with the PA models including embedded numerical, analytical, and empirical models to represent the physics of flow and transport in the containment system. The NRC Model Integration TRR for the DOE 2020 PA described the interfaces between each model in more detail (ML23017A090). In essence, the 2020 SDF PA uses one PA model, the Closure Cap Model, to estimate the amount and timing of water that passes below the ULDL, and other PA models use these flows as input to represent flow through the engineered closure cap down to the LLDL just above the SDSs (see Figure **3-*3***) and to the underlying water table. The 2020 SDF PA Vadose Zone Model uses the PORFLOW numerical model to explicitly represent individual disposal structures, including the LLDL, composite barriers above the SDS roof and in mud mats, as well as other select features of the disposal structure (see Figure 4.4-41 in SRR-CWDA-2019-00001, Rev. 0). Flow output from the Closure Cap model is applied to the top of two-dimensional (2-D) PORFLOW models. Degradation of cementitious materials in the disposal structures are modeled as changes to hydraulic and chemical properties over time, using input provided by other models and calculations as described in more detail below. The 2020 SDF PA Vadose Zone Transport Model uses PORFLOW to simulate radionuclide release and transport through the vadose zone to the water table, using the PORFLOW-calculated flow fields. The SDF flow velocity field in the local SDF SZ transport model, the Aquifer Transport Model, was generated directly from the regional GSA PORFLOW model as described in the TRR on Hydrogeology, Groundwater Monitoring, and Far-Field Modeling for the SDF (ML23017A084). Radionuclide fluxes at the bottom of the vadose zone (i.e., at the top of the water table) are used as input in the Aquifer Transport Model, which is used to simulate transport of radionuclides released from the disposal structures to a downgradient compliance point where a potential receptor could be exposed through groundwater dependent pathways.

A key component with regards to the Closure Cap Model calculations involving the ULDL are the performance of the composite barrier layer and its degradation. Downstream models (i.e., those below the Closure Cap Model) incorporate HDPE geomembrane layers and composite barrier layers in a simpler way (i.e., as equivalent porous media), which is closely equivalent to a conceptual model of a great many small defects in the HDPE geomembrane. The intact barrier concept used for the ULDL composite barrier layer in the Closure Cap Model assumes total flow through a defect is constrained by: (i) the head gradient across the GCL and (ii) the ease for flow to spread between the HDPE geomembrane and the GCL. The head driving flow is due to water ponded above the geomembrane; that ponded water can cause a steep head gradient across the thin GCL in an approximately circular zone. The depth of flow at the defect reflects the value that balances supply from the environment to flow through the

defect. The underlying foundation layer and backfill are assumed to be permeable enough that they can accept any flow from the GCL with only gravity driving flow, thus are not allowed to consume any of the head created by the ponded water. In this case, the underlying medium is partially saturated, balanced at the saturation value needed to match the hydraulic conductivity to the available supply of water under gravity drainage.

The 2020 SDF PA Closure Cap Model assumed that: (i) the HDPE geomembrane is impermeable unless a physical hole (defect) is present, (ii) almost all initial defects will be identified by testing and remediated, (iii) no new defects or holes will develop, and (iv) at 2,000 years the assumed initial defects are modeled as increasing in size. The Closure Cap Model calculated a service life for the HDPE geomembrane of 1975 years (rounded to 2000 years), based on estimates for: (i) rates of first antioxidant depletion and then material decomposition, and (ii) the consequences of material decomposition on break strength, break strain, and stress crack resistance. The 2020 SDF PA assumed that, even after the HDPE geomembrane service life is over, cap design and installation protocols will preclude the possibility that sufficiently large stresses, from any combination of sources, will be imposed on the geomembrane to overcome the remnant HDPE strength and form new breaches after the geomembrane is installed. Although no new breaches are formed, the 2020 SDF PA assumed that the initial defects increase in size after 2000 years. The Closure Cap Model assumed five 2-mm (0.08 in) diameter defects per hectare are initially present in the HDPE geomembrane and represents each of the initial defects degrading and growing to a 10-mm (0.4-in) diameter 2,000 years after composite barrier installation. This spacing corresponds to one defect per 2,000 m^2 (21,500 $ft.^2$) or approximately: (i) one defect each for SDS 2A, SDS 2B, SDS 3A, SDS 3B, and SDS 5A, SDS 5B (0.16 ha [0.40 acres]), (ii) five defects each for SDS 6 through SDS 12 (1 ha [2 acres]), (iii) three defects for SDS 1 (0.56 ha [1.4 acres]), and (iv) 5.5 defects for SDS 4 (1.1 ha [2.7 acres]). According to the authors of the 2018 DOE document SRRA107772-000009 (Benson, C.H., and Benavides, J.M.), the Closure Cap Model calculates flow through each defect using numerical modeling and an analytic solution, with rates that are dependent on the condition of the overlying sand in the ULDL and hydraulic conductivity of the GCL. The total flow through the defects is assumed to be evenly distributed across the top of the Vadose Zone Flow Model. With these assumptions, the initial infiltration rate is 0.006 mm/yr (0.0002 in./yr), almost five orders of magnitude smaller than the soil-only case, increasing to 0.13 mm/yr (0.0051 in./yr) after 2,000 years.

The PA models below the Closure Cap Model implement and simulate the composite barrier layers and the vertical HDPE geomembranes (generically called liners) differently than within the Closure Cap. These upstream liner degradation models, using equivalent porous medium (EPM), have a very different representation of liners compared to the upstream liners which are essentially intact barriers except for a few scattered defects. The EPM approach allows water and dissolved constituents to exchange across the entire outer surface of the disposal structure. Insofar as cementitious degradation (oxidation, decalcification) depends on exchange with the exterior environment, this one-dimensional (1-D) exchange means that connected flow pathways in degraded material develop along the exterior surface relatively quickly in the roof, walls, floor, and outer rind of the saltstone.

The Cementitious Degradation Model calculates degradation of disposal structure cementitious materials (e.g., saltstone and disposal structure roof, walls, floor, mud mats and grout). The Vadose Zone Flow Model uses the infiltration rates to calculate the distribution of liquid flow passing from the ULDL through and around each disposal structure to the water table. The Vadose Zone Transport Model combines the release rates with the vadose zone flows to calculate contaminant fluxes to the water table, and the Aquifer Transport Model uses these

fluxes to calculate contaminant concentrations at the receptor locations. The composite barrier layer in the ULDL is modeled in the Closure Cap Model, and the other HDPE geomembrane layers and composite barrier layers, including the LLDL, are considered explicitly or implicitly in the other models. The Vadose Zone Transport Model and Cementitious Degradation Model appear to use the same assumptions for liner properties and liner degradation.

The 2020 SDF PA included sensitivity analyses separately examining the effect of: (i) preferential discrete pathways that partially or fully pass through the saltstone and (ii) high infiltration rates through the ULDL. The 2020 SDF PA sensitivity cases for potential fast pathways used discrete gravel-filled pathways through the saltstone as a surrogate generic representation of fast pathways (represented with higher hydraulic conductivities and diffusivities), and the Compliance Case infiltration rates through the ULDL. The Compliance Case infiltration rate (i) peaks at 0.13 mm/yr (0.0051 in./yr) after 2000 yr when all ULDL and composite-layer degradation is assumed completed, (ii) is based on years with average inflow to the ULDL, and (iii) does not consider wet years, changing climate, or uncertainty in ULDL properties that might increase infiltration. The 2020 SDF PA concluded that transport within the disposal structure would be diffusion dominated during the performance period even with the fast pathways.

The 2020 SDF PA sensitivity cases with much larger infiltration rates than calculated by the Closure Cap model consider: (i) infiltration rates based on the 2009 SDF PA and (ii) infiltration rates based on drainage into the ULDL in the 2020 SDF PA. In the sensitivity cases based on the 2009 SDF PA, infiltration is initially small but increases over time, peaking at 269 mm/yr (10.6 in./yr). In the sensitivity cases based on the 2020 SDF PA, a soil-only closure cap is assumed (i.e., the Closure Cap Model has no ULDL barriers) under current climatic conditions after evapotranspiration and runoff is removed from precipitation, giving a steady infiltration rate of 418 mm/yr (16.5 in./yr) to the Vadose Zone Model. The LLDL and underlying composite barrier layer are present in both sensitivity sets; in the soil-only closure cap, the LLDL would presumably replace the barrier functionality of the ULDL because of the similarity in design. The two sets consider several assumptions about material degradation, but the high-infiltration sensitivity cases do not consider fast pathways through the SDS which contribute significantly to saltstone degradation. Output from cases with infiltration rates based on the 2009 SDF PA or a hypothetical soil-only closure cap showed earlier releases with higher peak doses relative to the Compliance Case.

Composite barriers and HDPE geomembranes influence degradation rates of cementitious materials in the 2020 SDF PA. The Cementitious Degradation Model considers changes in physical properties of cementitious materials (the effective hydraulic conductivity and effective diffusion coefficient), which both increase as the medium and embedded steel components degrade. Degradation of saltstone also allows radionuclides to transfer into the aqueous pore solution more readily. The Cementitious Degradation Model considers physical degradation of saltstone as occurring through decalcification. The barrier of a liner (a composite barrier layer or a HDPE geomembrane layer) reduces carbonization by reducing carbon dioxide ingress via: (i) diffusion from the surrounding environment and (ii) advective transport through the roof and reduces decalcification by limiting egress of dissolved components. The Cementitious Degradation Model represents the initial hydraulic properties of the liners using the same HDPE geomembrane defect frequency as in the Closure Cap Model but assumes that the defects are initially fully degraded (10-mm [0.4 in] defects) to calculate initial properties. The initial saturated hydraulic conductivity is based on representing the liner as an EPM based on assumed defects, and liner retention properties are based on concrete. The liner properties are assumed to

degrade to backfill between years 750 and 3,200, based on a decline in the stress crack resistance due to depleting (see page 391 in Section 4.4.2.7 of the DOE 2020 SDF PA).

The 2020 SDF PA Contaminant Release Model considers changes in the pore solution composition, which is influenced by ingress of oxygen into the disposal structures and removal of buffering components. The aqueous pore solution composition, in particular the oxidation state and pH, influence the retention of several important radionuclides (e.g., technetium, iodine), which affects the dissolved radionuclide concentration available for transport. The barrier of a liner reduces ingress of oxygen by: (i) reducing diffusion from the surrounding environment and (ii) reducing advective transport through the roof. The Contaminant Release Model considers pore solution evolution of disposal structure components and saltstone (as well as saltstone physical degradation) using a reaction path model based on waters advected through the roof. The reaction path model does not consider diffusive transport across the disposal structure exterior, thus the oxidation state at the base of the saltstone does not depend on diffusion across the floor even after the floor and composite barrier layer are fully degraded.

3.3.2 Characterization of Initial Defects

The 2020 SDF PA assumes that a high level of quality control will be applied during installation of all composite barrier layers, based on specifications for ongoing installations of composite barrier layers emplaced in mud mats (C-SPP-Z-00019). Although not called out in the 2020 SDF PA, the 2018 DOE document WSRC-STI-2008-00244 also provide detailed installation specifications for the 2009 SDF PA that appear consistent with the 2020 SDF PA descriptions of installation practices. The 2020 SDF PA Closure Cap Model uses five circular holes per hectare as the initial number of defects in the ULDL composite liner, based on the recommendation of Giroud and Bonaparte (1989) for seam defects remaining after quality assurance; other PA models represent HDPE geomembrane layers and composite barrier layers as an EPM with an equivalent areal-average saturated hydraulic conductivity. The 2020 SDF PA specifies that HDPE geomembrane installation, detection of defects, and repairs of defects shall all be performed according to standards established by the American Society for Testing and Materials (ASTM). Depending on the seam welding method used (allowed methods are single or double hot-wedge fusion seam welding or extrusion welding), each seam will be tested for defects and repaired using a vacuum testing device, spark testing device, or air channel pressure test for double wedge welded seams, or shear and peel testing.

The NRC Request for Supplemental Information for the DOE 2020 SDF PA (ML20254A003) included a request to consider the full range of uncertainty when simulating SDF performance in a probabilistic manner, including the full range of uncertainty associated with HDPE and GCL degradation. The DOE provided a range of uncertainties including the initial HDPE defect size as documented in the DOE document SRR-CWDA-2021-00033, Rev. 1 (ML21160A062). In that document, the DOE used information from Colucci and Lavagnolo (1995) on a landfill in China that had used HDPE layers. Reported geomembrane hole sizes from the 1995 study were given in Table 4.2-1 of SRR-CWDA-2021-00033, Rev. 1. Based on the assumed good quality assurance practices during HDPE installation, the DOE assumed that all repairs are made to the larger, more easily detected defects, leaving only 1 out of every 30 defects in the dataset. The recommended final defect diameter distribution (Figure A-5, SRR-CWDA-2021-00033, Rev. 1) resulted in an approximate median value of 1.1 mm (0.43 in). The maximum parameter value was set to 11.3 mm (0.445 in) based on the Colucci and Lavagnolo (1995) observation that, prior to repairs, roughly half of all observed defects were 11.3 mm (0.43 in) in diameter or less, thereby assuming that larger half of all defects will be identified and repaired. Initially a uniform distribution was assumed; however, the modeled cumulative distribution function for the

full range of defects (i.e., from 0 to 1,130 mm [0 to 44.5 in]) did not produce a smooth curve so that a log-uniform distribution was chosen instead. The log-uniform distribution was also applied after all defects greater than 5.05 mm (0.199 in) were removed from the dataset.

The Giroud and Bonaparte (1989) analysis focused on estimating leakage through liners to design leakage collection facilities. For analysis and design purposes, Giroud and Bonaparte (1989) recommended working assumptions of: (i) 1 seam defect per 300 m (984 ft.) of seam (3 to 5 seam defects per hectare) and (ii) a range of hole sizes from least 2 mm (0.08 in.) (representing seam defects), to at least 10 mm (0.4 in.) (representing accidental punctures that cannot be observed by quality assurance personnel). Giroud and Bonaparte (1989) do not quantify accidental puncture frequencies. Giroud and Bonaparte (1989) recommend a hole size of 3.1 mm^2 (0.0048 $in.^2$) (2 mm [0.08 in.] diameter) for evaluating performance of the lining system (e.g., flow in a leakage collection layer under typical operating conditions) and a hole size of 1 cm^2 (0.2 $in.^2$) (11 mm diameter [0.43 in.]) to provide design flows for components of a lining system (e.g., pipes and pumps).

Nosko and Touze-Foltz (2000) described 4,194 defects at more than 300 sites with geomembrane liners, with the defects found using electrical leak detection sensors installed below the geomembrane. Based on the technology, the NRC staff inferred that the liners generally had less than ten years in service. The total liner area was 325 hectares (803 acres), implying 12.9 defects/hectare (5.22 defects/acre) on average. For comparison, the total roof area of the set of 15 disposal structures is 9.8 hectares (24 acres). Nosko and Touze-Foltz (2000) placed the liner area into five defect categories, but do not quantify the fraction of area covered by each category. The category of flat areas is analogous to the ULDL and LLDL in the 2020 SDF PA, probably represents the vast majority of the total liner area and contained 78 percent of all identified liner defects. In flat areas, defect causes included stones (81 percent), heavy equipment (13.2 percent), worker (4 percent), cuts (1 percent), and welds (0.8 percent). Nosko and Touze-Foltz (2000) do not quantify the weld failure mode (e.g., initial defect, stress crack failure), but found that welds were a much more prevalent fraction of defects for the four categories that were not flat areas: (i) corners and edges (17.5 percent), (ii) under drainage pipes (27.2 percent), (iii) at pipe penetrations (90.9 percent, and (iv) others (e.g., road access, temporary storage) (16.7 percent). It may be that uncomplicated layouts in flat areas were more suited to single or dual track welded seams and areas with more challenging conditions are more likely to feature extrusion welding.

Peggs and Giroud (2014) described: (i) typical geomembrane hole sizes at the end of installation as between one and a few square millimeters; (ii) holes due to stress cracking around 10 mm^2 (0.02 in^2) expanding to 100 mm^2 (0.2 in^2) or larger if the geomembrane remains in tension; (iii) holes due to puncture by stones as >10 mm^2 (0.02 in^2); and (iv) holes due to tears from construction equipment as 100 to 1,000 cm^2 (15 to 155 in^2).

Gilson-Beck (2019) and Beck (2015) compared leakage data from 122 discrete landfill cells with double linings in upstate New York, in which leachate through a top geocomposite layer is collected above a second liner (the primary leachate collection system) and leakage rates are measured. Current specifications can be found in the 2021 CNWRA report (ML21287A328). Some sites may have used a GCL instead of clay liners. The top geocomposite layer is analogous to an undegraded composite barrier layer in the 2020 SDF PA.
Figure Error! No text of specified style in document.-5 contrasts the exceedance fraction for cells that underwent an electrical leak location (ELL) survey with cells that did not get surveyed, suggesting that repairs subsequent to the survey tend to mitigate large leaks. Beck (2015) suggested that leakage is underestimated through cells lacking an ELL survey, because those

cells are from older cells with very thick waste (which reduces flow) and some cells may have been capped. Gilson-Beck (2019) reported earlier data by Bonaparte and Gross (1993) from 14 sites, suggesting that more recent technology may have reduced leakage rates. Data from 2010 suggests that 27 percent exceeded 1.8 mm/yr (0.071 in./yr) and 3 percent was between 7.3 and 18.3 mm/yr (0.29 and 0.721 in./yr). Data from these studies illustrate that HDPE geomembrane quality and installation practices have improved over time. These measured leakage rates, representative of initial infiltration rates, have a median infiltration rate of ~2 mm/yr (0.08 in./yr), two orders of magnitude larger than any initial infiltration rate in the 2020 SDF PA's Closure Cap Model (
Figure Error! No text of specified style in document.-) and several times larger than the upper bound infiltration with both the HDPE geomembrane layer and the GCL fully degraded.

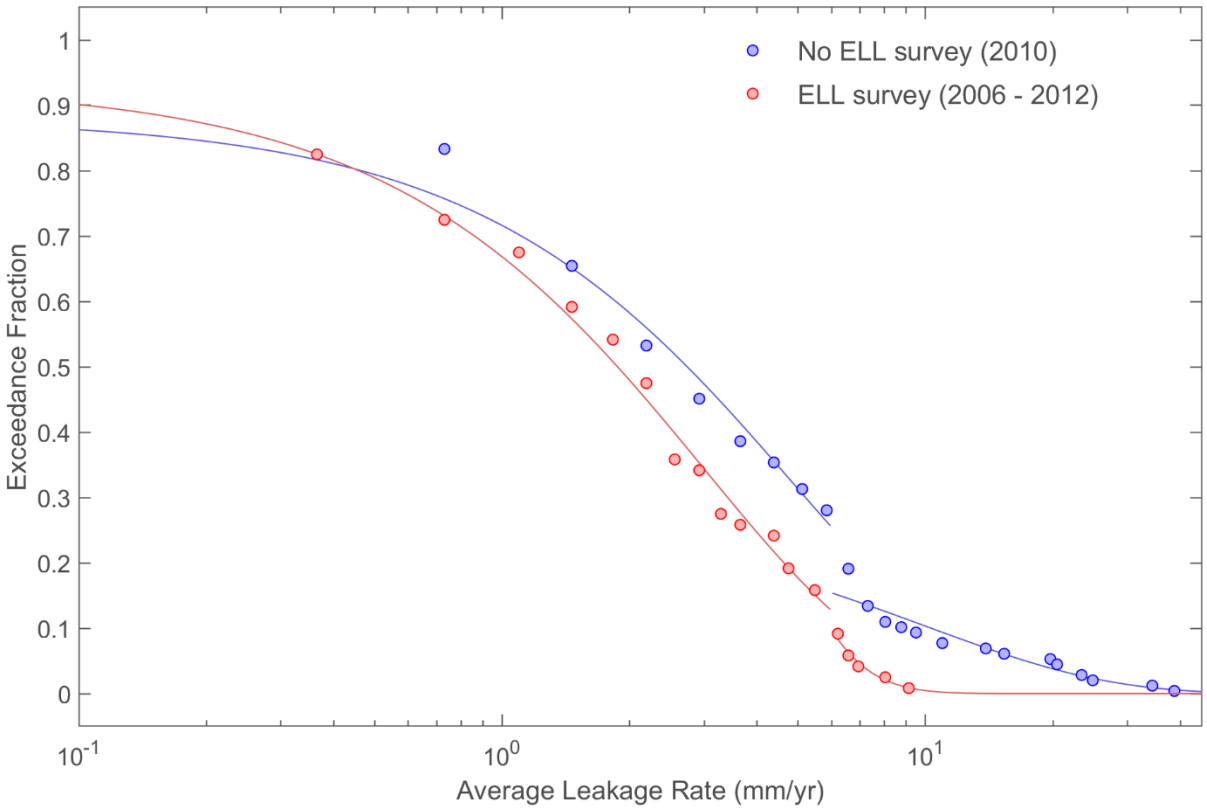

Figure Error! No text of specified style in document.**-5: Leakage Observations from Double-Lined Landfills in Upstate New York (Beck, 2015) Partitioned into Cells with and without ELL Surveys (data are fitted with exponential exceedance fractions, broken at 6 mm/yr (0.2 in./yr))**

3.3.3 HDPE Geomembrane Seam Factors

In North America, HDPE geomembrane seams are typically sealed using single or double hot-wedge fusion seam welding or by extrusion welding, and the DOE 2020 SDF PA specifies that one of these methods will be used. Hot-air fusion is a method similar to hot-wedge fusion, using hot air to melt the geomembrane, but the hot-air heating process is less controlled. The DOE specification document C-SPP-Z-00019 (describing GCL and HDPE geomembrane installation in the mud mats for SDS 8 and SDS 9) stated that hot-air welding is not acceptable.

Hot-wedge fusion is only used for initial installation and consists of running a semi-automatic device along the overlap between two geomembrane sheets, with a wedge heated by electrical resistance partially melting the geomembrane and rollers pinching the heated area together to form a permanent bond. The wedge may form a single welded track or dual tracks separated by an enclosed air gap. Extrusion welding can be used for initial installation or repairs and consists of extruding a ribbon of molten polymer over the edge of the overlying sheet, joining the two sheets. Both methods require that the seams overlap, typically approximately 15 cm (5.9 in).

Seam integrity may be compromised by improper installation, in which defects or gaps form due to water or soil in the seam, incomplete or excessive heating, improper pressure, or stresses applied prior to curing (e.g., physically adjusting the seaming device, walking on an incompletely cured seam). Seam testing shortly after installation can reveal these types of seam defects.

Both hot-wedge fusion and extrusion welding generate a seam that is thicker than the geomembrane, and therefore the thicker zone may be more robust than the original geomembrane. Adjacent to the seam, the partially melted material adjacent to the seam, called the heat-affected zone, tends to be weaker than the original geomembrane, may be thinned with improper installation, and depletes in antioxidants more rapidly than either the seam or the surrounding geomembrane (Rowe and Shoaib, 2017). The heat affected zone has been found to be more susceptible to shear failure (Zhizhou et al., 2019) and stress cracking. In addition, strains in the heat affected zone adjacent to seams are magnified by a factor of 2.3 to 4 (Kavazanjian et al., 2017). Stress crack failures on the weakened zones may occur months after installation, implying that seam testing shortly after installation may not reveal such delayed defects.

Single-track hot-wedge fusion generates two heat-affected zones on each side of the weld, one for each overlapping geomembrane; however, failure of the heat-affected zones on the overlapping flaps (two of the four zones per weld) would have no impact on overall geomembrane integrity. Dual-track hot-wedge fusion generates four weakened zones for each overlapping sheet; the outer weakened zones are like the single-track weakened zones, while the weakened zones between the two welds maintain containment unless an upper zone and a lower zone both fail. Extrusion welding creates a single weakened zone on each side of the weld. With extrusion welding, both weakened zones are visible, but hot-wedge fusion welding results in geomembrane covering at least one of the weakened zones.

3.3.4 Composite Barrier Layer Installation Factors

The DOE 2020 SDF PA assumed that the HDPE geomembrane and GCL have good contact conditions when calculating the flow through defects, based on: (i) installation or construction activities creating a smooth surface for the GCL emplacement, (ii) GCL placement will be performed using quality control standards to minimize wrinkles and irregularities, and (iii) constant pressure conditions placed on the HDPE geomembrane from overlying materials.

Good contact between the HDPE geomembrane and GCL is very important for limiting leakage from a defect, because total leakage is roughly proportional to the total surface area of the GCL that water can easily spread to under the geomembrane. Contact conditions between the geomembrane and GCL can deteriorate (i.e., gaps form) when the geomembrane: (i) contains wrinkles or (ii) bridges depressions and breaks in slope (the bridged condition is called trampolining). Both conditions increase tensile stresses on the geomembrane, promoting formation of new defects from stress cracking. In addition, thermal expansion and contraction of geomembranes over the course of one or more days may promote wrinkles and trampolines

that persist after the geomembrane is covered. Quality control measures can minimize these effects by: (i) assuring smooth planar surfaces for emplacement; (ii) carefully matching geomembrane temperatures to the expected long-term ambient temperature during the period that includes geomembrane placement, seaming, and covering; and (iii) prompt covering after seaming. In the RAI response CBs&DLs-3 of the DOE Comment Response Matrix for the Third Set of U.S. Nuclear Regulatory Commission Staff Requests for Additional Information on the PA for the SDF at the SRS from March 2022 (the DOE document SRMC-CWDA-2022-00003, and referred to in this TRR as the DOE 3rd Set of Responses), the DOE stated that the current practice is to install the upper mud mat at night, which reduces the risk of wrinkling and to use an HDPE coated with a white surface that better reflects solar radiation and reduces heating of the material.

In response to the NRC Request for Supplemental Information for the DOE 2020 PA (ML20254A003), the DOE considered the HDPE-to-GCL contact factor. In that document, the DOE described the HDPE-to-GCL contact factor as a unitless measure of the quality of the contact between the two components. The DOE assumed that there will be good contact between the HDPE and the GCL partly because flat installation is assumed which allows sufficient compressive stress to be applied and because the conceptual design of the closure cap is expected to allow such good contact to be created.

Repair patches may also be associated with poor contact between the HDPE geomembrane and the underlying GCL or substrate. For example, Gilson-Beck (2019) quantified leakage rates of ~230 liters/hectare/day (>8 mm/yr) through a 1.5 mm (0.059 in) HDPE geomembrane over a GCL due to six pinholes in extrusion welds and a 4-mm (0.16 in) puncture, with the pinholes appearing to be aligned with extrusion-welded repair patches along a seam. Gilson-Beck (2019) calculated leakage rates using a Rowe (1998) equation for a circular hole on a wrinkle and the Giroud (1997) leakage equation. These calculated leakage rates approximately matched observed leakage assuming a wrinkle width of 31 cm (12 in) and connected network length of 190 m (620 ft.). Leakage calculated with the Giroud (1997) leakage equation (the equation used in the 2020 SDF PA Closure Cap Model) was 1.5 to 1.7 percent as large assuming good contact and 8.2 percent to 9.3 percent as large assuming poor contact.

3.3.5 Initial GCL Properties and GCL Installation Factors

In response to the NRC Request for Supplemental Information for the DOE 2020 PA (ML20254A003), the DOE considered the initial saturated GCL hydraulic conductivities and GCL thicknesses in the DOE document SRR-CWDA-2021-00033, Rev. 1 (ML21160A062). In that document, the DOE used information from Rowe (2012) that recommended initial GCL hydraulic conductivity values for modeling with a minimum of $7.0x10^{-10}$ cm/s ($2.8x10^{-10}$ in./s), a maximum of $2.0x10^{-06}$ cm/s ($7.9x10^{-11}$ in./s), and $5.0x10^{-09}$ cm/s ($2.0x10^{-10}$ in./s) as a "most likely" value. Because the most likely or "reasonable value" from Rowe (2012) was more than five times higher than the highest GCL hydraulic conductivity value measured from the analog site at Barnwell, SC (Scalia et al. (2017)), the DOE scaled down the generic recommendations for the minimum and reasonable values from Rowe (2012) by a factor of 5. The DOE chose log-triangular distribution over the triangular distribution because the DOE is expected that variability in the initial GCL hydraulic conductivity values will vary logarithmically. Although the actual GCL thickness will be determined closer to the scheduled time of closure cap construction, the DOE document SRR-CWDA-2021-00033, Rev. 1 also discussed and provided recommended GCL thicknesses for the probabilistic modeling. Based on the document's literature review, a common range of thicknesses was found to be between 5 mm to 12 mm (0.2 to 0.5 in.), with the 2020 SDF PA assuming an 8 mm (0.3 in).

Currently there is no national standard for GCL seaming protocols. Unified Facilities Guide Specification UFGS 02 56 15 (U.S. Department of Defense, 2010) specified required minimum edge overlaps and requires that panels be oriented in the direction of slope, but otherwise defers to manufacturer's recommendations for overlap extent and seam sealing protocols. Recommendations from several representative manufacturers (ABG, AGRU America Inc., GSE Environmental Inc. (now, Solmax), CETCO®, and Jen-Hill) typically specify granular bentonite as the GCL sealing compound where site-specific conditions warrant sealing. Some manufacturers offer self-sealing products, in which the end of the sheet is manufactured to allow a controlled amount of bentonite to extrude where two sheets overlap along the seam. Some products combine the GCL with a factory-adhered HDPE geomembrane, allowing emplacement of the composite barrier layer with a single product, which aligns the HDPE geomembrane and GCL seams with little or no offset. Typically, two to four times as much overlap is recommended at sheet ends than for longitudinal seams.

GCL sheet alignment is typically intended to ensure little or no lateral shear forces at the overlap zone, but Rowe et al. (2010) report five instances where originally overlapped GCL panels separated between 0.2 and 1.2 m (0.7 and 3.9 ft.). Rowe et al. (2010) attribute the separations to panel shrinkage as a result of cyclic wetting and drying of uncovered panels, all exposed for multiple months (2 to 36 months).

A GCL seam with a bentonite-based seal typically requires that a certain amount of pressure be applied to the seal to limit leakage. Increasing cover thickness acts to increase pressure on a GCL seam. A wrinkle in an overlying HDPE geomembrane forms an arch that can shield an underlying strip of GCL from considerable overburden pressure; the geomembrane thickness determines how much pressure the arch can withstand (Joshi et al., 2016). HDPE geomembrane wrinkles are of concern because wrinkles concentrate stresses, enhancing stress cracking in the geomembrane; such cracks would be aligned with the axis of the wrinkle, so that defects will tend to be elongated and allow flow into the underlying gap. The partially melted zone adjacent to a HDPE geomembrane seam is more susceptible to stress cracking than the seam or bulk geomembrane, thus a wrinkle along or crossing a HDPE geomembrane seam would create conditions especially prone to stress crack defects. The gap under the

wrinkle is of concern because it provides an elongated flow path that greatly enlarges the surface area of the GCL where seepage through the GCL can occur. If a wrinkle crosses a GCL seam, the potential for significant leakage exists due to the combination of reduced pressure on the GCL seam and free flow along the wrinkle.

Thiel and Thiel (2009) proposed heat tacking the GCL seams to provide resistance to shear stresses, performed a field test using GCLs prone to shrinkage at the Carlota Mine in Arizona, and reported no evidence of shrinkage on heat-tacked seams. The heat tacking was performed using a flame torch followed by pressing together with light pressure from a sand-filled bag. Rowe et al. (2010) tested heat tacking methods in the laboratory, finding that the heat-tacked seams appeared to be as strong as the GCL adjacent to the seam after forty wet-dry cycles. No literature testing the shear resistance of a bentonite seal was identified, but the NRC staff expects that heat tacking would offer much greater shear resistance than a bentonite seal because heat tacking causes a physical bond to form between the geotextile layers and a bentonite seal does not cause a physical bond to form.

3.3.6 Detection of Composite Barrier Layer Defects After Installation

The DOE 2020 SDF PA stated that the HDPE geomembrane installation, detection of defects, and repairs of defects shall all be performed according to standards established by the ASTM, and each seam will be tested for defects and repaired. Hot-wedge fusion and extrusion welding both bond two HDPE geomembranes by partial melting, and both generate a seam in that is thicker than the geomembrane; however, the heat-affected zone, partially melted material adjacent to the seam, tends to be weaker than the original geomembrane, may be thinned with improper installation, and depletes in antioxidants more rapidly than either the seam or the surrounding geomembrane (Rowe and Shoaib, 2017). As described in Section 3.3.3, the heat affected zone has been found to be more susceptible to stress cracking and strains are magnified by a factor of 2.3 to 4 (Kavazanjian et al., 2017). The air channel pressure test commonly performed for dual hot-wedge fusion seams does not test for continuity in the heat-affected zones outside dual tracks, leaving a potential undetected gap. Where geomembranes overlap, a heat-affected zone in the lower geomembrane is poorly visible, potentially allowing a significant defect to go undetected.

Test methods

ASTM D7700 (Standard Guide for Selecting Test Methods for Geomembrane Seams) indicated that one destructive seam evaluation technique, six non-destructive techniques, and two general ELL approaches apply to HDPE geomembranes. Most methods test seam continuity, the shear and peel apparatus tests seam strength. Details of how each testing method (e.g., vacuum box, water puddle, water or air lance, or arc testing method) works are discussed and documented in the CNWRA Report (ML21287A328).

Test methods that are applicable after the geomembrane is covered may be especially useful for detecting construction damage and early-onset stress crack partings near welds, although such techniques have limits on the maximum cover thickness and moisture conditions during testing. Gilson-Beck (2019) suggests that: (i) bare geomembrane tests are strongly biased to detecting small (<1 cm [< 0.3 in]) holes, (ii) dipole tests are strongly biased to detecting large (>1 cm [>0.3 in]) holes, and (iii) holes on wrinkles are extremely difficult to detect unless the geomembrane has a conductive backing, or the hole is wet (because an air gap will not support a measurable current).

Leak detection surveys

Geoelectric leak detection surveys are used to detect geomembrane defects that allow measurable current to "leak" through the geomembrane. Forget et al. (2005) collected data from 57 geoelectric leak detection surveys performed on exposed (i.e., prior to covering) HDPE, PVC, and bituminous geomembranes totaling 229 hectares (566 acres), finding that of the 43 sites with a rigorous installation or construction quality assurance (CQA) program: (i) 80 percent had leak densities between 0 and 7 leaks/hectare (0 and 3 leaks/acre) and (ii) most of the remaining sites were small (<0.53 hectare). The remaining 14 sites without a rigorous CQA program averaged 22 leaks/hectare (8.9 leaks/acre). In sites with exposed HDPE geomembranes and a CQA program, leak density decreased with HDPE thickness. Nearly half of the 2.0-mm (0.08-in) sites with CQA and prior testing with the water puddle approach were retested with a dipole method after covering the geomembrane, which identified an additional 0.2 leaks/hectare (0.08 leaks/acre) (without CQA and prior water puddle survey, the dipole approach detected 15.6 leaks/hectare [38.5 leaks/acre]). The water puddle leak detection method detects >1 mm^2 (> 0.003 in^2) leaks and the dipole method generally detects >6 mm^2 (>0.009 in^2) holes.

Gilson-Beck (2019) discussed available ELL techniques for identifying defects in geomembranes, including general approaches and limitations. Gilson-Beck (2019) recommended performing an exposed geomembrane survey and a dipole survey for each site. Gilson-Beck (2019) provided a table of defects found at 50 sites in North America surveyed with one or more ELL techniques during or shortly after installation, all with at least 1.5 mm (0.059 in) thick HDPE geomembranes installed with CQA in place and the foreknowledge that leak detection procedures would be used. No leaks were found at 23 of the sites; at the remaining sites, the average area surrounding a defect ranged from 0.24 to 57 hectares/defect (0.02 to 4 leaks/hectare). Gilson-Beck (2019) reported that the selection of an ELL technique limits the size of defect that can be detected, with some techniques better at finding small defects and others at finding large defects, thus some unknown numbers of holes were likely missed during the surveys.

Figure 3-6 presents the number of detected leaks per hectare for the 50 Gilson-Beck (2019) sites, presented as the cumulative distribution for each method. This metric provides a way of assessing how potent the methods are at identifying defects. Assuming that the sites examined with each method have a reasonably similar distribution of actual leaks (which may be inaccurate with so few sites), the most effective method will have a larger identified leak density for each level of the cumulative distribution. There are too few single-method sites to draw strong conclusions about the relative ranks of the single-method techniques, but Figure 3-6 suggests that combining methods may be much better at identifying defects than relying on a single ELL technique. The "Multiple" categories include various combinations of arc testing, soil dipole, water puddle, water dipole, and water lance techniques (one site used three methods, the others used two). Note that the water dipole method was used three times under the Multiple categories, including the two sites with the largest number of identified leaks, suggesting that the water dipole method may be especially effective at detecting leaks.

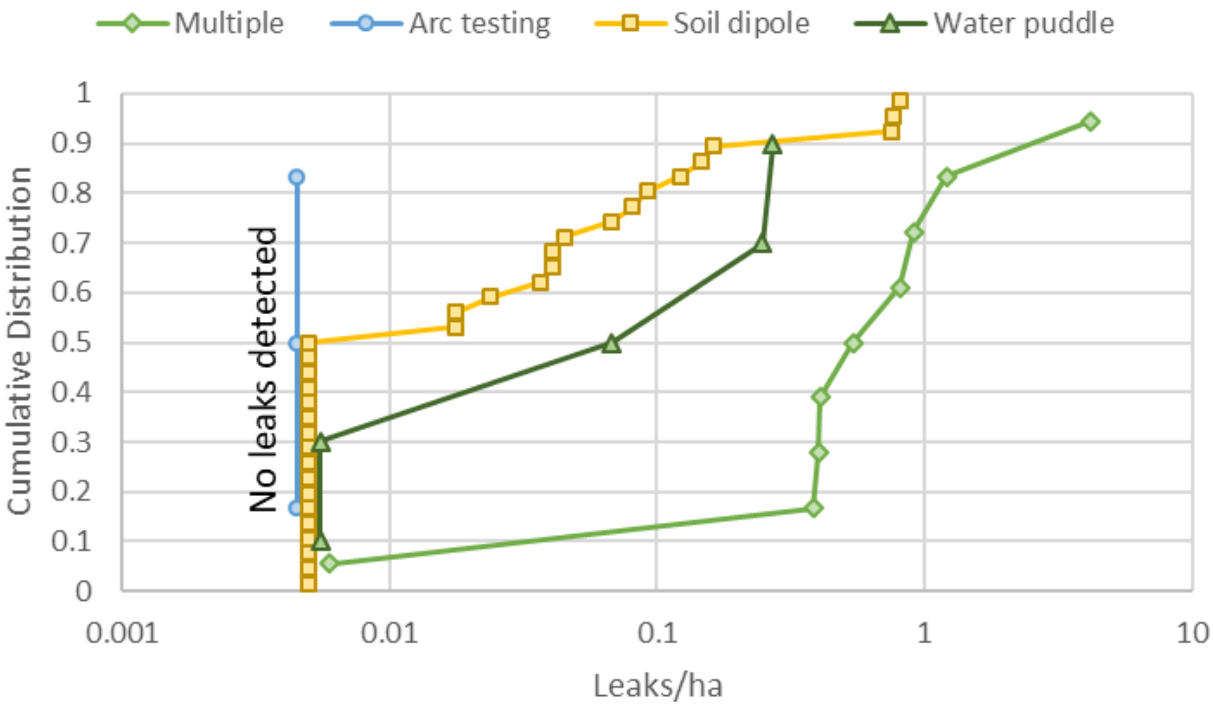

Figure 3-6: Cumulative Distribution of Observed HDPE Geomembrane Leak Density for 50 Sites in North America Determined with Different Test Approaches (data from Gilson-Beck, 2019), with Each Marker Representing a Different Site[1]

In response to the NRC Request for Supplemental Information for the DOE 2020 PA (ML20254A003), the DOE considered the initial HDPE defect frequency in the DOE document SRR-CWDA-2021-00033, Rev. 1 (ML21160A062). In that document, the DOE used information from a literature review of initial HDPE defect frequencies to recommend a distribution of frequency values. However, the DOE increased the mean from 2.775 defects per hectare to a more conservative 4.0 defects per hectare, and, in order to widen the range of variability, the standard deviation was increased by a factor of 10 from 0.65 to 6.5. A log-normal distribution was applied based on the interpretation of the cumulative distribution curve by one of the authors documented in the literature review.

3.3.7 Characterization of HDPE and GCL Degradation

The Closure Cap Model developed for the both the DOE 2020 PA and the DOE 2009 PA rely on the analysis by WSRC-STI-2008-00244 to identify potential HDPE and GCL degradation mechanisms. WSRC-STI-2008-00244 relied on the extensive Needham et al. (2004) report to guide analyses of degradation mechanisms, while Needham et al. (2004) compiled and summarized earlier documents related to generation of defects in HDPE geomembrane landfill barriers. Needham et al. (2004) segregated degradation causes into: (i) large-scale or catastrophic events, which occur as a result of poor design or avoidable operational practices and (ii) physical damage, inevitable material degradation, and stress cracking. Needham et al.

[1] Note that the curves are fit to data for different sites and so only indirect comparisons of different test methods are being provided. Category "Multiple" combines two or three approaches. Values that Gilson-Beck (2019) reported as zero are stacked at ~0.005 leaks/ha (0.002 leaks/acre), with curves offset slightly for visibility.

(2004) described an adequate standard of design as avoiding slope instability, down-drag stresses caused by settlement, and excessive differential settlements. Needham et al. (2004) recommended installing a fixed ELL system that is monitored annually after closure.

HDPE Geomembrane Degradation

The DOE 2020 SDF PA identified seven potential degradation mechanisms specific to the HDPE geomembrane in the SDF closure cap: (i) ultraviolet radiation, (ii) antioxidant depletion, (iii) thermal oxidation, (iv) high energy irradiation, (v) tensile stress cracking, (vi) biological (microbial, root penetration), and (vii) chemical (waste leachate). Six potential degradation mechanisms were identified that apply to multiple layers, including the HDPE geomembrane: (i) static loading induced settlement, (ii) seismic induced liquefaction and subsequent settlement, (iii) seismic induced slope instability, (iv) seismic induced lateral spread, (v) seismic induced direct rupture due to faulting, and (vi) disposal structure or saltstone subsidence. Seven potential degradation mechanisms were identified specific to the GCL, which may indirectly influence HDPE performance: (i) slope stability, (ii) freeze-thaw cycles, (iii) dissolution, (iv) divalent cations, (v) imbibition-desiccation (wet-dry cycles), (vi) biological (root penetration, burrowing animals), and (vii) chemical (waste leachate).

Both the 2020 SDF PA and WSRC-STI-2008-00244 dismiss several of these mechanisms from consideration, based on the following assumptions consistent with the 2009 SDF PA:

- installation protocols will cover the HDPE geomembrane long before ultraviolet radiation will significantly deteriorate the geomembrane
- HDPE degradation from high energy irradiation requires orders of magnitude greater radiation doses than are credible in the SDF closure cap
- exposure to significant leachate is precluded in the closure cap because of vertical separation from the disposal structures
- all GCLs will be buried far below the freeze/thaw penetration depth
- soils being considered for the cap are not susceptible to cracking from wet-dry cycles; the considered soils are predominantly highly leached quartz sand with a small clay fraction that is predominately kaolinite, which has low swelling capacity
- high-molecular-weight polymers used for geomembranes are judged insensitive to microbial biodegradation
- degradation from microbial growth is primarily associated with leachate collection layers receiving leachate containing organic and inorganic degradation waste products, while infiltrating water is expected to be very low in both mineral and organic content, so microbial growth in lateral drainage sand layers is not considered applicable at the site
- burrowing animals will be precluded by the erosion barrier design
- waste layer subsidence is assumed not to be applicable because the disposal structures are filled with grout

- seismic-induced lateral spread and direct rupture due to faulting are incompatible with site conditions (WSRC-STI-2008-00244)

The 2020 SDF PA indicated that future design analyses and design choices will ensure that the final cap will not be subject to degradation from:

- seismic slope instability
- static settlement: preliminary analyses in the 2007 DOE document WSRC-STI-2007-0018, Rev. 2 suggested that static settlement of a cover system would be less than 5 to 7.5 cm (2 to 3 in) and spatially uniform
- slope instability related to the GCL

The 2009 SDF PA Closure Cap Model explicitly considered:

- antioxidant depletion
- thermal oxidation (included in the antioxidant depletion model)
- tensile stress cracking
- biological degradation (root penetration of the composite barrier layer)
- silting-in of the lateral drainage layers

The 2020 SDF PA Closure Cap Model eliminates two mechanisms from consideration that strongly affected infiltration rates in the 2009 SDF PA:

- biological degradation, based on lack of evidence from analog sites (the DOE document SRRA107772-000009)
- Silting-in of the lateral drainage layers, based on lack of evidence from analog sites (the DOE document SRRA107772-000009)

The 2020 SDF PA describes thermal oxidation of HDPE as excluded from consideration based on arguments in WSRC-STI-2008-00244, but it appears that both the 2020 SDF PA Closure Cap Model and WSRC-STI-2008-00244 explicitly include thermal effects in the antioxidant depletion model.

The 2020 SDF PA Closure Cap Model is based on a model for HDPE antioxidant depletion and service life when exposed to low-level radioactive waste leachate (Tian et al., 2017). The model considers various experiments considering one- and two-sided immersion of 2-mm (0.08-in) HDPE strips with different leachate compositions. Tian et al. (2017) use a three-stage model (stages for antioxidant depletion, induction, and polymer degradation) for service life predictions, with predictions based on a 2-mm (0.08-in) HDPE geomembrane at 15 °C. Stage 1 calculations are based on one-sided exposure experiments with synthetic low-level radioactive waste leachate, with an estimated antioxidant depletion time of 750 years. Stages 2 and 3 are based on one-sided exposure experiments with municipal solid waste leachate, using rate parameters

reported by Rowe et al. (2009). Tian et al. (2017) calculate a total service life of at least 1975 years, based on a criterion of failure at 50 percent loss of stress crack resistance.

The 2020 SDF PA Closure Cap Model assumes that the initial defects immediately expand from 2 to 10 mm (0.08 to 0.4 in) at the end of the service life (rounded to 2,000 years). However, the 2020 SDF PA Section 1.4.3 assumed that stress cracks never form for 10,000 years, regardless of the degradation state, based on the rationale that the HDPE geomembrane is not subject to tensile loading as long as it remains under pressure (i.e., always buried beneath the upper layers of the closure cap).

Section 4.4.2.7 of the 2020 SDF PA represented HDPE geomembrane layer and composite barrier layer degradation associated with the LLDLs and mud mats, as tied to the Tian et al. (2017) model. The initial state is assumed to be the fully degraded version of the HDPE geomembrane in the Closure Cap Model (five 10-mm [0.4-in] holes per hectare). The model assumed that the HDPE geomembrane layer and composite barrier layer hydraulic properties decay to backfill, using geometric interpolation over time from 750 to 3,200 years (i.e., the logarithm of the hydraulic conductivity changes linearly in time). The time frame is selected based on stress crack resistance calculated in the Tian et al. (2017) model, which dropped from 100 percent to 50 percent during the period from year 750 to year 1975. Linear extrapolation to 0 percent stress crack resistance gives the year 3,200 endpoint.

The 2009 SDF PA Closure Cap Model performance was driven by biological degradation in the form of plant root penetrations through the composite barrier layer. However, the DOE document SRRA107772-000009 and the 2020 SDF PA dismissed the possibility that plant roots will penetrate the composite barrier because: (i) roots accumulate in regions where water is more plentiful and do not grow towards regions where water is more difficult to extract, (ii) water will tend to accumulate above the composite barrier while the soil dries below the composite barrier, and (iii) no root systems were observed below the composite barrier at any covers evaluated by Benson, C.H., et.al. in NUREG/CR-7028 (ML12005A110).

NUREG/CR-7028 examined three sites that had a composite barrier and were located in a humid or sub-humid climate (Cedar Rapids, IA; Omaha, NE; and Polson, MT); all had conventional covers with grasses or grasses and forbs, and none had existed for more than 9 years. Exhumations were limited to a 2 m by 2 m square at each site.

In response to the NRC Request for Supplemental Information for the DOE 2020 PA (ML20254A003), the DOE considered the service life of HDPE in the SDF closure cap in the DOE document SRR-CWDA-2021-00033, Rev. 1 (ML21160A062). In that document, the DOE used information from a literature review of HDPE degradation to recommend a distribution of service life values. Service life estimates of 1,975 to 3,550 years were recommended in the DOE document SRRA107772-000009 based on Tian et al. (2017) while Rowe (2005) and Rowe et al. (2009) suggested a minimum value may be on the order of 600 to 700 years. To reflect this variability, the DOE used a log-normal distribution with an assumed mean of 1,975 years and a standard deviation of 1,200 years resulting in a 5^{th} percentile of 671 years and a 95^{th} percentile of 4,244 years.

The DOE document SRR-CWDA-2021-00033, Rev. 1 also considered how to simulate degraded conditions of the HDPE. For simulating the degraded conditions of the HDPE, the DOE considered three potential end states: complete HDPE failure, partial HDPE failure, and no HDPE failure. When simulating the no-failure condition, the initial conditions for the HDPE remained the same, including the HDPE defect frequency and the HDPE defect size, while other materials in the system were allowed to degrade over time. For simulating partial failure condition, it was assumed that the area of existing defects would double on a regular basis, starting when the polymer degradation stage begins. The interval for doubling was based on the length of time estimated for the polymer degradation stage, such that by the end of the service life, the initial defects double in area relative to the initial conditions. This approach does not explicitly simulate the formation of any new defects, which may form over the very long time periods considered in PA modeling. However, the DOE assumed that increasing the areas of the defects implicitly addresses the potential impacts of any new defects which may form over time. For simulating the complete failure condition, once the end of the HDPE service life was reached, the HDPE geomembrane was ignored, and Darcy's law was used to estimate the infiltration rate through the GCL based on an attenuation layer approach developed by Rowe (2012) that the DOE modified based on DOE expert judgement for site-specific properties. A probability density function for the recommended HDPE failure conditions was provided with each of the three conditions assumed to be equally likely (i.e., 33.3 percent).

GCL Degradation

The 2020 SDF PA addresses GCL properties in the Closure Cap Model, with minimal discussion outside the Closure Cap Model. Infiltration rates are proportional to the GCL hydraulic conductivity raised to the power of 0.74 in the Giroud (1997) equation, with infiltration increasing by a factor of 5.5 for each order of magnitude increase in hydraulic conductivity. The 2020 SDF PA Closure Cap Model assumes that the GCL hydraulic conductivity does not significantly change due to divalent cations replacing monovalent cations, based on analyses by Scalia and Benson (2011) [also reported in NUREG/CR-7028 (ML12005A110)] of samples from GCLs exhumed after 4.7 to 6.7 yr of service in several closure caps and samples from GCLs exhumed after 14 years at the nearby Barnwell Disposal Facility (Scalia et al., 2017). The 2020 SDF PA cited the relevant samples as having hydraulic conductivities less than 5×10^{-9} cm/s ($2x10^{-9}$ in/s) and the Closure Cap Model uses 1×10^{-9} and 1×10^{-8} cm/s ($4x10^{-10}$ and $4x10^{-9}$ in/s) for the expected and upper bound values for the GCL, respectively. The expected value is representative of new GCL samples prior to installation. All tested exhumed samples had partial to complete cation replacement, and Scalia and Benson (2011) indicate that divalent cation exchange within GCLs would be expected at most sites. The NRC staff expects that the GCLs in the LLDL and mud-mat composite barriers would be especially prone to divalent cation replacement as a result of the decalcification process for the disposal structure cementitious materials.

Figure 7a and b present the Scalia and Benson (2011) and Scalia et al. (2017) measurements: (i) in comparison to the exhumed GCL water content and (ii) translated into the corresponding influence on infiltration calculations;
Figure 7c and d show the cumulative distribution of measurements from small to large. Scalia and Benson (2011) reported hydraulic conductivity measurements using: (i) a standard water (SW) with 10 millimolar (one thousandth of a mole per liter concentration [mM]) $CaCl_2$ solution (SW in
Figure 7) and (ii) deionized water (DW) and indicated that most pore waters should have chemistry between these extremes. Scalia et al. (2017) used an average water (AW) consisting

of 1.3 mM NaCl and 0.8 mM $CaCl_2$ to represent soil pore water, as well as three confirmatory SW measurements (the SW and AW samples had similar hydraulic conductivity measurements). Most of the Scalia and Benson (2011) measurements were performed with the SW permeant, as the variability in measured values was much smaller with deionized water. Some of the measurements were first reported by Meer and Benson (2007), and these were mostly sampled from exhumed GCL-only installations (labeled “SW GCL-only”). Samples obtained from GCLs in a composite barrier layer were labeled “DW composite” and “SW composite” to distinguish measurements made with deionized water and standard water. Dye tests performed on some of the SW samples exhibited undiagnosed fast pathways through the GCL associated with needle punching; these are labeled “SW penetration.” The few measurements made on samples of new (i.e., never installed) GCLs, with both standard water and deionized water, were plotted with the same symbol and labeled “New GCL”. The influence on infiltration is calculated using the ratio of measured hydraulic conductivity divided by the new-GCL hydraulic conductivity (1×10^{-9} cm/s [$4x10^{-10}$ in/s]), raised to the power of 0.74. Scalia and Benson (2011) inferred from those data that a GCL placed on a sufficiently moist subgrade and covered with a geomembrane will maintain a low hydraulic conductivity. The Scalia et al. (2017) measurements had bound cation mole fractions and swelling capacity similar to new-GCL values, consistent with essentially no cation replacement. Scalia et al. (2017) observed needle-punched pathways with mineral precipitation, but dye tests showed no flow through these pathways.

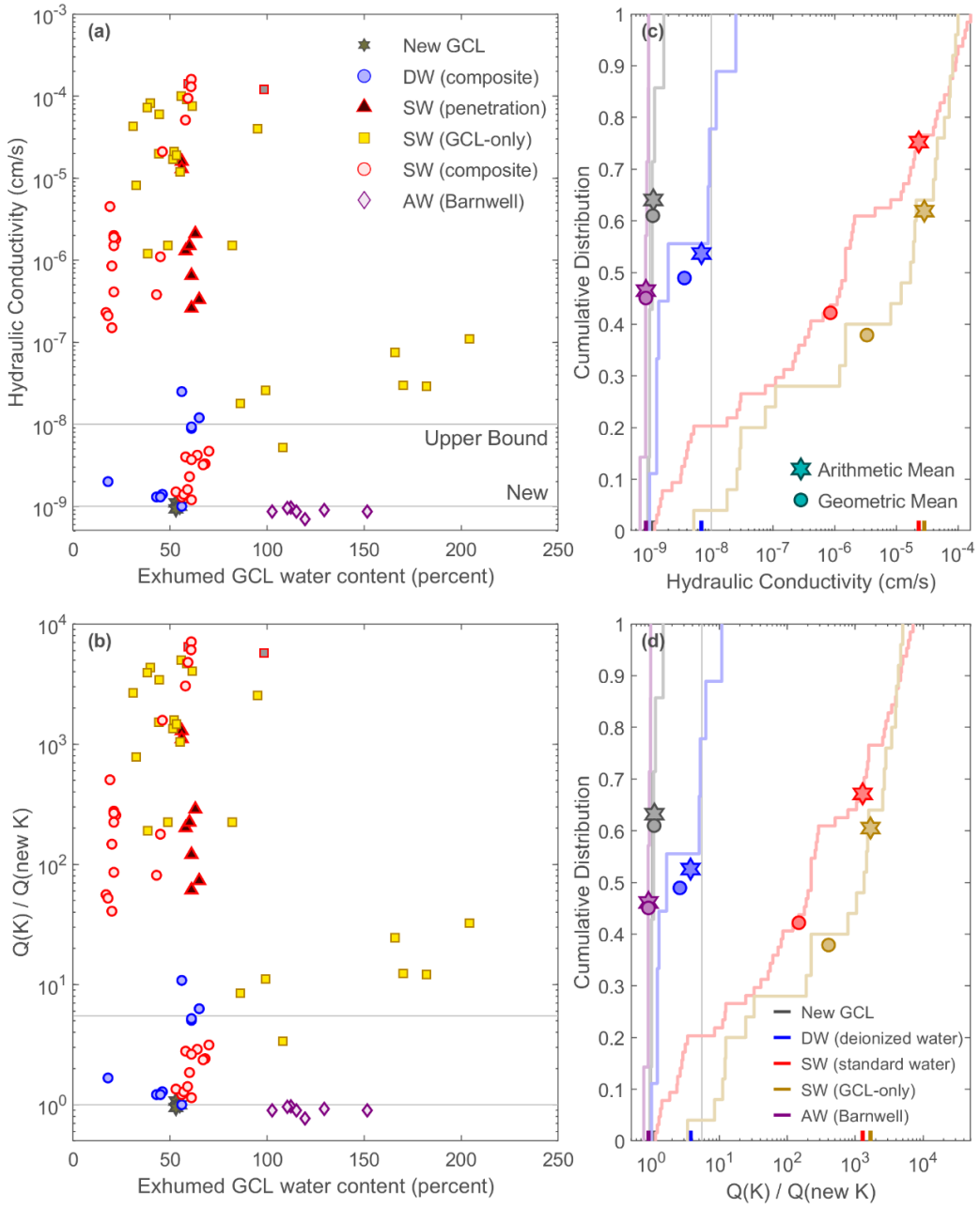

Figure 3-7: Measurements from New and Exhumed GCLs[2] (from NUREG/CR-7028)

[2] Hydraulic conductivity versus exhumed GCL water content: (a) measured values and (b) infiltration increase relative to a new GCL using the Giroud (1997) equation. Cumulative distribution of measurements for new GCLs and different water sources: (c) measured values and (d) corresponding infiltration increase. Horizontal lines in (a) and (b) and vertical lines in (c) and (d) represent a new GCL (2020 SDF PA Expected Value) and the 2020 SDF PA Upper Bound value. In (c) and (d), the arithmetic and geometric means are indicated by symbols; the arithmetic means are also indicated with tick marks on the x-axis.

In response to the NRC Request for Supplemental Information for the DOE 2020 PA (ML20254A003), the DOE provided a recommended approach for representing the GCL hydraulic conductivity in the DOE document SRR-CWDA-2021-00033, Rev. 1 (ML21160A062). In that document, DOE represented the GCL hydraulic conductivity with two independent distributions: (i) an initial value and (ii) a degradation multiplier. In that document, the DOE used information from literature reviews of GLC properties and GCL degradation to recommend for both properties: (i) a probability distribution and (ii) minimum, mode, and maximum values. DOE recommended reducing the distribution of initial GCL hydraulic conductivity derived from the literature review by a factor of 5 to account for site-specific conditions based on expert judgement. DOE recommended that the degradation factor distribution had a minimum of 1 (i.e., no GCL degradation occurs) and a mode of 10 (to acknowledge the long time periods being considered, based on expert judgement).

3.3.8 Calculated Properties for Composite Barrier Layers and HDPE Geomembrane Layers Below the Closure Cap Model

The Vadose Zone Flow Model treats all HDPE-geomembrane-containing barriers as an EPM with 2.54-cm (1-in) thickness. The DOE made that assumption for the horizontal HDPE/GCL composite barriers layers below the LLDL, the composite barrier layers between the upper and lower mud mats (except for SDS 1 and SDS 4 which do not have this layer), and the vertical HDPE geomembrane layer wrapping the exterior walls of the smaller cylindrical SDS 2A, SDS 2B, SDS 3A, SDS 3B, SDS 5A, AND SDS 5B. The 2020 SDF PA generically refers to such barriers as liners.

The EPM approach replaces the representation of the barrier as impermeable except for local defects with an alternative representation as a porous medium. Section 4.4.2.7 in the 2020 SDF PA described the approach in general terms as initially representing a scenario with five 10-mm (0.4-in) defects in the HDPE geomembrane per hectare, which is equivalent to the degraded state of the HDPE in the Closure Cap Model. Each barrier is assumed to degrade to backfill over time. More precisely, the barriers are assigned retention properties equivalent to concrete, which are assumed to be constant over time, and the degradation process is limited to changes in the saturated hydraulic conductivity (Ksat) and the effective diffusion coefficient (Deff). Based on the description of the degradation model, both Ksat and Deff are assumed to change according to

$$\log K = \log K_i + (t - t_i)\left(\frac{\log K_f - \log K_i}{t_f - t_i}\right) \tag{3-3}$$

where K represents either Ksat or Deff, t is time, and subscripts i and f represent the initial and final values during the change. The initial time is set to the calculated depletion time for antioxidants from the Closure Cap Model, and the final time is based on the complete loss of stress crack resistance extrapolated from the Closure Cap Model assumptions. The Closure Cap Model is based on 2-mm (0.08 in) [80 mil] HDPE geomembranes using the approach of Tian et al. (2017) to calculate antioxidant depletion and oxidation rates; the EPM approach does not adjust the timing to account for difference in rates for the HDPE geomembrane thicknesses (1.5 and 2.5 mm [0.06 and 0.1 in]]) in the lower barriers. The initial and final years for degradation are 750 and 3,200, respectively, with the basis described in Section 3.3.1 of this TRR.

3.3.9 Degradation of the Lateral Sand Drainage Layers

The 2020 SDF PA Compliance Case assumed that the portions of the two ULDL degrade from ingrowth of roots, but not due to infill, based on inferences in the DOE document SRRA107772-000009. However, the NRC Request for Supplemental Information for the DOE 2020 PA (ML20254A003) included a request to consider the full range of uncertainty when simulation SDF performance in a probabilistic manner, including the full range of uncertainty associated with lateral sand drainage layer degradation. The DOE provided a range of uncertainties including the effects of infill in the DOE document SRR-CWDA-2021-00031, Rev. 1 (ML21160A061). In that document the DOE discussed changes to the hydraulic conductivity values of the sand drainage layer due to degradation processes such as mineral precipitation and microbial growth, root penetration into the ULDL, and the silting-in of the layer. In SRR-CWDA-2021-00031, the DOE concluded that minerals and microbes typically associated with landfill leachates will not affect the performance of the UDL and LLDL. As for root penetration in the ULDL, SRR-CWDA-2021-00031 relied heavily on the DOE document WSRC STI-2008-00244, which estimated roots to potentially occupy up to 0.17 percent of the overall volume of the ULDL and decrease hydraulic conductivity by 0.2 percent as a worst-case assumption. Although the overall effect was considered negligible relative to other uncertainties in the long-term performance of the system, a root function multiplier of 0.998 (100 percent – 0.2 percent = 99.8 percent) was applied to the hydraulic conductivity values.

The DOE also considered the silting-in process as an unlikely process, but more likely than other processes. In order to obtain parameter values to use for modeling a degraded drainage layer, the DOE chose to determine: (i) the hydraulic conductivity of the backfill to be used in the closure cap, (ii) a distribution of hydraulic conductivity values between initial and fully degraded for sand drainage layers, and (iii) a distribution of the time required for complete sand drainage layer degradation. The DOE assumed that the hydraulic conductivity of the backfill will represent the end state hydraulic conductivity of the ULDL after full degradation. To develop a distribution for the hydraulic conductivity of the ULDL, the DOE used minimum and maximum values that also were based on probabilistic distributions. The minimum value was based on a distribution of hydraulic conductivity for backfill, and the maximum value was based on a distribution of initial hydraulic conductivity values for sand. In the distribution for the hydraulic conductivity of backfill, the minimum ($2x10^{-5}$ cm/s [$8x10^{-6}$ in/s]) and maximum ($1.4x10^{-4}$ cm/s [$5x10^{-6}$ in/s]) parameter values used for the distribution for modeling the hydraulic conductivity of backfill (Table 4.3-1, SRR-CWDA-2021-00031) were based on geometric mean of the SRS site-specific value ($4.1x10^{-5}$ cm/s [$1.6x10^{-5}$ in/s]), and the recommended minimum ($1.0x10^{-5}$ cm/s [$4x10^{6}$ in/s]) and maximum ($5.0x10^{-4}$ cm/s [$2x10^{-5}$ in/s]) from NUREG/CR-7028 (ML12005A110) (see Section 5.8.3.2 in the 2020 SDF PA). Using the hydraulic conductivity values for the initial sand (1.29 cm/s [0.5 in/s]) and the backfill ($2x10^{-5}$ cm/s [$8x10^{-6}$ in/s]) as the upper and lower bounds, respectively, a log-triangular distribution shape was applied to obtain the recommended values for the hydraulic conductivity of the ULDL (Table 4.3-2, SRR-CWDA-2021-00031). A log-triangular distribution was selected because the DOE expected that partial silt-in would be more likely than no, or complete, silt-in. Another reason for selecting that distribution was that a log-triangular distribution samples lower sand hydraulic conductivity values more frequently than a triangular distribution.

The DOE document WSRC-STI-2007-00184 postulated a flow rate through the backfill of 10 in. per 5,000 years based on evidence of the formation of B-horizons from the deposition of translocated clay particles. The DOE assumed that once half of the fines content of the backfill has migrated to the drainage layer, the two layers essentially become the same material, so only 50 percent of the fines are needed to reach equilibrium. Therefore, the DOE assumed the

silting-in degradation process would take 3,000 years for 50 percent of the fines to migrate from the backfill into the ULDL (i.e., 50 percent of the 6,000 years it would take for all the fine particles to flow through, and migrate out of, 30 cm (12 in.) of backfill), The DOE assumed a wide range for the uncertainty given that no field information is available as to the length of the silt-in process, choosing a log-triangular distribution where the minimum time is 300 years, the mode is 3,000 years, and the maximum time is 30,000 years until full degradation occurs. In addition, log-triangular samples lower or earlier times more frequently than a triangular distribution, resulting in faster degradation rates.

In Section 4.4.1.3.4 in the 2020 SDF PA, the DOE based hydraulic properties for the Closure Cap Model on analyses in WSRC-STI-2008-00244, developed for the 2009 Closure Cap Model. The 2009 SDF PA Closure Cap Model performance was influenced by transport of fine particles from the overlying backfill and deposition of the particles in sand drainage layers, because: (i) the projected perched water depth in the drainage layer is increased when silting reduces the saturated hydraulic conductivity and (ii) flow through defects is proportional to the perched water depth. Sensitivity analyses for the infiltration rate as a function of the drainage layer hydraulic conductivity suggest that increasing or decreasing the saturated hydraulic conductivity by a factor of 2 gives infiltration rates that are reduced or increased by a factor of 3 (Section 5.8.3.1, 2020 SDF PA). SRRA107772-000009 dismissed the possibility that the hydraulic conductivity is affected by the addition of fine particles because: (i) the authors did not observe infilling of fines when exhuming modern final covers or analog sites, (ii) the closure cap design includes a nonwoven polymeric geotextile filter above the drainage layer, and (iii) the DOE expects a natural filter will develop above the geotextile.

NUREG/CR-7028 (ML12005A110) exhumed geotextiles and geonets for modern-day covers, describing modest amounts of soil present in many of the geotextiles and a coating of fines in some of the geonets. A geonet is a manufactured product, typically with two sets of extruded HDPE ribs overlapped to form a mesh, that allows drainage flow in the plane of the mesh. The presence of fines on geonet ribs is direct evidence of transport from fine soil and deposition in a coarse medium, which was noticeable within a few years after installation.

The authors of the DOE document WSRC-STI-2008-00244 claimed that colloidal clay entering the sand drainage layer would likely be carried to the exit and indicated that clean sand layers are preserved below clayey layers at SRS yet developed a deposition model based on slow clay translocation formation of the B horizon in soil to account for uncertainties.

The 2020 SDF PA considered the LLDL in the Vadose Zone Flow Model and in the Airborne Pathway Release and Transport Model. In the 2009 SDF PA, FY 2013 SDF Special Analysis Document (SRR-CWDA-2013-00062, Rev. 2), and FY 2014 Special Analyses Document (SRR-CWDA-2014-00006, Rev. 2), the saturated hydraulic conductivity of the LLDL is reduced over time to account for inflow of colloidal particles into the coarser drainage layer, and eventually the drainage layer assumes the properties of the overlying backfill.

3.3.10 Calculation of Infiltration and Saturation in the Closure Cap Model

As discussed in Section 3.3.1 in this TRR, the 2020 SDF PA Closure Cap Model Compliance Case assumed that: (i) the HDPE geomembrane is impermeable unless a physical gap is present, (ii) almost all initial defects will be identified by testing and remediated, (iii) no new defects or holes will develop during the 10,000-yr Performance Period, and (iv) at 2,000 years the assumed initial defects are modeled as increasing in size. The 2020 SDF PA Compliance Case assumed that cap design and installation protocols will preclude the possibility that

sufficiently large stresses, from any combination of sources, will be imposed on the geomembrane to overcome the remnant HDPE strength to form new breaches even after the geomembrane is fully degraded. In response to the NRC Request for Supplemental Information for the DOE 2020 PA (ML20254A003) the DOE evaluated the effects of using a greater range of defect area increases. Section 3.3.7 in this TRR discusses what the DOE evaluated in more detail.

The 2020 SDF PA Closure Cap Model calculated infiltration in a multistep procedure. First, vertical inflow to the ULDL was calculated using a 1-D numerical model called WINUNSAT-H; the model calculates time-dependent inflow, but the inflow was averaged in time and assumed to be approximately spatially uniform across the cap. Second, infiltration was calculated for a single defect located at the most vulnerable location in the cap, assuming that inflow redistributes within the ULDL in an unconfined saturated layer perched on top of the composite barrier layer below the sand layer. Third, the single-defect infiltration flow was multiplied by the number of assumed defects to obtain a total infiltration. Finally, the total infiltration was averaged across the cap area and passed to the vadose zone flow model as the equivalent uniform infiltration. In essence, the three-step procedure assumed that: (i) the defects are so widely separated that flow calculations for a defect are not influenced by flow removed by any other defect and (ii) the sand layer remains unconfined (the perched water table within the sand layer does not rise to the top of the sand layer).

The 2020 SDF PA Closure Cap Model (Equation 4.4-4, Section 4.4.1.2.2) calculated flow through a defect based on an approximate solution (Giroud, 1997) that considered: (i) flow through the defect, (ii) lateral spreading along the interface between the HDPE geomembrane and GCL, and (iii) vertical flow through the GCL. Giroud (1997) identified head as the driver for flow through the defect and provided an approximation for head where the drainage layer was unconfined (the saturated flow is entirely within the drainage layer); for that case, the head driving flow was the same as the flow depth. The Giroud (1997) defect-flow equation summed two terms containing head, one proportional to $h^{0.9}$ and one proportional to $h^{1.85}$ (where h is head); the flow through the defect was either approximately linear or approximately quadratic, depending on the input parameters.

The 2020 SDF PA Closure Cap Model calculated average defect flow over the cap using the Giroud (1997) approximation for saturated flow depth, assuming a flow accumulation distance equal to 356.6 m, the longest slope in an alternative design for the cap, instead of the longest slope in the current design (311 m), in order to overestimate infiltration. The saturated flow depth was inversely proportional to the saturated hydraulic conductivity for the ULDL; in other words, decreasing hydraulic conductivity by a factor of five increases flow depth by a factor of five.

4.0 NRC Staff Evaluation

The authors of this TRR considered the 2020 SDF PA and supporting documents, supplemented with the DOE-provided input and output files from computer analyses used in the PA and reviewed the DOE approach to model methodology, model support, and model consequences related to: (i) HDPE/GCL composite barrier layers, (ii) HDPE geomembrane layers, and (iii) the ULDL and LLDL. Given the complexity of the physical processes, the modeling process, and potential interactions, additional information may be needed to clarify key performance issues as the time nears for surface cover construction (i.e., currently estimated in the early 2030s).

The authors of this TRR evaluated four barriers in the 2020 SDF PA that rely on HDPE geomembranes: (i) the ULDL barrier (the combined ULDL and composite barrier layer), (ii) the LLDL barrier (the combined LLDL and composite barrier layer), (iii) the mud-mat composite barrier layers, and (iv) the vertical HDPE geomembrane layers. Figure 4-1 shows the first three of the evaluated barriers. The ULDL and LLDL barriers both include a sand drainage layer and a composite barrier layer while the mud mat only includes the composite barrier layer.

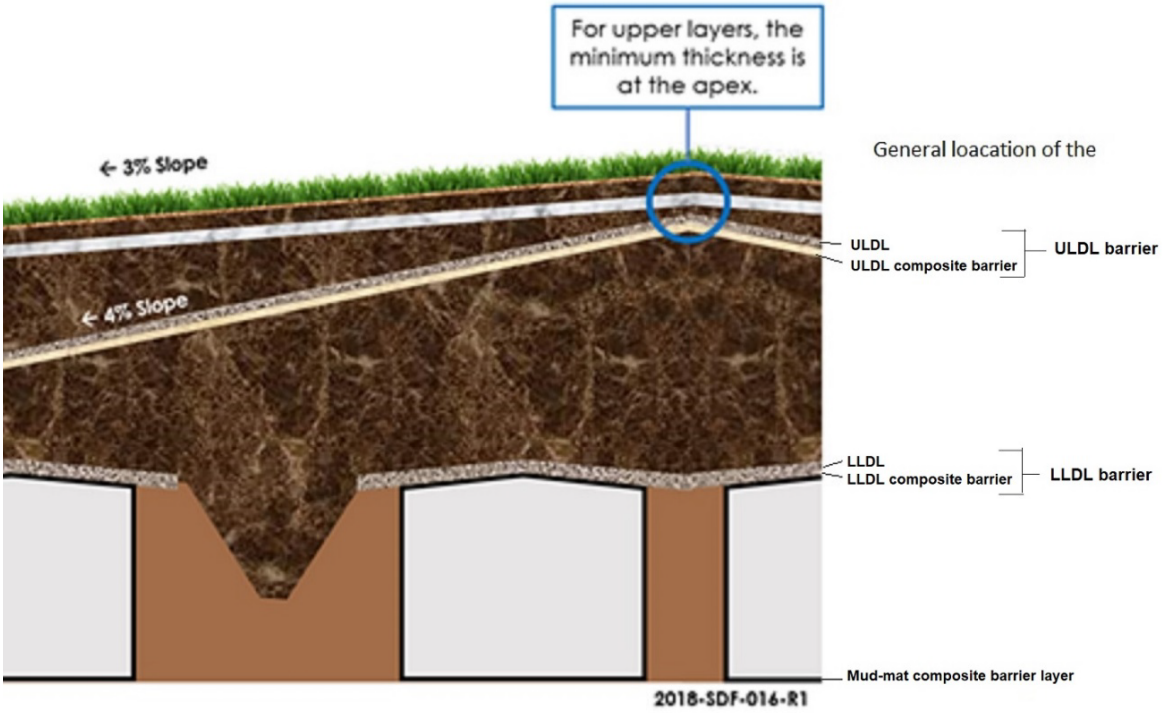

Figure 4-1: SDF Conceptual Close Cap Configuration and the General Location of Composite Barrier and Geomembrane Layers (modified from Figure 3.2-32 of the 2020 DOE PA)

4.1 Evaluation of Information from the DOE 2020 SDF PA and Related Documents

4.1.1 Influence of Composite Barrier Layers and HDPE Geomembrane Layers on Performance

As discussed further in the rest of Section 4, the authors of this TRR concluded that there is a high likelihood that the ULDL barrier (the combined ULDL and composite barrier layer) would permit larger infiltration rates than calculated in the 2020 SDF PA Compliance Case due to: (i) studies from other sites indicating that measured leakage rates are typically much larger than calculated in the 2020 SDF PA; (ii) seasonal and annual periods of high inflows are not accounted for; (iii) and the 2020 SDF PA did not consider GCL properties that affect performance only under a flowing defect.

For the vertical HDPE geomembrane layer, the NRC staff determined the risk significance of this layer is relatively low since the vertical HDPE geomembrane is only used on the smaller cylindrical disposal structures and covers just 2.3 percent of the combined exterior area over all the disposal structures. Although omitting the barrier may increase the overall transfer rates

from those disposal structures, the dose consequence of the increase is likely to influence the overall dose consequence only incrementally.

4.1.2 Characterization of Initial Defects

The DOE provided a range of recommended initial HDPE defect size, as documented in the DOE document SRR-CWDA-2021-00033, Rev. 1 (ML21160A062). In that document, the DOE used information from Colucci and Lavagnolo (1995) to provide a full range of initial HDPE defect sizes based on field work. The subsequent DOE assumption that all larger defects will be detected and repaired during installation so that larger initial defects need not be considered in the PA is a risk-significant assumption. The NRC staff did not see a technical basis provided by the DOE to support that important assumption. In addition, the NRC staff could not find a sound technical basis for the use of the log-uniform distribution for the recommended defect diameter dataset. Initial model results using the entire dataset from Colucci and Lavagnolo (1995) were the justification for the adoption of a log-uniform distribution; however, no results were shown by the DOE for uniform distribution after the reduced dataset (i.e., 3.3 percent of original dataset) was selected for consideration.

Section 3.1.2 in this TRR described various field studies that suggested that initial and installation or construction-related defects historically have tended to be more frequent and larger than assumed for the 2020 SDF PA. In particular, construction-related defects have historically been much larger than the weld defects assumed for the Closure Cap Model and at least one large study suggested that construction defects dominate weld defects in flat areas. The Giroud and Bonaparte (1989) recommendations were based on the analysis of six case histories using extrusion welded seams. Recognizing the advances in HDPE formulations and installation techniques that have taken place over the last 30 years, it is not clear that these recommendations fully capture the range of uncertainty given the small sample size. Although the clay layers described in some of those field studies may allow somewhat greater leakage than a GCL for an identical HDPE geomembrane defect, and some of the landfills in the studies used 1.0-mm (0.04 in) HDPE geomembranes instead of the 1.5 mm (0.06 in) HDPE geomembrane planned for the SDF, those leakage data suggest that the calculated leakage rates in the 2020 SDF PA may be an optimistic outlier compared to existing installations. The authors of this TRR recognize that: (i) placing the HDPE geomembrane directly on a GCL will tend to mitigate against defects caused during construction, and (ii) material properties and construction quality have improved over time. The DOE assumption that construction-related defects will be precluded by careful construction practices (equivalent to the assumption that all defects are weld defects) may be an achievable goal, but the available data from Section 3.1.2 in this TRR suggest that the calculated infiltration rates in the 2020 SDF PA Closure Cap Model are often orders of magnitude larger in actual covers.

Recommendation CBDL-01

> *Therefore, the NRC staff recommends observing monitoring the installation of the HDPE/GCL composite barriers and the repairs to cuts and defects in the HDPE under a new MF entitled "Confidence in Quality Assurance and Quality Control for the HDPE/GCL Composite Barrier and Drainage Layer Installation" in MA 2 (Infiltration and Erosion Control) under both 10 CFR 61.41 and 10 CFR 61.42.*

4.1.3 HDPE Geomembrane Seam Factors

The DOE 2020 SDF PA did not explicitly discuss defects within the heat-affected zone, which is known to have low resistance to stress or large local stresses. Heat-affected features adjacent to the welded seam (i.e., the weakened areas where two geomembrane layers overlap without being attached to each other) would be prone to developing defects even when stress levels are too small to develop defects over most of the geomembrane and would be the most likely location for hidden initial defects. Seams with heat-affected zones could also be the locations where defects develop later in time. As discussed in Sections 3.3.3 and 3.3.6 in this TRR, Rowe et al. (2019) considered welded seams to be the most critical locations for failure. Heat-affected zones, which occur near welded seams, are known to have enhanced leaching of antioxidants and low resistance to stress cracking.

The NRC staff requested additional information on heat-affected zones near welded seams in the Third Set of RAI Questions and Comments for the DOE 2020 SDF PA, referred to in this TRR as the NRC 3rd Set of RAIs (ML21341A551). In the DOE response to CBs&DLs-6, (the DOE document SRMC-CWDA-2022-00003, DOE 3rd Set of Responses), the DOE indicated that, for the SDF, locations where the HDPE layers are seamed together, the thickness of the HDPE will double due to the required overlapping of HDPE panels when welding the panels togethers, either with typical fillet extrusion welds or with typical hot wedge double track fusion welds. The DOE also indicated that they evaluated the risk associated with potential defects through the seams of the HDPE originating at the initial time of installation but did not address potential delayed defects occurring at the weakened heat-affected seam zone after year 0 and assumed no new defects occurred after that.

Although the thickness of the HDPE layer may increase to twice the thickness after the seams have been welded, the authors of the studies discussed above were aware of the thickness of the HDPE at and near the seam when their findings were published. This thickness did not prevent them from stating that the heat-affected zones near the locations of seams may be the most critical locations for failure based on their experiments. In addition, the cross-sectional view of a typical fillet extrusion weld (the DOE intends to use extrusion welds for any necessary repairs and patches) as shown in Figure CBs&DLs-6.1 in SRMC-CWDA-2022-00003 shows that one side of the weld is a single geomembrane and shows a thickening at the immediate weld but not the heat-affected zone adjacent to the weld. Therefore, the authors of this TRR do not agree with DOE's conclusion in the response to CBs&DLs-6 that the presence of the overlapping layer will ensure adequate protection from additional defects from occurring over time.

In addition, SDS 3A had issues with water collecting in the liquid collection box. Liquid had been observed in the SDS 3A liquid collection box since the it was brought online. The cell interior currently did not contain liquid, yet liquids continue to collect in the collection box. The liquids were presumed by the DOE to be rainwater in the surrounding soils that had found a pathway through the HDPE and into the collection sump (the DOE document SRR-CWDA-2014-00070).

The SDS 3A collection box was extrusion welded as were two HDPE pipes penetrating the top of the collection box for instrumentation access and pumping capability. Either the pathways were not initially detected, if they existed, at the completion of the installation, or the defects originated at some point in time after that. As of 2022, excess water containing radionuclides was observed in one of the four SDS 6 leak detection sumps, indicating that waste had a leak path out of the SDS 6 containment system and possibly through the HDPE geomembrane (the DOE document SRMC-CWDA-2022-00025). The four sumps include a 5-cm (2-in) diameter

HDPE pipe that penetrates through the top HDPE to allow water to be removed from the sumps. While HDPE installation plans typically require a minimum of 10 cm (4 in) of overlap when seaming the HDPE together, exceptions to this overlapping requirement include welds to objects with more complex geometry where overlapping the sheets is not possible, such as connections to the HDPE embeds, HDPE pipes, or to the leak detection boxes. For these connections, only extrusion welds are possible.

Due to the considerations discussed above, the NRC staff determined that the future occurrence of degradation of heat-affected zones near welded seams is plausible.

Recommendation CBDL-02

Therefore, the NRC staff recommends opening a new monitoring factor entitled "Long-Term HDPE/GCL Composite Barrier and Drainage Layer Degradation" under MA 2 and monitoring the development of additional information relevant to HDPE degradation in the heat-affected zones near welded seams and at edges, HDPE degradation due to root penetration, GCL degradation due to HDPE defects, and drainage layer degradation due to diminishing hydraulic conductivity under a new MF in MA 2 (Infiltration and Erosion Control) under both 10 CFR 61.41 and 10 CFR 61.42.

4.1.4 Composite Barrier Layer Installation Factors

Good contact between the HDPE geomembrane and GCL is very important for limiting leakage from a defect. Poor contact can be minimized if strict quality control measures are taken. The NRC staff requested additional information in RAI Question CBs&DLs-3 documenting the high level of Quality Assurance/Quality Control (QA/QC) applied during the emplacement and installation of the composite barrier layers in mud mats in the NRC 3rd Set of RAIs (ML21341A551). DOE responded in the DOE 3rd Set of Responses (the DOE document SRMC-CWDA-2022-00003) and provided a summary of documents that the DOE indicated demonstrate the high level of QC applied during installation of the composite barrier layers.

The DOE response to CBs&DLs-3 described the DOE experience with reducing and preventing wrinkles in the HDPE geomembrane layer. Lessons learned included: (i) increasing the thickness of the upper mud mat to create a better contact between the HDPE and GCL layers, (ii) tensioning the HDPE layer, and pouring the mud mat concrete mixture, at night when the HDPE wrinkles "relaxed" and subsided, (iii) switching to a white-coated HDPE that better reflected solar radiation and reduced heating of the material, (iv) upper mud mat concrete mixture poured starting from the middle of the disposal structure, so that any "waves" or wrinkles will then be pushed towards the outer edge as the concrete is poured, (v) when waves cannot be "pushed" to the edge of the HDPE, creating a cold joint in the upper mud mat concrete cutting the HDPE geomembrane layer, and patching to remove the wave, and (vi) minimize using heavy equipment to place concrete over the HDPE or installing plywood sheeting to protect the HDPE from damage.

As discussed in Section 3.3.4 in the TRR, the DOE expected the HDPE geomembrane layer and the GCL to have good contact because flat installation was assumed, which allows sufficient overburden pressure to be created. The NRC staff requested additional information in RAI Question CBs&DLs-4 regarding the DOE plans for avoiding wrinkle formation on conical surfaces in the NRC 3rd Set of RAIs (ML21341A551). The NRC staff also requested additional information in RAI Question CBs&DLs-4 demonstrating that leakage rates through repair patches will not become risk-significant. Repair patches also may cause good contact to be lost between the HDPE geomembrane and the underlying GCL or substrate. The DOE responded in

the DOE 3rd Set of Responses (the DOE document SRMC-CWDA-2022-00003) and indicated that when the DOE is near establishing the final closure cap design additional considerations may be given to ensuring good contact between the HDPE and GCL layers and to the curvatures and slopes in the layout of the HDPE to minimize areas where the HDPE surface is not planar. Consideration will also be given to ensuring high integrity of the HDPE welded surfaces.

With respect to applying HDPE to more complex geometry, the DOE response discussed the vertical HDPE geomembrane sheets that had been applied to the outside wall of each smaller cylindrical disposal structure (SDS 2A, SDS 2B, SDS 3A, SDS 3B, SDS 5A, and SDS 5B) and installed from the roof embed down to the upper mud mat embed. The DOE stated that, “The bottom of this [disposal structure] design include curved slopes, so installation of the liner required relief cuts and additional HDPE patch materials to be placed over the relief cuts with extrusion welds,” and that this work was an example of HDPE geomembrane layers being applied on the curved slopes demonstrating that HDPE geomembranes can be shaped to ensure good contact with curved surfaces. The DOE expects that the same care will be given to HDPE installation of complex configurations as is the current practices when repairing damaged HDPE and verifying the integrity of each weld.

There is uncertainty regarding the impact of a penetrating defect created in the heat-affected zone. With two overlapping geomembranes, both geomembranes would need to have a defect for a vertical flow pathway. However, the contact area between overlapping HDPE geomembranes is not sealed, which may allow a lateral flow pathway between the geomembranes. Poor contact between the geomembranes may be analogous to poor contact between the HDPE geomembrane and underlying GCL.

The authors of this TRR understand that the final design of the engineered surface cover at the SDF is many years in the future and that additional considerations will be given to the technical issues raised in this section of this TRR. However, one of the above-mentioned disposal structures (i.e., SDS 3A) had issues, as discussed in the section above, with rainwater in the surrounding soils that had found a pathway through the HDPE and into a collection sump (the DOE document SRR-CWDA-2014-00070). The SDS 3A incident demonstrates that not all HDPE/GCL composite barrier installations will be on flat surfaces. HDPE geomembranes are being applied to more complex geometry (e.g., the two HDPE pipes that lead to the liquid collection box, and the collection box itself, are extrusion welded). In addition, although plywood sheeting is installed with the intention to protect the HDPE from damage during the pouring of the upper mud mat concrete, it is not clear to the authors of this TRR that DOE’s QA/QC program is able to ensure that no damage is done when heavy equipment is used to place concrete over the HDPE. It is also not clear to the authors of this TRR if inspections are performed to check for potential damage due to heavy equipment use during the construction of the upper mud mat. In addition, wrinkles or waves created during installation of the mud mat HDPE geomembrane layer that cannot be eliminated sometimes need to be cut and patched in order to remove the wave. It is not clear to the authors of this TRR how frequently this procedure needs to be performed or if the DOE considers that future cutting and patching of the HDPE geomembrane layers for the mud mat, roof, and the closure cap will be a relatively common or uncommon procedure during installation. Additional cutting and patching to remove wrinkles or waves, or additional patching to repair damage due to heavy equipment use, increases the uncertainty that the HDPE/GCL composite barrier layer will perform as intended.

Recommendation CBDL-03

Therefore, the NRC staff recommends observing and monitoring the cutting of the HDPE geomembrane to remove wrinkles and waves under the new monitoring factor entitled "Confidence in Quality Assurance and Quality Control for the HDPE/GCL Composite Barrier and Drainage Layer Installation," which the staff recommended opening in recommendation CBDL-01 under both 10 CFR 61.41 and 10 CFR 61.42.

4.1.5 Initial GCL Properties and GCL Installation Factors

GCL seams are not welded and rely on continued panel overlap, additional bentonite applied within the seams for sealing, and applied overpressure to maintain integrity, unlike HDPE geomembranes. Factory-adhered HDPE/GCL composites may share some of the same seaming issues as GCLs, depending on the seaming technique. Although it is expected that promptly covering a GCL will preclude significant panel shrinkage from cyclic hydrothermal forcing, it appears that augmenting the GCL design to include heat tacking is a good approach for maintaining GCL seam integrity. In addition, the probability of reducing the potential for large bypass flow from an HDPE geomembrane seam to a GCL seam increases if HDPE geomembrane panel seams are offset from GCL panel seams when separate products are used.

In SRR-CWDA-2021-00033, Rev. 1, the DOE used information from Rowe (2012) to obtain recommended initial GCL hydraulic conductivity values, combined with measurements from exhumed GCLs obtained from the nearby Barnwell Disposal Facility site (Scalia et al., 2017) that the DOE used to justify reducing the values recommended by Rowe (2012) by a factor of 5. The exhumed samples were obtained beneath an HDPE geomembrane; thus, the properties reflect initial rehydration and slow diffusive equilibration with the underlying medium. Note that the lower bound value for initial GCL hydraulic conductivity reported in Table 7.3-1 of SRR-CWDA-2021-00033, Rev. 1 is 1.4×10^{-11} cm/s, but the approach described in the text would result in 1.4×10^{-10} cm/s (i.e., $7x10^{-10} \div 5$). The values associated with initial GCL hydraulic conductivity are very risk significant based on modeling results from the DOE documents SRR-CWDA-2021-00066 and SRR-CWDA-2021-00066. Therefore, the assigned log-triangular distribution for the initial GCL hydraulic conductivity values has risk significant implications that require a strong technical base. The DOE chose the log-triangular distribution over the triangular distribution due to an assumption that the variability in the initial GCL hydraulic conductivity values will vary logarithmically. The authors of this TRR could not find a technical basis provided by the DOE to support this important assumption. The authors of this TRR determined that the actual initial GCL hydraulic conductivity value used for PA modeling should be analogous with an independently validated GCL value originally defined by the manufacturer. As for the recommended distribution for modeling GCL thicknesses, the NRC staff found the information provided to support the recommended thicknesses to be adequate.

Recommendation CBDL-04

Therefore, the NRC staff recommends monitoring the initial GCL hydraulic conductivity value used in the PA modeling be analogous with an independently validated GCL value originally defined by the manufacturer once that information is definitively known under the new monitoring factor that the NRC staff recommended opening in recommendation CBDL-01 under both 10 CFR 61.41 and 10 CFR 61.42.

4.1.6 Detection of Composite Barrier Layer Defects After Installation

Based on information presented in Section 3.3.6 in this TRR, augmenting testing programs with an ELL survey once the composite barrier layer has been covered with the overlying sand drainage layer appears to increase the likelihood of detecting installation-related defects. In the 2020 DOE SDF PA, the DOE indicates that each HDPE geomembrane seam will be tested for defects and repaired using a vacuum testing device, spark testing device, or air channel pressure test for double-wedge welded seams, or shear and peel testing, and indicates that installation procedures will be similar to ongoing installations for composite barrier layers emplaced in mud mats (C-SPP-Z-00019). Procurement specifications for SDS 8 and SDS 9 (C-SPP-Z-00019) require use of single or double hot-wedge fusion seam welding or extrusion welding for HDPE geomembrane seams.

In SRR-CWDA-2021-00033, Rev. 1, the DOE recommended a distribution for modeling initial HDPE defect frequencies. Although the NRC staff has no immediate concerns with regard to the distribution provided, much of the information to support the recommended initial HDPE defect frequencies is dependent on the assumed high level of quality control expected (i.e., installation, detection, repairs shall all be performed according to standards established by the ASTM and that each seam will be tested for defects using good quality practices). To provide confidence that good quality control will be integral to the entire installation process of HDPE/GCL composite barriers and drainage layers,

Recommendation CBDL-05

> *Therefore, the NRC staff recommends that the NRC monitor QA/QC as discussed in both TRR Section 4.1.4 and TRR Section 7.3 under the new MF entitled "Confidence in Quality Assurance/Quality Control for HDPE/GCL Composite Barrier and Drainage Layer Installation," which the NRC staff recommended opening in CBDL-01 under both 10 CFR 61.41 and 10 CFR 61.42.*

4.1.7 Characterization of HDPE and GCL Degradation

The 2020 DOE SDF PA described the combination of an HDPE geomembrane and GCL as essentially impermeable where either component is intact. The 2020 SDF PA Closure Cap Model represented the HDPE geomembrane in the ULDL as remaining essentially impermeable for an indefinite period of time (other than flow through defects), even though the geomembrane strength degrades over time. In contrast, the 2009 DOE SDF PA assumed root activity would penetrate the HDPE geomembrane, significantly degrading the ULDL performance over time. The 2020 SDF PA Cap Closure Model assumed that no new defects will be created because the DOE expects that the cap design and installation protocols preclude the possibility that sufficiently large stresses will be imposed on the geomembrane to overcome the remnant HDPE strength (including root stresses), but the Cementitious Degradation Model assumed that the initial performance of HDPE geomembrane adjacent to the disposal structures with respect to CO_2 ingress degrades from the initial state to backfill during the period between years 750 and 3,200. The Vadose Zone Flow model also assumed that the initial hydraulic performance reverts to backfill, presumably using the same representation. The 2020 SDF PA does not explicitly address degradation associated with seams.

In SRR-CWDA-2021-00033, Rev. 1, the DOE recommended a distribution for modeling the service life of HDPE in the SDF closure cap. As discussed in Section 3.3.7 of this TRR, service life estimates of 1,975 to 3,550 years were recommended in SRRA107772-000009 based on Tian et al. (2017); however, based on the information from Section 8.1.2.2 in

SRR-CWDA-2021-00033, Rev. 1, it would seem that the correct lower number for that range should be 1,300 years instead of 1,975 years: “At 15°C, Tian et al. (2017) reported a minimum service life estimate of 1,975 years for HDPE exposed to municipal solid waste leachates. Alternatively, using an assumed subsurface temperature of 22°C (based on information in Appendix I of WSRC-STI-2008-00244) and exposure to water instead of leachates, the minimum estimated service life for HDPE is lower (approximately 1,300 years).” In addition, the authors of this TRR determined that the DOE did not consider all possible processes that could shorten the service life of a HDPE geomembrane as discussed below.

The authors of this TRR identified several aspects of the 2020 SDF PA Closure Cap Model approach for HDPE degradation that may result in overestimating the HDPE degradation times:

- The NRC staff expects that the ULDL will have an episodic or perennial water table perched on the composite barrier layer in order to drain inflow. The scenario of a HDPE geomembrane that is saturated on one side and has a GCL on the lower side was not tested. Soil gas oxygen available below the GCL may diffuse through the GCL, allowing at least partial degradation on the bottom of the geomembrane.

- Degradation rates for the 1.5 mm (0.06 in.) HDPE geomembranes were based on one-sided exposures of a 2.0 mm (0.08 in.) HDPE geomembrane. As pointed out in Section 4.4.2.1 of the 2020 SDF PA, the time for a reaction front to penetrate a fixed distance is proportional to the square of the distance. Accordingly, degradation of the 1.5 mm (0.06) material will take approximately 56 percent as long as the 2.0 mm (0.08 in.) material.

- Degradation rates are strongly temperature dependent. The relative change in degradation time is $t_2 = t_1 \exp[-(E_a/R)(1/T_1 - 1/T_2)]$, where t is the degradation time, T is absolute temperature, E_a is the activation energy, and R is the universal gas constant. Tian et al. (2017) service life calculations assumed a temperature of 15°C. WSRC-STI-2008-00244 used 22°C for HDPE degradation calculations, based on three years of measured subsurface temperatures within an onsite well with a shallow water table (reported mean and median monthly temperatures are 21.64°C and 21.03°C). Using the Tian et al. (2017) values for the three degradation stages with the 22°C site temperature, overall degradation time would decrease from 1,975 years to 953 years (48 percent as long). Two of the numbers in Table 3-1 by Tian et al. (2017) are incorrectly reported, based on independent regressions, and Tian et al. (2017) do not provide a criterion for calculating the antioxidant depletion time; the reported time of 215 years for a Stage I depletion time is consistent with the independently regressed coefficients and a criterion of 99 percent removal of antioxidants above the residual. Assuming fully immersed degradation at defects with the 22°C site temperature, but not accounting for edge effects or seam stress effects, overall degradation time would decrease to 513 years. Multiplying this time by 0.56 to account for a 1.5-mm (0.06-in.) geomembrane, rather than a 2-mm (0.08-in) geomembrane, results in an overall degradation time of 287 years for defects.

The NRC RAI Question CBs&DLs-5 in the NRC 3rd Set of RAIs (ML21341A551) requested information describing the DOE plans for reducing the uncertainties associated with: (i) the assumed degradation rates for the 1.5-mm (0.06-in.) HDPE geomembrane based on one-sided exposures of a 2.0-mm (0.08-in.) geomembrane, (ii) HDPE geomembranes underlying the ULDL and LLDL may have different conditions on the two sides, and (iii) service life calculations assuming a temperature of either 15°C (59°F) or 22°C (72°F). Section 8.1.2 in

SRR-CWDA-2021-00033, Rev. 1, provided additional insight with respect to one- and two-sided degradation rates of HDPE under various temperatures and conditions. Analysis results showed a minimum (bounding) HDPE degradation time for the 1.5-mm (0.6 in.) HDPE at 22°C (72°F) to be approximately 665 years when using the expected SDF cover field conditions. The authors of this TRR determined that this analysis and its results are useful information that could be used in the PA. However, the DOE believes that the 2,000-year service life assumed in the 2020 SDF PA (SRR-CWDA-2019-00001) is a reasonable assumption. The DOE responded to RAI Question CBs&DLs-5 in the DOE 3rd Set of Responses (the DOE document SRMC-CWDA-2022-00003) by indicating that much of the data from studies by R.K. Rowe used to derive service life estimates for HDPE were derived in experiments in which the HDPE was immersed in synthetic leachates similar to municipal solid waste leachates. While the DOE concluded that 665-year value provides a bounding estimate, they decided that it was appropriate to examine other studies to determine what they described as more reasonable value. To support the 2,000-year service life and in regard to HDPE thickness and the temperature and chemistry of the tests, the DOE stated that, “The implied assumption is that the differences in the temperature and thickness of the HDPE tests are balanced by the differences in the leachate chemistry and by other conservatisms applied by Tian et al. (2017).” The authors of this TRR agree that there is validity to this argument if the features and processes being discussed had moderate or less risk significance on the final outcome of the 2020 SDF PA; however, that is not the case. The risk significance of the ULDL composite barrier is high and therefore their modeled performance must be supported by strong technical bases. For example, although 20°C is relatively close to the 22°C expected in the SDF closure cap, it is not clear what sensitivity each degree Celsius has on HDPE geomembrane degradation and DOE has not provided a related sensitivity analysis. Nor is it clear with what degree of certainty 22°C can be assumed to be the subsurface temperature for all depths below grade. Sappington et al. (2005) determined the subsurface temperatures within a well screened within a shallow water table aquifer at SRS and was considered representative of the depth that the SDF Closure Cap HDPE geomembrane will be located in (i.e., a comparable shallow depth of 2 m (6 ft.) below ground surface). It is not clear if all of SRS has a temperature close to this value at this depth or if temperature at various depths below the natural land surface differs within an engineered surface cover.

In Section 1.4.3 of the 2020 SDF PA, the DOE described a HDPE geomembrane as not subject to tensile loading as long as it remains under pressure (i.e., always buried beneath the upper layers of the closure cap), in which case stress cracks will not open and the material will perform well for 10,000 years. In effect, the degradation model has little or no effect on performance because of this assumption.

The Rowe et al. (2019) analysis suggested that the 2020 SDF PA characterization of HDPE geomembranes as not subject to tensile loading while under pressure may not consider relevant sources of tensile stress. For example, gravel penetration, wrinkle deformation, and tensile stresses on trampolines all increase with increasing overburden pressure so that quantifying the expected tensile stresses on the most vulnerable HDPE locations (e.g., heat affected zones) and comparing these stresses to the defect formation resistance would provide support for the given defect formation rate.

Moisture would be expected to equilibrate through a defect, so the geomembrane adjacent to the defect would be expected to experience conditions similar to the edge of a fully immersed sample. Tests of fully immersed samples do not measure degradation of edges, which are likely to degrade faster than areas away from edges because of the diffusion perpendicular to the exposed edge. However, the 2020 SDF PA degradation calculations for enlarging a defect were

based on Tian et al. (2017) calculations for one sided diffusion during Stage I antioxidant depletion, which multiplies the calculated time determined using full-immersion tests by a factor of 3.4 instead of reducing the calculated time to account for edge effects.

The NRC staff requested additional information in RAI Question CBs&DLs-7 regarding the degradation rates at the edges of defects in the HDPE geomembranes to determine whether degradation in those areas will lead to an increased risk-significant degradation of the composite barrier layers in the NRC 3rd Set of RAIs (ML21341A551). DOE responded to RAI Question CBs&DLs-7 in the DOE 3rd Set of Responses (the DOE document SRMC-CWDA-2022-00003) and provided leakage rate calculation considerations. The results of these calculations caused the DOE to conclude that while larger defect diameters do increase the leakage rate estimates, other model simplifications and conservatisms likely outweigh these potential impacts and that the risk significance is not large. The authors of this TRR agree that the risk significance of enlarging a circular defect diameter does appear to be less risk significant than the total number of defects assumed at the beginning and over time.

The HDPE geomembrane in the composite barrier layer underlying the LLDL is likely to have very different conditions on the two sides. The upper side is likely to remain under unsaturated or minimally perched conditions almost continually, depending on infiltration rates through the cap, but with high dissolved oxygen levels. When first installed, the bottom side of the GCL will contact concrete that has been exposed to the atmosphere for years to decades, so initially the concrete will have relatively low saturation levels and high oxygen levels. Over time, moisture will wick from lower saturated concrete towards the GCL but the initial oxygen in the concrete will be consumed without replacement unless resupplied through defects. Over time, dissolved saltstone and concrete constituents (including radionuclides) will diffuse from the saltstone towards the GCL. The DOE predicted that the disposal structure roof concrete will have a pH of at least 12.5 for at least 565 yr (SDS 4) to 793 yr (SDS 9) for the Compliance Case assumptions (Section 4.4.3.4.3 of the 2020 SDF PA). A highly alkaline environment may speed antioxidant depletion rates without additives to the HDPE geomembrane (Abdelaal and Rowe, 2017). Section 8.1.3.2 of SRR-CWDA-2021-00033, Rev. 1 took most of these factors into account and the service life of the HDPE at the roofs of the cylindrical disposal structures were assumed to be 1/3rd of the value sampled by the distribution recommended in Table 8.1-8 of the same document.

The HDPE geomembrane in the composite barrier layer encased within a mud mat will be surrounded by essentially saturated concrete with low levels of oxygen (at least until significant concrete degradation allows oxygen diffusion from the backfill in the gas phase) and pH >12.5 for at least 25,000 yr (150-Foot disposal structures) to >55,000 yr (375-Foot disposal structures) under Compliance Case assumptions (Section 4.4.3.4.3 of the 2020 SDF PA). Over time, dissolved saltstone constituents (including radionuclides) will diffuse from the saltstone towards the upper side of the composite barrier layer. Any differential movement of concrete, such as cracks or offsets at joints, may impose locally intense shear stresses on the geomembrane, which may promote formation of HDPE geomembrane defects. Section 8.1.3.3 of SRR-CWDA-2021-00033, Rev. 1 took most of these factors into account and the service life of the HDPE between the mud mats of the cylindrical disposal structures were assumed to be 1/3rd of the value sampled by the distribution recommended in Table 8.1-8 of the same document.

The HDPE geomembrane layer wrapping an exterior disposal structure wall will have moisture and geochemical conditions similar to the HDPE geomembrane layer above the roof, exposed to unsaturated backfill on one side and concrete that had been exposed to the atmosphere for an extended duration on the other. However, gaps are more likely to form on both sides of the

geomembrane without an expansive GCL adjacent to the geomembrane, especially if there is some differential settlement of backfill. Differential settlement along the disposal structure wall, if it occurred, also may impose additional strains on the geomembrane. As far as the authors of this TRR know, the DOE did not consider these aspects of HDPE service life at exterior disposal structure walls.

In SRR-CWDA-2021-00033, Rev. 1, the DOE considered how to simulate degraded conditions of the HDPE and provided a probability density function for the recommended HDPE failure conditions: complete, partial, and no failure of the HDPE. Section 8.1.3.4 in SRR-CWDA-2021-00033, Rev. 1 suggested that the partial failure condition is probably the most likely representation of the HDPE failure condition. Because the results of the probabilistic sensitivity analysis of total doses in Section 4.2.1 in SRR-CWDA-2021-00066 showed the HDPE failure condition being the most risk significant parameter influencing both infiltration and saltstone degradation rates, it is important that the partial failure condition is represented correctly. A key assumption with regards to this failure condition is the assumption that the formation of new defects need not be explicitly simulated. The rationale behind this assumption is that the results will implicitly address the potential impacts of any new defects which may form over time since this approach continuously and exponentially increases the areas of the defects. However, the leakage rate calculation considerations from the addendum to the DOE CBs&DLs-7 response in SRMC-CWDA-2022-00003 demonstrated that that while larger defect diameters do increase the leakage rate estimates, “other model simplifications and conservatisms already built into the application of the Equation 4.4-5 [Page 89, SRMC-CWDA-2022-00003] likely outweigh these potential impacts. As such, concerns about a potential through defect resulting in faster degradation rates are not expected to be risk significant.” Probabilistic sensitivity analysis results in Section 6.2 in SRR-CWDA-2021-00066 confirmed that the defect diameter parameter is not as risk significant as number of defects per hectare (see Tables 6.2-1 and 6.2-3). Therefore, the assumption, that by increasing the areas of the defects formation of new defects need not be explicitly simulated, is incorrect and the partial failure condition may not be represented correctly.

Sections 3.3.3 and 4.1.3 of this TRR discuss reason why additional long-term defects may form in the HDPE especially near the seams. It is not clear that the degradation rates that the DOE modeled for intact HDPE geomembranes apply to the most vulnerable locations. As discussed in Sections 3.3.3 and 3.3.6 in this TRR, Rowe et al. (2019) consider welded seams to be the most critical locations for failure because of observed increased degradation rates and strains. These findings bolster the argument that the partial failure condition should include the formation of new defects in the HDPE.

Although the 2009 SDF PA Closure Cap Model performance was driven by biological degradation in the form of plant root penetrations through the composite barrier layer, SRRA107772-000009 dismissed the possibility that plant roots will penetrate the composite barrier because: (i) roots accumulate in regions where water is more plentiful and do not grow towards regions where water is more difficult to extract, (ii) water will tend to accumulate above the composite barrier while the soil dries below the composite barrier, and (iii) no root systems were observed below the composite barrier at any covers evaluated in NUREG/CR-7028 (ML12005A110).

The authors of this TRR offer the following counterarguments to the DOE document SRRA107772-000009 basis for eliminating biological degradation of the HDPE geomembrane:

- Although root systems tend to accumulate in wetter areas such as the sand drainage layer above the composite barrier layer, this would imply that the root system would find the base of the ULDL drainage layer adjacent to the HDPE geomembrane especially appealing. If a root did penetrate the geomembrane, the defect would result in a leak that saturates the GCL and underlying soil below it, encouraging root systems to expand below the defect.

- The SDF site is humid subtropical, and tree roots are assumed for the biological degradation model. NUREG/CR-7028 examined three sites that had a composite barrier and were located in a humid or sub-humid climate (Cedar Rapids, IA; Omaha, NE; and Polson, MT); all had conventional covers with grasses or grasses and forbs, and none had existed for more than 9 years. Exhumations were limited to a 2 m by 2 m square at each site. It is not at all clear that strong conclusions regarding the penetration of tree roots over thousands of years can be drawn from 12 m^2 of exhumations with grassland covers over 9 years.

The NRC RAI Question CBs&DLs-1 in the NRC 3rd Set of RAIs (ML21341A551) requested information regarding the DOE plans for reducing the risk-significant uncertainty associated with root penetration of the ULDL, HDPE, and GCL in the closure cap and the resulting reduction of performance due to that degradation. DOE responded to RAI Question CBs&DLs-1 in the DOE 3rd Set of Responses (the DOE document SRMC-CWDA-2022-00003) by providing detailed information on the loblolly pine, which is the current dominant pine tree in the SRS area. This information included root mass per rooting depths for loblolly pines (Figure CBs&DLs-1.1 and 1.2 in CWDA-2022-00003) and estimated line fits and maximum rooting depths for loblolly pine plots (Table CBs&DLs-1.1 in the same DOE document) and numerous references with information on this tree species. Based on the data gathered and subsequently analyzed by the DOE on the loblolly pine, the authors of the TRR agree that the probability of future extensive damage to the 2-m (6-ft.) deep or deeper HDPE geomembrane layer due to loblolly pine taproots is unlikely because loblolly pine roots generally do not exceed 2 m (6 ft.) depth. However, the DOE has not provided similar data and analyses for the longleaf pine. Although this tree species is much less common, longleaf pine forests once spanned an estimated $3.7x10^{11}$ sq. m (92 million acres) in a range that stretched from southwest Virginia to eastern Texas (U.S. Department of Agriculture, 2012). As such, it is not unreasonable to assume that this species could make a comeback in the future. If one longleaf pine grew at the center of each of the two SDF closure caps every 50 years, this would amount to 20 trees growing above the shallower portion of the HDPE geomembrane layer (i.e., that portion of the cover with a relatively thin middle backfill) within the compliance period. This could be risk significant since the tap roots of the longleaf pine may extend deeper than 2 m (6 ft.), which is the minimum thickness needed to reach the HDPE geomembrane layer if the effects of erosion are not included.

The NRC Clarifying Comment-9 (CC-9) in the NRC's 4th Set of RAI Questions and Comments (ML22026A397) requested clarification on whether the DOE evaluated other trees and flora native to the general surrounding region of the Z-Area in the past and in the present, and potentially native in the future, other than the loblolly pine. The DOE responded to CC-9 in the DOE 4th Set of Responses (the DOE document SRMC-CWDA-2022-00016) by presenting facts about various potentially destructive species that supported the DOE low-risk conclusions for each species that came into question. Most species were evaluated in SRMC-CWDA-2022-00016 as being low risk because the species' root systems were generally shallow, or the species grew in areas moister than that of the SDF. However, the DOE response stated that the longleaf pine taproot commonly grew longer than 2 m (6 ft.), although the growth

of the taproot would be restricted due to poor structure, low porosity, and slow permeability, such as the clays and compacted soils similar to the soils planned for use in the closure cap system. However, as the DOE stated in Section 4.4.1.3.4 of the 2020 SDF PA, the closure cap material is assumed to have undergone pedogenesis and lost compaction, and as stated in DOE response to CBs&DLs-2 (SRMC-CWDA-2022-00003), “the backfill is expected to be a predominantly sandy material, with some clay and silt mixed in.” Based on (South Carolina Department of Natural Resources, 2020), longleaf pines grow on sandy soil with low organic content and poor to excessive drainage.

The information presented by the DOE is not sufficient to exclude the potential for tree roots to penetrate the composite barrier layer. Therefore, the NRC staff considered the potential for and consequences of root penetration. The most vulnerable locations for roots newly penetrating the HDPE geomembrane may be heat affected zones covered by an overlapping geomembrane flap, because root growth under the flap would exert tensile forces on the heat affected zones. If nothing else, root systems would be expected to penetrate initial defects and enlarge them over extended periods of time. The authors of this TRR recognize that root penetrations would be unlikely over portions of the cap with the HDPE geomembrane below the rooting depth; however, based on the 2020 SDF PA surface and ULDL slopes (0.03 and 0.04, respectively), roots would potentially reach the geomembrane up to 183 m from the ridgeline with the 3.66 m [12-ft.] maximum rooting depth used in the 2009 SDF PA. Based on the SDF Closure Cap design configuration map (Figure 3.2-29, 2020 SDF PA), it appears that all SDSs except SDS 3A, SDS 3B, SDS 5A, and SDS 5B would be at least partially within the potential root degradation area.

Therefore, the NR staff expects that biological degradation in the form of plant root penetrations through the composite barrier layer and its HDPE remains a viable process that could cause the formation of new defects in partial failure condition mode.

With regards to GCL degradation and an increasing hydraulic conductivity related to long-term GCL performance, the authors of SRRA107772-000009 indicated that it is more relevant to assess the cover performance based on the seven Barnwell GCL samples than it is to use the other data shown in
Figure . Scalia et al. (2017) noted that the Barnwell data did not have the same type of changes in the swell index and sodium mole fraction observed with the Scalia and Benson (2011) samples and hypothesized that this discrepancy was due to a different soil barrier pore water chemistry, but the data necessary to confirm the hypothesis were not obtained as part of the study. The selected values for the expected value and upper bound values for GCL hydraulic conductivity may not be appropriate for use in the Closure Cap Model, given the model assumptions, even if the selected properties described the vast majority of the ULDL composite barrier layer. The Closure Cap Model assumed that the only defects are initial defects. Initial defects will experience flowing conditions starting soon after installation; therefore, the section of the GCL that controls performance will also experience flowing conditions that allow continual modification of the bentonite chemistry. None of the Barnwell samples were described as experiencing flow through a defect. Accordingly, the most relevant GCL properties for PA may be associated with GCL-only samples, because these samples experienced a continual flow of pore water through the GCL. In essence, the GCL under a defect is the sole barrier to flow through the defect. NUREG/CR-7028 (ML12005A110) concluded that GCLs used as the sole barrier layer typically become very permeable within several years after installation and cease functioning as a hydraulic barrier. Logically, that conclusion may equally apply to GCLs exposed to flow from defects. The Barnwell samples hinted that the disposal structure cap pore water

may have relatively dilute chemistry, reducing the cation replacement rate, but it is not clear that slower rates of cation replacement will avoid GCL deterioration.

Because a geomembrane-covered GCL typically experiences no flow after the initial rewetting event is completed, chemical changes to the bentonite are driven by the chemistry of the rewetting water and diffusion from the stagnant pool of pore water beneath the GCL. Measured values of GCL saturated hydraulic conductivity cited by SRR-CWDA-2021-00033, Rev. 1 showed strong responses to various permeant chemistries, but the laboratory experiments and exhumed samples were also based on single pore-volume rehydration responses (i.e., not considering through flow). In contrast, GCLs beneath a defect may experience multiple pore volumes flowing through the GCL annually, given typical head gradients across the GCL to the unsaturated backfill. Single-pore-volume samples may not provide information regarding the cumulative consequences of flow through the GCL after rehydration has completed. That is, it is not clear that changes to the GCL saturated hydraulic conductivity are completed after a single pore volume of a permeant has entered the GCL. The Ksat could continue to change until all exchangeable ions have been exchanged. Accordingly, exhumed geomembrane covered GCL samples may represent an optimistic bound for GCLs beneath a defect so that the NRC staff will be monitoring this issue in the future.

Without a firm basis for rejecting the hypothesis that cation exchange will degrade the GCL hydraulic conductivity beneath defects relatively rapidly compared to the time scales of interest, and with no data specifically relating to GCL hydraulic conductivity under conditions when the GCL is exposed to flow through a defect, the NRC staff considered the entire population of samples for determining long-term GCL performance, including the range of observed samples has substantial impact on estimated infiltration rates. For example, using either the complete set of standard water samples reported by Scalia and Benson (2011) or the GCL-only samples as a representative population of values after degradation, the calculated infiltration rate for this value would be approximately three orders of magnitude larger than calculated in the Closure Cap Model, or 6 mm/yr (2 in./yr) instead of 0.006 mm/yr (0.002 in./yr).

The DOE recommended a distribution for modeling the GCL hydraulic conductivity degradation multiplier in SRR-CWDA-2021-00033, Rev. 1. Table 9.3-3 provided a summary of estimated GCL hydraulic conductivity values for the GCL in the cover for realizations with partial failure. The saturated hydraulic conductivity value for backfill is not represented within the recommended range (i.e., the highest hydraulic conductivity value at 10,000 years is less than that of backfill with 4.1×10^{-5} cm/s [1.6×10^{-5} in/s]). The authors of this TRR would suggest that "complete failure of the GCL," as discussed in Section 8.2.2 in SRR-CWDA-2021-00033, Rev. 1, would be represented in the model by the parameter values of the adjacent backfill based on the arguments discussed above. The GCL in the closure cap is intended to be no more than 5 mm (0.2 in) thick and, if there is no HDPE geomembrane layer above it to keep it relatively isolated (e.g., if there is a hole or a tear in the HDPE), will be exposed to the processes described above for 1,000s of years. Due to the risk significance of this layer to overall dose results, the technical basis supporting minimal degradation during long-term performance cannot be described as adequate.

The DOE did subsequently model the HDPE/GCL composite layer with a hydraulic conductivity value equal to that of the lower backfill. The NRC staff requested additional information in RAI Question CBs&DLs-9 demonstrating that the degradation of the GCL immediately below defects in the HDPE geomembrane will not occur or lead to a risk-significant increase in the infiltration rate below the ULDL barrier in the NRC 3rd Set of RAIs (ML21341A551). The DOE responded in the DOE 3rd Set of Responses (the DOE document SRMC-CWDA-2022-00003) and provided

an analysis that included degraded composite barriers below the closure cap (i.e., composite barriers with hydraulic conductivity values of $4.1x10^{-5}$ cm/s [$1.6x10^{-5}$ in/s]). As the DOE stated, "It is important when interpreting these results to be aware of what this modeling case represents; it effectively assumes complete and catastrophic failure of both the HDPE and the GCL at the [disposal structure] roof and between the [disposal structure] mud mats." However, since the NRC staff had asked for an analysis with a degraded GCL only immediately below HDPE geomembrane defects, gaining insights on the performance of partially degraded GCL layer based on the modeling results provided is not as direct. The analyses provided did show increased dose within the 2020 SDF PA Compliance Period ($9.4x10^{-03}$ to >14 mrem/yr) and within 10,000 years (1.2 to >16 mrem/yr) due to the increase infiltration rates and degraded composite barrier layers below the closure cap (Figure CBs&DLs-9.7, SRMC-CWDA-2022-00003). If the localized defects within the GCL caused a fraction of the increase within the compliance period, the authors of this TRR would still consider the results risk significant. Due to the risk significance of these composite barriers and a low to moderate technical basis, it cannot be assumed that the GCL can mitigate flow through those breaches indefinitely, but that instead, the GCL will degrade, and performance will decrease.

Due to the considerations discussed above, the NRC staff determined that the future occurrence of degradation of the GCL immediately below defects in the HDPE geomembrane is plausible.

Recommendation CBDL-06

> *Therefore, the NRC staff recommends that the NRC monitor information and planned activities related to degradation of the ULDL barrier, which includes the GCL, under the new MF entitled "Long-Term HDPE/GCL Composite Barrier and Drainage Layer Degradation," which the NRC staff recommended opening in recommendation CBDL-02 under both 10 CFR 61.41 and 10 CFR 61.42.*

4.1.8 Calculated Properties for Composite Barrier Layers and HDPE Geomembrane Layers Below the Closure Cap Model

The 2020 DOE SDF PA provided values for initial and final Ksat for all the EPM-related HDPE-geomembrane-containing barriers below the Closure Cap Model domain. The horizontal and vertical barriers are assigned initial Ksat values of 1.8×10^{-12} and 2.0×10^{-13} cm/s ($7.1x10^{-13}$ and $7.9x10^{-14}$ in/s), respectively; both are assigned final values of 4.1×10^{-5} cm/s ($1.6x10^{-5}$ in/s). With those values, the assigned barrier Ksat is the same as the initial saltstone Ksat for compliance modeling (5×10^{-10} cm/s [$2x10^{-10}$ in/s]) in years 1,564 and 1,752, respectively. After that time, the dominant barrier becomes the saltstone.

The authors of this TRR did not find a specific description of how the initial EPM Ksat values were calculated. Typically, the equivalent Ksat value is calculated so that the same flow would occur through a given thickness of material with the same head difference across the medium. However, the EPM Ksat value is not unique, because flow is a nonlinear function of the head difference in the Giroud (1997) formula. The head difference across the GCL beneath a defect may strongly depend on the Ksat values of the underlying porous media; the GCL Ksat is much smaller than backfill Ksat but is larger than concrete and saltstone Ksat.

Although the method for calculating the Ksat values of the barrier EPMs was not explained in detail, the modeled barriers do not appear to significantly impede flow through the disposal structures (at least when no fast pathways that contribute to saltstone degradation are included). The lack of influence can be seen in comparisons of calculated intermediate flow

rates through various levels of the disposal structures (Section 4.4.4.4, 2020 SDF PA). The combined barrier effect would be most clearly seen as gradually increasing flow through the disposal structures from year 750 through year 1100, as the barrier EPM Ksat values increase (the section labeled “EPM degradation” in Figure 4-2). The modeled increase is, at most, barely discernable, implying that the barrier effect is minimal. Once the barriers are fully degraded, the saltstone Ksat controls how much water is able to pass through the disposal structures; the remainder diverts within the LLDL in the DOE model.

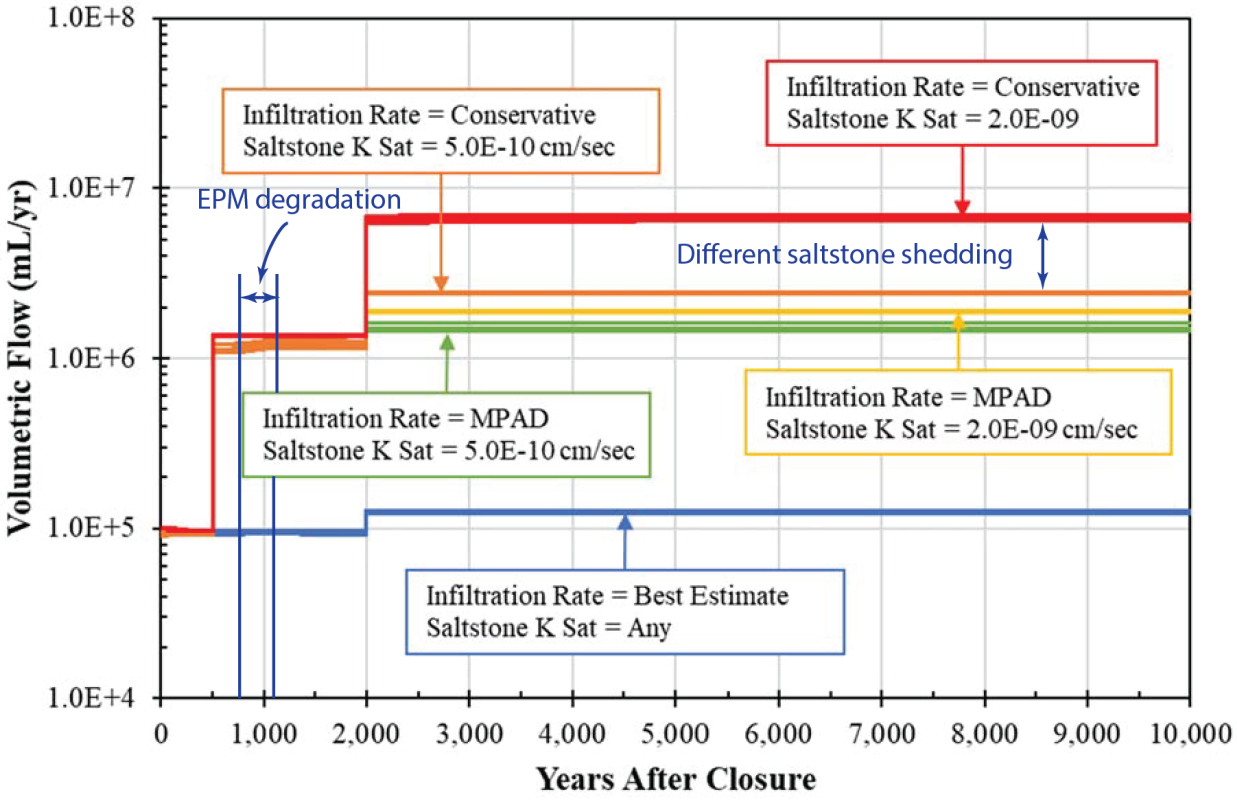

Figure 4-2: Calculated Volumetric Flow through SDS 7 for 54 Flow Cases Varying Infiltration Rate, Cementitious Degradation Rate, Backfill Ksat, and Saltstone Ksat[3]

4.1.9 Degradation of the Lateral Sand Drainage Layers

The DOE 2020 SDF PA assumed that the ULDL degrades from ingrowth of roots, but not due to infill, based on inferences in the DOE document SRRA107772-000009. The 2020 SDF PA bases hydraulic properties for the Closure Cap Model on analyses in WSRC-STI-2008-00244 (Section 4.4.1.3.4, 2020 SDF PA), developed for the 2009 Closure Cap Model. The 2009 SDF PA Closure Cap Model performance was influenced by transport of fine particles from the overlying backfill and deposition of the particles in sand drainage layers, because: (i) the perched water depth in the drainage layer is increased when silting reduces the saturated hydraulic conductivity and (ii) flow through defects is proportional to the perched water depth. Sensitivity analyses for the infiltration rate as a function of the drainage layer hydraulic

[3] The modified underlying figure is Figure 4.4-78 from the 2020 DOE PA with blue annotations indicating the timing of EPM degradation and the influence of saltstone Ksat on flow diversion in the LLDL

conductivity suggest that increasing/decreasing the saturated hydraulic conductivity by a factor of 2 gives infiltration rates that are reduced/increased by a factor of 3 (Section 5.8.3.1, 2020 SDF PA). SRRA107772-000009 dismisses the possibility that the hydraulic conductivity is affected by the addition of fine particles because: (i) the authors did not observe infilling of fines when exhuming modern final covers or analog sites, (ii) the closure cap design includes a nonwoven polymeric geotextile filter above the drainage layer, and (iii) the DOE expects that a natural filter will develop above the geotextile.

However, eliminating the reduction of the saturated hydraulic conductivity in the drainage layers requires a strong technical basis and the arguments made in SRRA107772-000009 are not in and of themselves adequate. For example, it is not clear that the visual presence of a persistent sharp interface between different layers precludes the migration of fines. Direct measurement of fines is needed to strengthen this argument.

Cumulative fine migration into a coarser medium is dependent on the cumulative number of pore volumes passing from fine to coarse, and the SDF location is designed to have large flow into the ULDL over long periods of time. The SRRA107772-000009 discussion does not address differences in cumulative pore volumes:

- The provided example of a modern cover in Nebraska was specifically designed to minimize flow into the sand layer and was only in place for 8 years. The Nebraska inflow likely represents a fraction of a year of SDF inflow.

- The Kyushu burial mound and Tu-Dun tombs described in SRRA107772-000009 are expressly designed to shed flow; the alternating layers are clay and loam (Kyushu) and clay and fine sand (Tu-Dun). It is questionable how many pore volumes penetrated the clay layers into the coarser loam and fine sand layers at these sites.

The NRC RAI Question CBs&DLs-2 in the NRC 3rd Set of RAIs (ML21341A551) requested information regarding the DOE plans for reducing the risk-significant uncertainty associated with fine-grain deposition of particles in the ULDL and the resulting reduction of performance due to this degradation. The DOE responded to RAI Question CBs&DLs-2 in the DOE 3rd Set of Responses (the DOE document SRMC-CWDA-2022-00003) by providing an evaluation of the quantities of fines, an evaluation of the flow rates from the middle backfill layer into the ULDL, and discussion on the function of the geotextile filter fabric. Based on the formation of B-horizons from the deposition of translocated clay, the DOE document SRR-CWDA-2021-00031, which the DOE provided in response to the NRC Request for Supplemental Information for the DOE 2020 PA (ML20254A003), used a rate of 25 cm (10 in) per 5,000 years to calculate how long it would take for the silting-in process to fully degrade the sand. Various times were calculated, including in the DOE response to CBs&DLs-2 in SRMC-CWDA-2022-00003. However, the rate of 25 cm (10 in) per 5,000 years was based on one source and on naturally deposited sediments with some structure. The closure cap soil will be backfilled and will have lost its structure so that the rate of translocation due to eluviation will likely differ from the one rate given in SRR-CWDA-2021-00031 and SRMC-CWDA-2022-00003. Therefore, the NRC staff did not find the projected infilling rates the DOE provided in response to the NRC Request for Supplemental Information Question RSI-2 to be sufficiently supported to answer the NRC questions about the infilling rate. That is, the NRC staff determined that the infilling rate could be greater than the range of rates the DOE considered in SRR-CWDA-2021-00031, Rev. 1.

The DOE also responded to RAI Question CBs&DLs-2 in SRMC-CWDA-2022-00003 by providing flow rates from the middle backfill layer into the ULDL. Using the Hjulström-Sundborg diagram, which illustrates the relationship between particle size and the tendency for those particles to be transported or deposited as part of streambed erosion, the critical velocity needed to initiate transport for clays in a streambed was calculated and determined to be much higher than calculated actual velocities in the middle backfill during an episodic rainfall event suggesting that clay particles will not be transported into lower closure cap layers. The DOE utilized the Hjulström-Sundborg diagram although the DOE stated that, "… this figure is not directly applicable to the subsurface conditions in the SDF closure cap…" While the SDF closure cap materials are not under the same conditions as a streambed, the information provided in the figure is used, nonetheless. The Hjulström-Sundborg plot shows several key concepts about the relationships between erosion, transportation, and deposition within a streambed. For particle sizes where friction is the dominating force preventing erosion, the curves follow each other closely and the required velocity increases with particle size. However, for cohesive sediment, mostly clay, but also silt, the erosion velocity increases with decreasing grain size, as the cohesive forces are relatively more important when the particles get smaller. This is an important fact for the vertical transport of clay particles within an engineered cover system because the soil particles in the backfill will have lost their natural depositional structure and no longer have cohesive forces. The erosion velocity will no longer need to increase, but can decrease with decreasing grain size (i.e., the erosion velocity would again decrease with decreasing grain size). In addition, the Hjulström-Sundborg plot is intended for lateral streambed particle transport and not for vertical gravity-assisted particle transport. Therefore, the authors of this TRR determined that calculated rates presented in the DOE response for CBs&DLs-2 cannot contribute to a strong technical basis supporting the exclusion of deposition within the ULDL.

The authors of NUREG/CR-7028 (ML12005A110) exhumed geotextiles and geonets for modern-day covers, describing modest amounts of soil present in many of the geotextiles and a coating of fines in some of the geonets. Geonets are used for internal drainage and are typically made of a mesh of HDPE ribs. The presence of fines coating geonet ribs is direct evidence of transport from fine soil and deposition in a coarse medium, noticeable within a few years after installation. That suggests that given a sufficient supply of fines, fines may move vertically into a geotextile filter above the ULDL and also deposit within the ULDL sand layer and reduce the hydraulic conductivity. However, fines accumulating on and above the overlying geotextile filter can also increase the filtration capability over time, thus the rate of fine migration into the ULDL can decrease over time. The DOE document WSRC-STI-2008-00244 indicated that insufficient data is available to estimate the service life of the fabric, although they did argue that colloidal clay entering the sand drainage layer would likely be carried to the exit and indicated that clean sand layers are preserved below clayey layers. Given that the sand drainage layer is intended to contain an unsaturated zone in the upper part of the layer, which may act as a natural filtration mechanism trapping clay on the upper bed, it is not clear that clay will be carried significant horizontal distances within the sand drainage layer. Furthermore, WSRC-STI-2008-00244 did not describe whether the flow direction is vertical through the clayey layer to the clean sand layer in the unsaturated zone (analogous to the closure cap configuration), or essentially horizontal parallel to bedding (typical of groundwater systems). If the system has essentially bedding-parallel flow, clay transport from fine to coarse likely to be small regardless of clay mobility.

With regard to potential fine-particle deposition within lateral sand drainage layers, the authors of this TRR recognize that it is intrinsically difficult to demonstrate that such slow infill processes will not occur over relevant time scales but do not consider the provided bases for neglecting

transport of fines to convincingly demonstrate that clay infill is unlikely or inconsequential in the ULDL. That is, the authors of this TRR recognize the great uncertainty associated with that process and also with the process of potential significant deposition above the ULDL that could significantly slow flow and transport into the drainage layer. In addition, the NRC staff also have determined that there is great uncertainty with regard to clay particle eluviation within the upper backfill (i.e., could it occur? and how a possible contribution to deposition above the erosion barrier or ULDL, or within the ULDL, could affect performance?)

Recommendation CBDL-07

Therefore, the NRC staff recommends that the NRC monitor information and activities associated with fine-particle transport and deposition within the ULDL under the new monitoring factor entitled "Long-Term HDPE/GCL Composite Barrier and Drainage Layer Degradation," which the NRC staff recommended opening in recommendation CBDL-02 under both 10 CFR 61.41 and 10 CFR 61.42.

This topic will also be discussed in the TRR on Future Scenarios and Conceptual Models (ML23017A088).

The 2020 SDF PA considered the LLDL in the Vadose Zone Flow Model and in the Airborne Pathway Release and Transport Model. In the 2009 SDF PA, FY 2013 Special Analysis Document (SRR-CWDA-2013-00062, Rev. 2), and FY 2014 Special Analysis Document (SRR CWDA-2014-00006, Rev. 2), the saturated hydraulic conductivity of the LLDL is reduced over time to account for inflow of colloidal particles into the coarser drainage layer, and eventually the drainage layer assumes the properties of the overlying backfill. Information pertaining to the conceptual model for degradation (or lack of degradation) specifically for the LLDL was not found in the 2020 SDF PA, but two sensitivity cases modified the hydraulic conductivity values for both the ULDL and the LLDL in the Vadose Zone Flow Model and Vadose Zone Transport Model (Section 5.8.3.1, 2020 SDF PA). Unfortunately, the individual effect on the dose results caused by the degraded ULDL versus the degraded LLDL were difficult to interpret and both the interdependencies and interrelationships between the two lateral sand drainage layers were difficult to recognize based on the description provided in Section 5.8.3.1.

The authors of this TRR considered the model assumption that the LLDL will have inconsequential degradation to be consistent with the very small infiltration rates calculated by the 2020 SDF PA Closure Cap Model because: (i) such small flow rates are unlikely to induce significant cumulative colloidal transport into large volumes of a sand drainage layer and (ii) roots are not expected to penetrate to the LLDL, so potential degradation from root penetration is unlikely. The authors of this TRR will revisit the LLDL model approach if the Vadose Zone Flow Model used significantly larger infiltration rates. The potential concern is that infill causes such a reduction in the drainage capability that a significant thickness of perched water exists above the roof, increasing flow through the disposal structures.

Recommendation CBDL-08

Therefore, the NRC staff recommends that the NRC monitor the modeled flow rate to and through the LLDL for significantly larger infiltration rates to determine if the LLDL modeling approach within the Vadose Zone Flow Model needs to be reevaluated under the new monitoring factor entitled "Long-Term HDPE/GCL Composite Barrier and Drainage Layer Degradation," which the NRC staff recommended opening in recommendation CBDL-02 under both 10 CFR 61.41 and 10 CFR 61.42.4.1.10 Calculation of Infiltration and Saturation in the Closure Cap Model

The authors of this TRR considered the 2020 DOE SDF PA approach of applying a 1-D vertical numerical model to estimate inflow to the drainage layer in the cover to be reasonable when unconfined conditions exist throughout the sand layer of the ULDL. This is because: (i) the very shallow slopes and uniform properties are likely to produce essentially vertical flow above the sand layer, (ii) the bottom boundary condition is isolated from the surface, and (iii) the lateral redistribution in the highly conductive ULDL drainage layer would mask any deviation from the vertical in the overlying backfill. Using the calculated inflow from the most adverse location across the entire cap is a conservative approach.

In contrast, the authors of this TRR determined that the approximation may substantially underestimate risks for some of the cases presented in the 2020 SDF PA, especially the sensitivity cases described in Section 5.8.3.1. The cases of concern arise when the ULDL becomes confined (the depth of flow completely fills the drainage layer in order to create a large enough gradient to drive flow) before reaching the outlet at the edge of the cap; the middle backfill has a much smaller hydraulic conductivity than the drainage layer, acting as a confining unit, and the constriction pressurizes the ULDL drainage layer. Pressurization may have two consequences: (i) a near-quadratic increase in flow through the defect and (ii) a perched water table existing in the overlying backfill that may limit the capacity for inflow to the backfill, thereby increasing runoff and cap erosion. The NRC staff recognized that assumed inflow rates become unrealistically large when the perched water table induces additional runoff beyond the rates assumed in the 1-D vertical model, which implies that there is a limiting flow through the defect.

The authors of this TRR constructed a one-dimensional steady-state numerical flow model to extend the analytical approach used to calculate head in the ULDL for the 2020 SDF PA. The numerical model differs from the analytical model by considering: (i) end effects at the toe of the slope and (ii) confined flow within the ULDL. The numerical model assumed that the downslope outlet has a seepage boundary condition, and the ridgeline represents a no-flow boundary. The seepage condition assumes that the water table is parallel to the ULDL whenever the perched water table is below the top of the ULDL (i.e., essentially the same solution as the analytic approach); otherwise, the layer is assumed fully saturated at the boundary and the pressure is set to atmospheric. For each grid cell, the water balance equation is

$$wb_2q_2 = wb_1q_1 + Aq_d \tag{3-4}$$

$$q = -K\frac{dh}{dx} \tag{3-5}$$

$$b = \min(B, h - z) \tag{3-6}$$

where q is the Darcy flux, q_d is drainage into the ULDL, h is head, b is flow depth, B is ULDL thickness, K is ULDL saturated hydraulic conductivity, z is the elevation of the ULDL base, w is the width of the flow path, and A is the area of the drainage inflow to the grid cell. A comparison value for infiltration was calculated using Equation 4.4-4 from the 2020 SDF PA with head from the CNWRA numerical model.

Table 5.8-10 of the 2020 SDF PA provided recommended infiltration rates based on assumed ULDL properties. For the Compliance Case, the ULDL saturated hydraulic conductivity was assumed to be 0.05 cm/s (0.02 in/s) initially, which is assumed to drop by a factor of five after 500 years. The degradation of the HDPE geomembrane, represented by an enlargement of the initial defect size from 2 to 10 mm (0.08 to 0.4 in), is assumed to occur at 2,000 years.

Table 5.8-10 provides the same sequence for two additional sensitivity cases (in addition to the Compliance Case), in which the initial saturated hydraulic conductivity is larger or smaller by a factor of two but the same degradation takes place, resulting in a set of nine calculated infiltration rates (three time periods [from 0-500 years; 500-2000 years; and 2000+ years to cover changes in the size of the defects and change in the ULDL saturated hydraulic conductivity] for each of three initial ULDL saturated hydraulic conductivities). All of the cases in Table 5.8-10 of the 2020 SDF PA assume an inflow of 400 mm/yr (16 in./yr) to the ULDL and calculate average infiltration assuming five defects per hectare.

The numerical model was run by the DOE for each of the nine combinations plus the same combinations with an increased inflow (650 mm/yr [26 in./yr]), with the cases reported in **Error! Reference source not found.**. Selected combinations from **Error! Reference source not found.** are displayed in **Error! Reference source not found.**4-3. The higher inflow rate is the assumed upper bound for average inflow. The calculations presented for the 2020 SDF PA suggest that this inflow rate is not unusual for wet years, as it was calculated in each of the four out of ten years in the representative wet decade that had at least 1,400 mm (55 in) of precipitation. Eleven out of 53 years in the period of record exceeded 1,400 mm (55 in), so the higher inflow rate would be expected regularly; three of these years had larger precipitation than any year in the wet decade. Figure 4.4-7 of the 2020 SDF PA suggested that there may be significant seasonal variability in inflow, which would also result in occasional seasonal inflow rates >650 mm/yr (>26 in./yr) (e.g., during wet winter months).

Error! Reference source not found.4-3 illustrates the numerical model results for all combinations of two inflow rates to the ULDL (400 and 650 mm/yr [16 and 26 in./yr]), two ULDL hydraulic conductivity multipliers (1 and 0.2), and two slope distances (183 and 356.6 m [600 and 1170 ft]). Because most of the closure cap has a shorter slope length than the 356.6 m (1170 ft) assumed in the 2020 SDF PA, a more typical slope length of 183 m (600 ft) is provided for comparison. A vertical gray line in **Error! Reference source not found.** 4-3 indicates the end of the 183-m (600-ft) domain.

Error! Reference source not found.4-3a shows the infiltration rate that the Giroud (1997) equation would provide for a 2-mm (0.08-in) defect at the calculated water table thickness at each slope location (assuming no other defects exist), scaled to the area of 5 defects/ha. The left axis indicates the infiltration rate with the GCL hydraulic conductivity representing a new GCL (10^{-9} cm/s [$4x10^{-10}$ in/s]); the right axis indicates the infiltration rate for the identical assumptions except that the GCL is highly degraded (2×10^{-5} cm/s [$8x10^{-6}$ in/s], approximately the average GCL-only hydraulic conductivity in
Figure). The location of the peak calculated infiltration is indicated with a symbol, which is echoed on the left and right axes for simulations with a fully unconfined perched water table. **Error! Reference source not found.**4-3b from the 2021 CNWRA report (ML21287A328) shows the head in the ULDL at each location of the slope, represented as the equivalent water table thickness, given the provided inflow rate with no losses through defects. The ULDL is fully saturated (i.e., the perched water table is confined) where the curves indicating infiltration and water table thickness are dotted. In common with the 2020 SDF PA approach, the calculated infiltration value does not account for infiltration losses through other defects and the calculated head value does not account for the local gradients near the defect. The calculated infiltration value can be larger than the assumed inflow rates under confined conditions, because confined conditions allow upslope flow and the area for scaling is much smaller than the cap area.

The DOE approximation for flow depth and the numerical model compare closely for cases with the ULDL saturated hydraulic conductivity is at least as large as the Compliance Case value,

with the numerical model calculating a slightly different maximum infiltration because of the outlet boundary condition (see **Error! Reference source not found.**). However, the numerical model calculates increasingly larger infiltration rates as the ULDL saturated hydraulic conductivity becomes smaller. The infiltration rates increase dramatically if the ULDL becomes confined before the end of the cap (a confined zone is indicated by dotted lines), which also moves the location of the peak infiltration towards the center of the cap (see **Error! Reference source not found.**4-3). The calculated infiltration rate with the numerical model is more than 80 times larger than the values in Table 5.8-10 for the Compliance Case values after 500 years (i.e., the ULDL saturated hydraulic conductivity decreases by a factor of 5); increasing the inflow rate to the ULDL from 400 to 650 mm/yr (16 to 26 cm/yr) increases the infiltration four-fold.

Confined conditions occur even with the shorter slope, with the smaller hydraulic conductivity, resulting in peak infiltration values much larger than used in the 2020 SDF PA.

Table 4-1: Comparison of Calculated Maximum Infiltration Rates between Numerical Water Balance Model and 2020 SDF PA Table 5.8-10 (assuming 5 defects/ha and a 356.6-m (1170 ft) domain)

Time Period (years)	ULDL Ksat* Multiplier	Defect Diameter (mm)	Inflow to Sand Layer (mm/yr)			Ratio of Numerical Model to DOE Table 5.8-10 Infiltration Rate [q_d = 400 mm/yr]
			Water Balance (q_d = 400 mm/yr)†	Water Balance (q_d = 650 mm/yr)	Table 5.8-10 (q_d = 400 mm/yr)	
Compliance Case						
0–500	1	2	0.0062‡	0.022‡	0.006	1.04
500–2,000	1/5	2	8.2§	33§	0.091	90.0
>2,000	1/5	10	11‡,§	45‡,§	0.13	86.9§
Compliance Case Except with Doubled Sand Layer Saturated Hydraulic Conductivity						
0–500	2	2	0.0023	0.0046§	0.0021	1.11
500–2,000	2/5	2	0.47§	4.1§	0.027	17.3
>2,000	2/5	10	0.64§	5.6§	0.037	17.4
Compliance Case Except with Halved Sand Layer Saturated Hydraulic Conductivity						
0–500	1/2	2	0.11§	1.7§	0.019	5.84
500–2,000	1/10	2	55§	170§	0.31	176
>2,000	1/10	10	75§	230§	0.43	175

*Ksat is saturated hydraulic conductivity
†q_d is inflow to the ULDL
‡These scenarios provide the inflow rates and sand layer hydraulic conductivities considered in **Error! Reference source not found.**
§Numerical model calculates a confined zone in the ULDL perched water

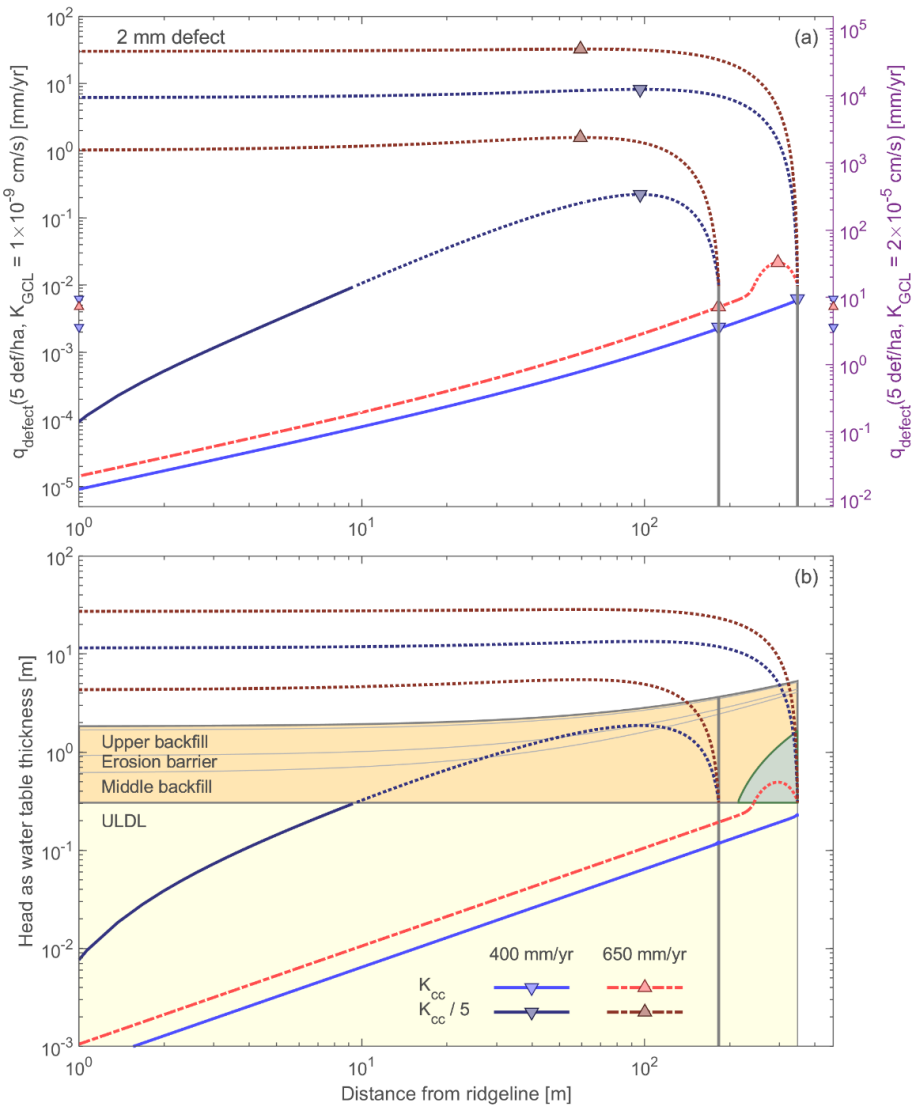

Figure 4-3: Calculated: (a) infiltration rate and (b) head (as perched water table thickness) representing the initial (0–500 years) and fully degraded (>2000 years) Compliance Case property sets in Table 4-1[4]

[4] Each property set is considered for all combinations of two slope lengths (183 and 356.6 m [600 and 1170 ft.]) and two infiltration rates (400 and 650 mm/yr [16 and 26 in./yr]). In (a), the symbols mark the point with maximum infiltration, calculated assuming a GCL hydraulic conductivity representative of a new or degraded GCL at the defect location (left and right axis, respectively). The degraded GCL represents the average GCL-only sample from Figure 3-7. Symbols with internally consistent simulation assumptions are copied onto the axis to provide reference scales. The dark yellow zone in (b) represents layers of backfill above the sand layer in the ULDL, and the greenish gray zone represents areas below a potential maximum 3.66 m (12 ft.) rooting depth. Curves above the light-yellow zone indicate an area where the ULDL is confined, and curves above the dark yellow zone indicate an area where the perched water table would rise above the ground surface.

The largest calculated infiltration rates using the numerical model may not be realistic, because the implied perched water table is located in the backfill above the ULDL or above the ground surface wherever the ULDL becomes confined. An elevated perched water table is inconsistent with the vertical 1-D inflow calculation assumption of a free drainage condition into the sand drainage layer and may interfere with infiltration by reducing soil moisture storage capacity during rainfall events. If the calculated perched water table is above the ground surface, then the assumed inflow to the ULDL is clearly too large, so that water would be forced to pond on the surface or run off instead of infiltrating. Increased runoff implies that there is a potential for increased erosion. The numerical model results suggested that this condition may occur during wet years if the ULDL saturated hydraulic conductivity is just a factor of two smaller than the Compliance Case value (e.g., bottom rows in **Error! Reference source not found.**). It is primarily for this reason that the priority of MF 2.02 will be increased in NRC's TRR entitled Percolation Through and Potential Erosion near the Closure Cap (ML23017A083).

Seasonable variability also may substantially influence annual-average infiltration. For example, assuming that annual inflow is 400 mm/yr (16 in./yr), with half of the year at the average rate and a quarter each at 250 mm/yr (9.8 in./yr) higher (650 mm/yr [26 in./yr] in "winter") or lower (150 mm/yr [5.9 in./yr] in "summer"). For the example case in **Error! Reference source not found.**, the "summer" infiltration is at the rate of 0.0035 mm/yr (1.4×10^{-4} in./yr). Averaging the seasonal infiltration yields 0.45 mm/yr (0.018 in./yr), which is 4.8 times larger than the infiltration with the annual-average inflow. Seasonal inflow is likely to be substantially larger than 650 mm/yr (26 in./yr) in wet years.

The NRC RAI Question CBs&DLs-8 in the NRC 3rd Set of RAIs (ML21341A551) requested information regarding the ULDL to determine whether the ULDL could plausibly become confined and, if it could, whether a confined ULDL will lead to a risk-significant increase in the infiltration rate below the ULDL barrier and to the LLDL. The current design of the SDF cover has typical maximum slope length of approximately 183 m (600 ft.) and one slope length is approximately 311 m (1020 ft.). The RAI Question CBs&DLs-8 raised a concern about the potential for water levels rising above the drainage layer. The calculations with the SDF drainage layer material and thickness suggest that this is a potential concern for the part of the cover with slopes longer than 183 m (600 ft.) especially for those relatively long slopes reaching 311 m (1020 ft.). The DOE responded to RAI Question CBs&DLs-8 in the DOE 3rd Set of Responses (the DOE document SRMC-CWDA-2022-00003) by providing information on recently constructed engineered surface covers located on Cape Breton Island in Nova Scotia, Canada constructed over waste rock piles from mining activities. The covers at Lingan, Summit, Victoria Junction, and Franklin have similar precipitation, but less evapotranspiration than the SRS site. The Summit and Victoria Junction sites are most similar to the SDF. The Lingan site has no drainage layer, and the Franklin site is very small and steep, so these are not comparable. Estimated maximum slope lengths are approximately 366 m (1200 ft.) and less than 183 m (600 ft.) for the Summit and Victoria Junction sites, respectively. The Victoria Junction site is the most similar in design to the SDF closure cap, both have the same side slope angle and include a lateral drainage layer; however, the Victoria Junction site has a thicker drainage layer than the SDF cover and is it composed of gravel which has a higher hydraulic conductivity than sand. This results in the Victoria Junction drainage layer having a greater capacity than the SDF drainage layer. In addition, none of the slopes at the Victoria Junction site are as long as those on the planned SDF cover, and the resulting percolation through the HDPE geomembrane layer is approximately 5 mm/yr (0.2 in./yr).

The Summit site is more similar to the SDF closure cap based on size of the cover and the risk-significant slope lengths and could provide insight into the potential head if the planned SDF

cover system did not include a lateral drainage layer or if the drainage layer becomes silted-in. The DOE stated in SRMC-CWDA-2022-00003 that measured heads above the HDPE for the Summit site typically ranged between 50 cm and 65 cm (20 in. and 26 in.) and sometimes exceeded 70 cm (28 in.). The Summit site has only 50 cm (20 in) of backfill above the HDPE layer Given the relatively thin backfill, and that this site does not include a drainage layer, it has been observed to become waterlogged at various times throughout the year indicating that the water level had risen as high as physically possible, and that surface runoff was occurring.

The NRC RAI Question CBs&DLs-8 (ML21341A551) also described the results of modeling in the CNWRA Report (ML21287A328) that showed that confined conditions can occur when the ULDL hydraulic conductivity decreases resulting in increased infiltration rates. The DOE RAI Question CBs&DLs-8 Response stated that the CNWRA modeling results are an artifact of the conservative modeling approach used and do not reflect actual expected conditions. The response concluded that while the one-dimensional CNWRA modeling approach provides a defensible estimate of leakage rates through the HDPE and GCL composite barrier, it does not provide an accurate reflection of the expected head above the HDPE that occur under normal field conditions. However, the DOE did not attempt to demonstrate how closely the one-dimensional modeling results matched the data at the sites nor use a two-dimensional model to demonstrate that two-dimensional flow will prevent pressurization. Although it must be emphasized that the results of the CNWRA one-dimensional modeling did not pertain to the entire cover, but rather those areas associated with longer surface slopes where the thickness of the ULDL appeared to be insufficient.

The authors of this TRR suggest that the 2020 SDF PA calculations related to infiltration may not be applied consistently with their theoretical underpinnings:

- The flow system may have very different behavior when the perched water table is confined instead of unconfined. Once the threshold creating a confined system is crossed, there is a dramatically increased potential for elevated infiltration, elevated surface runoff, and elevated cap surface erosion.

- The ULDL hydraulic conductivity is an important parameter for calculating infiltration. A small uncertainty in this parameter appears to have potentially large consequences for infiltration, surface runoff, and closure cap erosion.

- The inflow to the ULDL has a large influence on whether the ULDL perched water table becomes confined when the water table nearly fills the ULDL. It may be more appropriate to consider seasonal and interannual variability in inflow when calculating total infiltration and designing the ULDL.

The DOE considered flow through the composite barrier with the assumption of complete failure of the HDPE geomembrane in SRR-CWDA-2021-00040. Instead of using the Giroud (1997) relationship for flow through a defect, after complete failure, the model approach uses Darcy's Law, as modified by Rowe (2012), driven by head loss across the GCL and underlying layers. The approach accounts for the local thickness of the subsoil below the liner (i.e., below the GCL) in calculating the head loss. In essence, the head loss across the GCL was closely related to the head above the GCL plus the elevation difference between ULDL GCL and the HDPE geomembrane above the roof of the disposal structure. What this approach implies is that inflow rates could be larger across the ULDL GCL at the center of the closure cap (with a thick lower backfill) than at the edge of the cover (with a relatively thin lower backfill) if the thickness of perched water level in the ULDL above the GCL were equal.

Due to the considerations discussed above, the NRC staff determined that the future occurrence of confined conditions in some portion of the ULDL is plausible.

Recommendation CBDL-09

Therefore, the NRC staff recommends that the NRC monitor information and activities associated modeled confined conditions within the ULDL under the new monitoring factor entitled "Potential Confined Conditions in the ULDL" under both 10 CFR 61.41 and 10 CFR 61.42.

5.0 Teleconference or Meeting

There were no teleconferences or meetings with the DOE related to this TRR.

6.0 Follow-up Actions

There are no specific Follow-up Actions related to this TRR. The NRC staff will continue to monitor groundwater and far-field modeling under the MFs listed below in Section 7.

7.0 Conclusions

The NRC staff evaluated the DOE's technical bases for modeled performance of the HDPE geomembrane, HDPE/GCL composite barriers, the lateral sand drainage layers, especially the ULDL, in the 2020 SDF PA. After evaluating the technical bases provided by the DOE, the NRC staff determined that the calculations and models used to calculate and simulate flow rates into the lower backfill through the ULDL barrier is not adequate for modeling the projected dose from the SDF for the purpose of the DOE demonstrating compliance with the 10 CFR 61.41 and 10 CFR 61.42. The NRC staff made that determination because a number of plausible degradation processes that affect long-term performance of the ULDL barrier, especially long-term processes with the potential to degrade the GCL, were not included or used to calculate or simulate flow rates through the ULDL barrier and into the lower backfill in the SDF PA to determine compliance. Although sensitivity analyses involving the DOE's central scenario and current conceptual model have shown performance that demonstrate compliance, there are other potentially plausible future scenarios and alternative conceptual models (see NRC TRR on Future Scenarios and Conceptual Models [ML23017A088]), where the DOE PA results may have trouble demonstrating compliance given the significant uncertainty associated with composite barrier and drainage layer performance. In addition, the NRC staff considers confined conditions in the planned ULDL located in the lower portions at the end of long slope lengths to be plausible. Such conditions would cause saturated conditions to occur above the ULDL with potentially detrimental results for the stability of the site and the health of the flora (relevant for transpiration) growing on the closure cap surface. Finally, the NRC staff determined that long-term performance of the composite barrier layers relies heavily on a QA/QC component to ensure future emplacements and installations are managed and executed at a very high standard. Holes, tears, rips, and wrinkles need to be identified and repaired in such a way as to minimize reduction in long-term performance. The NRC staff needs to monitor the DOE QA/QC program to ensure that the DOE implementation and execution of risk-significant components will reduce or bound risk-significant uncertainty. Therefore, the NRC staff have developed several new MFs (see below) and will make a final determination on demonstrating compliance when the Closure Cap design and construction is finalized.

The NRC staff determined that the calculations and models used to calculate and simulate flow rates through the LLDL, and mud-mat barriers is adequate for modeling the projected dose from the SDF for the purpose of the DOE demonstrating compliance with the 10 CFR 61.41 and 10 CFR 61.42 in the 2020 SDF PA. The NRC staff made that determination because the technical basis and justification associated with those features is sufficient in relation to their significance to performance. As simulated and presented in the 2020 SDF PA, the ULDL barrier is the dominant barrier that reduces flow between the upper and lower portions of the closure cap (i.e., the input and output of the Closure Cap Model) by many orders of magnitudes. As such, the LLDL and mud-mat barriers are best seen as backup barriers; however, if the compliance cases should change to include significant flow through the LLDL barrier and significant surface area of saltstone being exposed to fast pathways through the disposal structures, then the adequacy of these barriers for modeling the projected dose from the SDF would need to be reassessed.

The future monitoring recommendations made by the NRC staff in Sections 4.1.2, 4.1.3, 4.1.4, 4.1.5, 4.1.6, 4.1.7, 4.1.9, and 4.1.10 in this TRR have been compiled and incorporated in three new MFs as described below:

Recommendations CBDL-01, CBDL-03, CBDL-04, and CBDL-05,
Confidence in Quality Assurance/Quality Control for HDPE/GCL Composite Barrier and Drainage Layer Installation

- The NRC staff recommends opening a new high-priority monitoring factor entitled "Confidence in Quality Assurance/Quality Control for HDPE/GCL Composite Barrier and Drainage Layer Installation" under MA 2 (Infiltration and Erosion Control) under the performance objectives of §61.41 and §61.42 due to the importance of proper composite barrier and drainage layer installation in the closure cap. The NRC staff expects to close the new monitoring factor when the NRC staff has observed the installation of portions of the ULDL HDPE/GCL composite barrier and the ULDL in both of the planned engineered surface covers of the SDF. In addition, the NRC staff will observe HDPE repairs carried out on defects and cuts, and the installation of the composite barrier layers above the roof and the lower mud mat, and of the LLDL, for those disposal structures the NRC staff deems to be risk significant. Also, the NRC staff will monitor that the initial GCL hydraulic conductivity value used in the PA modeling is comparable to the given value of the GCL manufacturer once that information is definitively known and independently verified.

Recommendations CBDL-02, CBDL-06, CBDL-07, and CBDL-08
Long-Term HDPE/GCL Composite Barrier and Drainage Layer Degradation

- The NRC staff recommends opening a new high-priority monitoring factor entitled "Long-Term HDPE/GCL Composite Barrier and Drainage Layer Degradation" under MA 2 (Infiltration and Erosion Control) under the performance objectives of §61.41 and §61.42 due to the importance of composite barrier and drainage layer performance in the closure cap. The NRC staff expects to close the new monitoring factor when the NRC staff has confidence that HDPE degradation in the heat-affected zones near welded seams and at edges, HDPE degradation due to root penetration, GCL degradation due to HDPE defects, and drainage layer degradation due to diminishing hydraulic conductivity will not occur or adversely affect performance (i.e., dose). In addition, the NRC staff will monitor the modeled flow rate through the LLDL barrier for significantly larger infiltration rates so as to determine if the LLDL barrier modeling approach within the Vadose Zone Flow Model needs to be reevaluated.

Recommendation CBDL-09

Potential Confined Conditions in the ULDL

- The NRC staff recommends opening a new high-priority monitoring factor entitled "Potential Confined Conditions in the ULDL" under MA 2 (Infiltration and Erosion Control) under the performance objectives of §61.41 and §61.42 due to the importance of drainage layer performance in the closure cap. In addition to the processes creating potential confined conditions within the cover, the NRC staff will monitor variations in the modeled infiltration rates between the center and the edges of the closure cap. The NRC staff expects to close the new monitoring factor when the NRC staff has confidence that confined conditions in the ULDL will not occur or adversely affect performance (i.e., dose).

8.0 References

Abdelaal, F.B., and R.K. Rowe. "Effect of high pH found in low-level radioactive waste leachates on the antioxidant depletion of a HDPE geomembrane." *Journal of Hazardous, Toxic, and Radioactive Waste*. Vol 21, No 1. D4015001, DOI: 10.1061/(ASCE)HZ.2153-5515.0000262. 2017. https://ascelibrary.org/doi/full/10.1061/%28ASCE%29HZ.2153-5515.0000262

Beck, A. "Available Technologies to Approach Zero Leaks." In Proceedings of Geosynthetics 2015, Portland, Oregon. pp. 38–47, 2015.

Benson, C.H., I.E. Kucukkirca, and J. Scalia. "Properties of Geosynthetics Exhumed from a Final Cover at a Solid Waste Landfill." *Geotextiles and Geomembranes*. Vol 28, No 6. pp. 536-546, DOI:10.1016/j.geotexmem.2010.03.001. 2010. https://www.researchgate.net/publication/223594633_Properties_of_geosynthetics_exhumed_from_a_final_cover_at_a_solid_waste_landfill

Bonaparte, R. and B.A. Gross. "LDCRS Flow from Double-Lined Landfills and Surface Impoundments." Washington. DC: U.S. Environmental Protection Agency. 1993. https://nepis.epa.gov/Exe/ZyPURL.cgi?Dockey=30002TE7.TXT

Center for Nuclear Waste Regulatory Analyses (CNWRA), *Technical Report: Performance of HDPE Geomembrane Layers, Composite Barrier Layers, and Lateral Sand Drainage Layers of the 2020 Saltstone Disposal Facility Performance Assessment*. Stuart Stothoff, San Antonio, Texas, September 2021. ML21287A328

Colucci, P., and Lavagnolo, M.C. (1995). *Three years field experience in electrical control of synthetic landfill liners*. In Proceedings of the Fifth International Landfill Symposium, October 2-6, Cagliari, Italy, T.H. Christensen, R. Cossu, and R. Stegmann, eds. Environmental Sanitary Engineering Centre, Cagliari, Italy, pp. 437-452.

Forget, B., A.L. Rollin, and T. Jacquelin. "Lessons Learned from 10 Years of Leak Detection Surveys on Geomembranes." In Proceedings of the Sardinia Conference 2005, Sardinia, Italy. 2005. http://leak-location-alphard.com/assets/img/lessons-learned-from-10-years-of-leak-detection-surveys-on-geomembranes.pdf

Gilson-Beck, A. "Controlling Leakage Through Installed Geomembranes Using Electrical Leak Location." *Geotextiles and Geomembranes*. Vol 47, No 5. pp. 697–710. 2019.

Giroud, J.P. “Equations for Calculating the Rate of liquid Migration Through Composite Liners Due to Geomembrane Defects, Special Issue on Liquid Migration Control Using Geosynthetic Liner Systems.” *Geosynthetics International*. Vol 4, Nos. 3–4. pp. 335–348. 1997. https://www.icevirtuallibrary.com/doi/abs/10.1680/gein.4.0097

Giroud, J. and R. Bonaparte. “Leakage Through Liners Constructed with Geomembranes—Part I.” *Geotextiles and Geomembranes*. Vol 8, No. 1. pp. 27–67. DOI 10.1016/0266-1144(89)90009-5. 1989. ML18215A331

Joshi, P., R.K. Rowe, and R.W.I. Brachman. “Physical and Hydraulic Response of Geomembrane Wrinkles Underlying Saturated Fine Tailings.” *Geosynthetics International.* DOI: 10.1680/jgein.16.00017. 2016. https://www.icevirtuallibrary.com/doi/10.1680/jgein.16.00017

Kavazanjian, E., J. Andresen, and A. Gutierrez. “Experimental evaluation of HDPE Geomembrane Seam Strain Concentrations.” *Geosynthetics International.* Vol 24, No 4. pp. 333–342. 2017. https://www.icevirtuallibrary.com/doi/10.1680/jgein.16.00017

Needham A., E. Gallagher, I. Peggs, G. Howe, and J. Norris. “The Likely Medium to Long-Term Generation of Defects in Geomembrane Liners.” R&D Technical Report P1-500/1/TR. Bristol, England: Environment Agency. 2004. ML12185A058

Nosko, V. and N. Touze-Foltz. “Geomembrane Liner Failure: Modelling of Its Influence on Contaminant Transfer.” Proceedings of the Second European Geosynthetics Conference, Pàtron Editore, Bologna, Italy. pp 557–560. 2000. https://library.geosyntheticssociety.org/proceedings/2-06-geomembrane-liner-failure-modelling-of-its-influence-on-contaminant-transfer-pdf/

Peggs, I.D. and J.P. Giroud. “Action Leakage Rate for Reservoir Geomembrane Liners.” 10th International Conference on Geosynthetics, ICG 2014, 21–2, 21–25 September 2014.

Rowe, R.K. “Geosynthetics and the Minimization of Contaminant Migration Through Barrier Systems Beneath Solid Waste.” In: Proceedings of the 6th International Conference on Geosynthetics, Atlanta, GA, 25–29 March. Vol. 1. St. Paul, Minnesota: Industrial Fabrics Association International. pp. 27–103. 1998. https://www.researchgate.net/publication/291698097_Geosynthetics_and_the_minimization_of_contaminant_migration_through_barrier_systems_beneath_solid_waste

Rowe, R.K., “Long-term performance of contaminant barrier systems,” Géotechnique, Volume 55 (9), pp. 631-678, November 2005. DOI: 10.1680/geot.2005.55.9.631 https://www.icevirtuallibrary.com/doi/abs/10.1680/geot.2005.55.9.631

Rowe, R.K., “Short- and Long-Term Leakage through Composite Liners,” Canadian Geotechnical Journal, Vol. 49 (2012), pp. 141-169, January 2012. DOI:10.1139/T11-092 https://cdnsciencepub.com/doi/10.1139/t11-092

Rowe, R.K. and M. Shoaib. “Long-Term Performance HDPE Geomembrane Seams in MSW Leachate.” *Canadian Geotechnical Journal*. Vol 54, No. 12. pp. 1,623–1,636. 2017. DOI: 10.1139/cgj-2017-0049. https://cdnsciencepub.com/doi/10.1139/t11-092

Rowe, R.K. and M. Shoaib. “Durability of HDPE Geomembrane Seams Immersed in Brine for Three Years.” *Journal of Geotechnical and Geoenvironmental Engineering*. Vol 144, No. 2. 2018.

DOI: 10.1061/(ASCE)GT.1943-5606.0001817.
https://ascelibrary.org/doi/full/10.1061/%28ASCE%29GT.1943-5606.0001817

Rowe, R.K., L. Bostwick, and R. Thiel. “Shrinkage Characteristics of Heat-Tacked GCL Seams.” *Geotextiles and Geomembranes*. Vol 28, No. 4. pp. 352–359. 2010.
DOI: 10.1016/j.geotexmem.2009.11.001. 2010.
https://www.sciencedirect.com/science/article/abs/pii/S0266114409001253

Rowe, R.K., P. Joshi, R.W.I. Brachman, and H. McLeod. “Leakage Through Holes in Geomembranes Below Saturated Tailings.” *Journal of Geotechnical and Geoenvironmental Engineering*. Vol 143, No. 2. 2019.
DOI: 10.1139/cgj-2019-0572. 2019
https://www2.deq.idaho.gov/admin/LEIA/api/document/download/3633

Rowe, R.K., D. Priyanto, and R. Ponnan. “Factors Affecting the Service-life of HDPE Geomembranes in an LLW Disposal Facility.” WM2019 Conference, March 3–7, 2019, Phoenix, Arizona, USA. 2019.
http://www.geoeng.ca/members/Rowe/Rowe%20et%20al%20SI%20of%20HDPE%20in%20LLW%20WM%20Symp%202019.pdf

Rowe, R.K., Rimal, S., and Sangam, H., (2009), *Ageing of HDPE geomembrane exposed to air, water and leachate at different temperatures*, Geotextiles and Geomembranes, Vol. 27 (2009), pp. 137-151, April 2009.
DOI: 10.1016/j.geotexmem.2008.09.007. 2009.
https://www.academia.edu/9825429/Ageing_of_HDPE_geomembrane_exposed_to_air_water_and_leachate_at_different_temperatures

Scalia, J. and C. Benson. “Hydraulic Conductivity of Geosynthetic Clay Liners Exhumed from Landfill Final Covers with Composite Barriers.” *Journal of Geotechnical and Geoenvironmental Engineering.* Vol 137, No. 1. pp.1–13. 2011.
https://www.researchgate.net/publication/245294865_Hydraulic_Conductivity_of_Geosynthetic_Clay_Liners_Exhumed_from_Landfill_Final_Covers_with_Composite_Barriers

Scalia, J., C.H. Benson, W.H. Albright, B.S. Smith, and X. Wang. “Properties of Barrier Components in a Composite Cover after 14 Years of Service and Differential Settlement.” *Journal of Geotechnical and Geoenvironmental Engineering.* Vol 143, No. 9. 2017.
DOI: 10.1061/(ASCE)GT.1943-5606.0001744. 2017.
https://ascelibrary.org/doi/10.1061/%28ASCE%29GT.1943-5606.0001744

Schweitzer, P.A. *Corrosion Resistance Tables, Vol. 1-4.* 5th Ed. New York City, New York. Marcel Dekker. 2004. https://openlibrary.org/books/OL3382028M/Corrosion_resistance_tables

South Carolina Department of Natural Resources. “Longleaf Pine (Pinus palustris).” 2020.
https://www.dnr.sc.gov/marine/mrri/acechar/speciesgallery/Plants/LongleafPine/index.html

Thiel, R., and C. Thiel. “GCL Shrinkage: A Possible Solution.” *Geosynthetics*. Vol 27, No. 1. pp. 10–21. 2009. https://www.cetco.com.au/Left-Side-Navigation/Lining-Technologies/Technical-Data?EntryId=8153&Command=Core_Download

Tian, K., C. Benson, J. Tinjum, and T. Edil. “Antioxidant Depletion and Service Life Prediction for HDPE Geomembranes Exposed to Low-Level Radioactive Waste Leachate.” *Journal of Geotechnical and Geoenvironmental Engineering.* Vol 143, No. 6. 2017. DOI 10.1061/(ASCE)GT.1943-5606.0001643. 2017. https://ascelibrary.org/doi/10.1061/%28ASCE%29GT.1943-5606.0001643

U.S. Bureau of Reclamation, *Design Standards No. 13, Embankment Dams, Chapter 20: Geomembranes*. DS-13(20)-16.1: Phase 4 (Final), 2018. https://www.usbr.gov/tsc/techreferences/designstandards-datacollectionguides/finalds-pdfs/DS13-20.pdf

U.S. Department of Agriculture, *History and current condition of longleaf pine in the Southern United States*. Oswalt, Christopher M. and Cooper, Jason A. and Brockway, Dale G. and Brooks, Horace W. and Walker, Joan L. and Connor, Kristina F. and Oswalt, Sonja N. and Conner, Roger C., U.S. Department of Agriculture Forest Service, Southern Research Station, 2012. https://www.srs.fs.usda.gov/compass/2013/01/15/longleaf-pine-forests-in-the-south-past-and-future/

U.S. Department of Defense. *Unified Facilities Guide Specifications UFSG 02 56 15 Geosynthetic Clay Liner (GCL)*. 2010. https://www.wbdg.org/FFC/DOD/UFGS/UFGS%2002%2056%2015.pdf

U.S. Department of Energy (DOE), DOE M 435.1-1, Chg. 3, DOE Manual 435.1-1 Change 3, *Limited Change to DOE Manual 435.1-1 Change 3 – Radioactive Waste Management Manual*, January 11, 2021. ML21035A232

_____, C-SPP-Z-00019, Rev. 0, *Saltstone Disposal Unit (SDU) 8&9: GCL, HDPE Geomembrane, Specification*, April 2019. ML20206L006

___, SRR-CWDA-2009-00017, Rev 0, *Performance Assessment for the Saltstone Disposal Facility at the Savannah River Site*, 2009. ML101590008

___, SRR-CWDA-2013-00062, Rev. 2, *Fiscal Year 2013 Special Analysis for the Saltstone Disposal Facility at the Savannah River Site*, October 2013. ML14002A069

___, SRR-CWDA-2014-00006, Rev. 2, *Fiscal Year 2014 Special Analysis for the Saltstone Disposal Facility at the Savannah River Site*, September 2014. ML15097A366

___, SRR-CWDA-2014-00070, Rev. 0, *Evaluation of Potential Breach of Side Wall High Density Polyethylene (HDPE) Liner on Saltstone Disposal Unit Cell 3A*, July 2014. ML14322A315

___, SRR-CWDA-2014-00099, Rev. 1, *Comment Response Matrix for NRC Staff Request for Additional Information on the Fiscal Year 2013 Special Analysis for the Saltstone Disposal Facility at the Savannah River Site*, January 2015. ML15020A672

___, SRR-CWDA-2016-00004, Rev. 1, *Comment Response Matrix for NRC Staff Request for Additional Information on the Fiscal Year 2014 Special Analysis for the Saltstone Disposal Facility at the Savannah River Site*, March 2016. ML16105A043

___, SRR-CWDA-2019-00001, *Performance Assessment for the Saltstone Disposal Facility at the Savannah River Site*, March 2020. ML20190A056

___, SRR-CWDA-2021-00031, Rev. 1, *Closure Cap Model Parameter Evaluation: Saturated Hydraulic Conductivity of Sand*, May 2021. ML21160A061

___, SRR-CWDA-2021-00033, Rev. 1, *Closure Cap Model Parameter Evaluation: High Density Polyethylene (HDPE) and Geosynthetic Clay Liner (GCL) Composite Barrier Performance*, May 2021. ML21160A062

___, SRR-CWDA-2021-00040, *Evaluation of the Uncertainties Associated with the SDF Closure Cap and Long-Term Infiltration Rates*, June 2021. ML21160A064

___, SRR-CWDA-2021-00065, *Response to NRC Request for Supplemental Information #8: Upper Three Runs Aquifer - Upper Aquifer Zone Lateral Flow Analysis*, August 2021. ML21217A082

___, SRMC-CWDA-2022-00003, *Comment Response Matrix for the Third Set of U.S. Nuclear Regulatory Commission Staff Requests for Additional Information on the Performance Assessment for the Saltstone Disposal Facility at the Savannah River Site*, March 2022. ML22083A049

___, SRMC-CWDA-2022-00016, *Comment Response Matrix for the Fourth Set of U.S. Nuclear Regulatory Commission Staff Requests for Additional Information on the Performance Assessment for the Saltstone Disposal Facility at the Savannah River Site,* April 2022. ML22026A397

___, SRMC-CWDA-2022-00025, Rev. 3, *Leak Rate Considerations Related to the SDU 6 Sumps,* June 2022. ML22189A149

___, SRR-CWDA-2021-00066, *Evaluation of the Combined Uncertainties Associated with the Long-Term Performance of Saltstone Disposal Facility Flow Barriers*,2021. ML21217A083

___, SRRA107772-000009, *Predicting Long-Term Percolation from the SDF Closure Cap*, Benson, C.H., and Benavides, J.M., Report No. GENV-18-05, April 2018. ML16105A043

___, WSRC-TR-2005-00017, *D-Area Sulfate Reduction Study Comprehensive Final Report,* February 11, 2005. ML23058A061

___, WSRC-STI-2007-0018, Rev. 2, *FTF Closure Cap Concept and Infiltration Estimates*, October 2007. ML111240597

U.S. Environmental Protection Agency, *Geosynthetic Clay Liners Used in Municipal Solid Waste Landfills*. EPA530-F-97-002, December 2001. https://www.epa.gov/sites/default/files/2016-03/documents/geosyn.pdf

U.S. Nuclear Regulatory Commission (NRC), NUREG/CR-7028, *Engineered Covers for Waste Containment: Changes in Engineering Properties and Implications for Long-Term Performance Assessment*, Vol. 1, December 2011. ML12005A110

___, *Technical Evaluation Report for the U.S. Department of Energy 2009 Performance Assessment for the Savannah River Site Saltstone Disposal Facility*, May 2012. ML121170309

___, *Plan for Monitoring Disposal Actions Taken by the U.S. Department of Energy at the Savannah River Site Saltstone Disposal Facility in Accordance with the National Defense Authorization Act for Fiscal Year 2005*, Rev. 1, September 2013. ML13100A113

___, *Technical Review: Performance of the High Density Polyethylene Layer, High Density Polyethylene/Geosynthetic Clay Liner Composite Layer, and the Lower Lateral Drainage Layer*, April 12, 2017. ML17081A187

___, *Report for the July 9 - 11, 2018, Onsite Observation Visit to the U.S. Department of Energy Savannah River Site Saltstone Disposal Facility*. November 1, 2018. ML18219B859

___, *Technical Review: Groundwater Monitoring At and Near the U.S. Department of Energy Savannah River Site Saltstone Disposal Facility*, May 2018. ML18117A494

___, *Supplement to the 2013 NRC Monitoring Plan for the U.S. Department of Energy Savannah River Site Saltstone Disposal Facility*, October 2018. ML18219B035

___, *Preliminary Review of the U.S. Department of Energy 2020 Performance Assessment for the Savannah River Site Saltstone Disposal Facility*, October 2020. ML20254A003

___, *Third Set of Request for Additional Information Questions for the Technical Review Reports for the U.S. Department of Energy 2020 Performance Assessment for the Savannah River Site Saltstone Disposal Facility*, March 2022. ML21341A551

___, *Technical Review: Model Integration of the U.S. Department of Energy 2020 Performance Assessment for the Savannah River Site Saltstone Disposal Facility*, May 2022. ML22116A184

___, *Fourth Set of Request for Additional Information Questions for the Technical Review Reports for the U.S. Department of Energy 2020 Performance Assessment for the Savannah River Site Saltstone Disposal Facility*, April 2022. ML22026A397

___, *Technical Review: Future Scenarios and Conceptual Models for the 2020 Performance Assessment for the Saltstone Disposal Facility at the Savannah River Site*, Rev. 1, April 18, 2023. ML23017A088

___, *Technical Review: Hydrogeology, Groundwater Monitoring, and Far-Field Modeling for the 2020 Performance Assessment for the Saltstone Disposal Facility at the Savannah River Site*, Rev. 1, April 18, 2023. ML23017A084

___, *Technical Review: Model Integration for the 2020 Performance Assessment for the Saltstone Disposal Facility at the Savannah River Site*, Rev. 1, April 18, 2023. ML23017A090

___, *Technical Review: Percolation Through and Potential Erosion near the Closure Cap for the 2020 Performance Assessment for the Saltstone Disposal Facility at the Savannah River Site*, Rev. 1, April 18, 2023. ML23017A083

Zhizhou, G., Z. Chengfeng, and X. Kai., *IOP Conference Series*. Earth and Environmental Science. pp 304, 042028. 2019.
DOI: 10.1088/1755-1315/304/4/042028. 2019. https://iopscience.iop.org/article/10.1088/1755-1315/304/4/042028/pdf